State University of Londrina
Center of Technology and Urbanization
Department of Electrical Engineering
Electrical Engineering Master Program

Otávio Seidi Nishimura

Random Access Protocols for Extra-Large and Massive MIMO Systems

Londrina,
March 19, 2021

Otávio Seidi Nishimura

Random Access Protocols for Extra-Large and Massive MIMO Systems

The Dissertation submitted to the Electrical Engineering Graduation Program at the State University of Londrina in fulfillment of the requirements for the degree of Master in Electrical Engineering.

Area: Telecommunications Systems

Supervisor: Taufik Abrão

Londrina,
March 19, 2021

Nishimura, Otávio Seidi

Random Access Protocols for Extra-Large and Massive MIMO Systems. Londrina, 2021. 96 p.

Supervisor: Taufik Abrão

Dissertation (Master) – Department of Electrical Engineering – State University of Londrina

1. Random access protocol, 2. Grant-based access protocols, 3. Machine Type Communication, 4. XL-MIMO, 5. Telecommunications Systems

Otávio Seidi Nishimura

Random Access Protocols for Extra-Large and Massive MIMO Systems

The Dissertation submitted to the Electrical Engineering Graduation Program at the State University of Londrina in fulfillment of the requirements for the degree of Master in Electrical Engineering.

Area: Telecommunications Systems

Examination Board

Dr. Taufik Abrão
Department of Electrical Engineering
State University of Londrina
Supervisor

Dr. José Carlos Marinello Filho
Department of Electrical Engineering
Federal University of Technology - Paraná
Member

Dr. Ricardo Tadashi Kobayashi
Department of Electrical Engineering
ITAIPU Binacional
Member

Londrina,
March 19, 2021

Acknowledgements

This study was financed in part by the Coordenação de Aperfeiçoamento de Pessoal de Nível Superior - Brasil (CAPES) - Finance Code 001.

Abstract

Emerging technologies as Internet-of-Things (IoT) and Machine-to-Machine (M2M) communications predict a rapid growth in the number of independent devices. Therefore, the challenge is to manage the huge amount of network connection attempts and intermittent data transmission. 5G wireless systems are expected to provide services as massive Machine-Type Communications (mMTC) and crowded Mobile-Broadband (cMBB), where it is possible to deal with a great number of user equipments (UEs) with low complexity and high efficiency. An assumed technique to manage such demands relies on massive Multiple-Input Multiple-Output (MIMO) with random access (RA). These methods have presented promising results, opening opportunities for new researches and deepen analyses. An actual challenge is how to adapt conventional techniques in novel structures, such as extra-large arrays with massive MIMO and cell-free systems. Therefore, this work proposes an adaptation of three conventional grant-based RA protocols for massive MIMO systems into extra-large massive MIMO (XL-MIMO) structures. Numerical results show appreciable system performance improvements in various figures-of-merit in overcrowded XL-MIMO scenarios. The adapted protocols, namely Strongest-User-Collision Resolution for XL-MIMO (SUCRe-XL) and Access Class Barring with Power Control for XL-MIMO (ACBPC-XL), are able to manage a greater number of UEs sporadically trying to access the network. As a consequence, an average connection delay decrease is observed in the pilot allocation step. The proposed ACBPC-XL protocol presents improved fairness, offering almost equal access opportunities (access fairness) for all UEs along the entire cell. The last adapted protocol, namely Graph-Based Pilot Access for XL-MIMO (GBPA-XL), has shown preliminary yet promising results for scenarios with median number of UEs, despite increasing computational complexity at the base station (BS).

Keywords: 1. Random access protocol, 2. Grant-based access protocols, 3. Machine Type Communication, 4. XL-MIMO, 5. Telecommunications Systems.

Resumo

Tecnologias emergentes como comunicações IoT (*Internet-of-Things*) e M2M (*Machine-to-Machine*) preveem um rápido crescimento no número de dispositivos independentes. Portanto, o desafio é manejar a imensa quantidade de tentativas de conexão na rede e transmissão intermitente de dados. É esperado que sistemas *wireless* 5G proporcionem serviços como mMTC (*massive Machine-Type Communications*) e cMBB (*crowded Mobile-Broadband*), onde é possível administrar um grande número de dispositivos (UEs - *user equipments*) com baixa complexidade e alta eficiência. Uma técnica já assumida para manejar tais demandas é o MIMO (*Multiple-Input Multiple-Output*) massivo com acesso aleatório (RA - *Random Access*). Estes métodos apresentaram resultados promissores, abrindo oportunidades para novas pesquisas e análises aprofundadas. Um desafio vigente é como adaptar técnicas convencionais em estruturas novas, como *extra-large arrays* com MIMO massivo e sistemas *cell-free*. Portanto, este trabalho propõe uma adaptação de três protocolos de acesso aleatório *grant-based* de sistemas MIMO massivo, para estruturas *extra-large massive MIMO* (XL-MIMO). Os resultados numéricos obtidos mostram melhorias apreciáveis em várias figuras de mérito de desempenho do sistema em cenários *overcrowded* XL-MIMO. Os protocolos adaptados, denominados SUCRe-XL e ACBPC-XL, são capazes de manejar um grande número de UEs tentando acessar a rede esporadicamente. Como consequência, há uma diminuição no atraso médio de conexão na etapa de alocação dos pilotos. O protocolo proposto ACBPC-XL apresenta uma melhora em termos de *fairness*, oferecendo quase a mesma oportunidade de acesso (*access fainess*) para todas as UEs em toda área da célula. O último protocolo adaptado, denominado GBPA-XL, tem revelado resultados ainda preliminares, porém promissores, para cenários com número mediano de UEs, apesar do incremento da complexidade computacional na estação radio-base (BS - *base station*).

Palavras-chave: 1. Protocolo de acesso aleatório, 2. Protocolos de acesso *grant-based*, 3. *Machine Type Communication*, 4. XL-MIMO, 5. Sistemas de telecomunicações.

List of abbreviations and acronyms

3GPP	3rd Generation Partnership Project
5G	5th Telecommunication Generation
ACB	Access class barrier
ACBPC	Access class barrier with power control
AP	Access point
AWGN	Additive White Gaussian Noise
AMP	Approximate message passing
BER	Bit Error Rate
BS	Base Station
CPU	Central Processing Unit
CSI	Channel state information
CS	Compressed sensing
cMBB	crowded Mobile BroadBand
D2D	Device-to-Device
DL	Downlink
EE	Energy Efficiency
eMBB	enhanced Mobile BroadBand
XL	extra-large
GBPA	Graph-based pilot access
HetNet	Heterogeneous Network
IPA	Idle Pilots Access
iUE	inactive user equipment
ITU-R	International Telecommunication Union Radiocommunication Sector
IoT	Internet of Things

LoS	Line-of-Sight
M2M	Machine-to-Machine
ML	Machine Learning
mMTC	Massive Machine-Type communications
mMIMO	massive multiple-input multiple-output
mmWave	millimeter Wave
MMSE	Minimum-mean-square-error
METIS	Mobile enablers twenty-twenty society
MIMO	Multiple-Input Multiple-Output
NOMA	Non-Orthogonal Multiple Access
NLoS	Non-Line-of-Sight
NMSE	Normalized mean square error
PC	Power control
PRC	Probability to resolve collision
RF	Radio Frequency
RA	Random Access
RAP	Random access to pilots
RAPiD	Random access to pilots and data transmission
RIS	Reconfigurable Intelligent Surfaces
SNR	Signal-to-Noise Ratio
SA	Subarray
SUCRe	Strongest-User Collision Resolution
SIC	Successive interference cancellation
TDD	Time-division-duplexing
URLLC	Ultra-Reliable Low Latency Communications
ULA	Uniform linear array

UL	Uplink
UE	User equipment
VR	Visibility region

List of Notations

a	scalar numbers are denoted by lower case letters;
$\mathbf{a}$	vectors are denoted by lower case bold letters;
$\mathbf{A}$	matrices are denoted by upper case bold letters;
$[\mathbf{A}]_{i,k}$	element present in the ith row and kth column of $\mathbf{A}$;
$\mathbf{A}^{-1}$	matrix inversion;
$\mathbf{A}^{T}$	matrix transposition;
$\mathbf{A}^{*}$	matrix conjugation;
$\mathbf{A}^{H}$	matrix conjugate-transposition;
$\mid . \mid$	cardinality of a set;
$\|\mathbf{A}\|$	norm-2 of $\mathbf{A}$;
$\mathbf{I}_N$	$N \times N$ identity matrix;
j	$\sqrt{-1}$;
$\Re(\cdot)$	real part operator;
$\Im(\cdot)$	imaginary part operator;
$\mathcal{B}(\cdot,\cdot)$	binomial distribution;
$\mathcal{N}(\cdot,\cdot)$	Gaussian distribution;
$\mathcal{CN}(\cdot,\cdot)$	circularly-symmetric complex Gaussian distribution;
$\mathbb{E}\{ \cdot \}$	expectation of a random variable;
$\mathbb{V}\{ \cdot \}$	variance of a random variable;
$\mathbb{C}$	space of complex-valued numbers;
$\mathbb{R}$	space of real-valued numbers;
$\Gamma(\cdot,\cdot)$	gamma function;
$\lceil \cdot \rceil$	nearest higher integer round operator;
$\odot$	Hadamard product.

List of Symbols

a	lowercase letter is a scalar;
$\mathbf{a}$	bold lowercase letter represents a vector;
$\mathbf{A}$	bold uppercase letter represents a matrix;
$\mathbf{A}^*$	conjugate of a matrix $\mathbf{A}$;
$\mathbf{A}^T$	transpose of a matrix $\mathbf{A}$;
$\mathbf{A}^H$	conjugate-transpose of a matrix $\mathbf{A}$;
$\mathbf{I}_M$	$M \times M$ identity matrix;
M	number of base station antennas;
B	number of subarrays;
M_b	number of antennas per subarray;
$\mathcal{M}$	set composed by all the subarrays, $1, \ldots, B$;
$\mathcal{V}_k$	set of visible subarrays related to user k, $\mathcal{V}_k \subset \mathcal{M}$;
P_b	success probability of the Bernoulli distribution associated to each subarray;
$\mathcal{U}$	set of user equipments in the cell;
$\mathcal{A}$	set of active user equipments in the cell, $\mathcal{A} \subset \mathcal{U}$;
$\mathcal{K}$	set of inactive user equipments in the cell, $\mathcal{K} = \mathcal{U} \setminus \mathcal{A}$;
K	number of inactive user equipments, $K = \lvert\mathcal{K}\rvert$;
τ_p	number of available mutually orthogonal pilot sequences;
$\mathbf{s}_i$	i-th pilot sequence, $\mathbf{s}_i \subset \mathbb{C}^{\tau_p \times 1}$;
$\mathbf{h}_k^{(b)}$	channel vector between user equipment k and subarrray b, $\mathbf{h}_k^{(b)} \subset \mathbb{C}^{M_b \times 1}$;
$\beta_k^{(b)}$	large scale fading coefficient between user k and subarray b;
$\mathbf{R}_k^{(b)}$	correlation matrix between user k and subarray b;
$\theta_k^{(b)}$	angle between user k and subarray b;
r	correlation index, $r \in (0; 1)$;
$d_{k.m}^{(b)}$	distance between user k and antenna m at subarray b;
g	pathloss at the reference distance;
κ	pathloss exponent;
φ	shadow fading;
σ_{sf}	shadow fading standard deviation;

P_a probability of an inactive user equipment realizing an access attempt;

$\mathcal{S}_t$ set of inactive user equipments indices transmitting pilot t;

ρ_k transmit power of user equipment k;

ρ_k^{pc} transmit power of user equipment k using power control;

ρ^{max} maximum transmit power;

$\bar{\rho}$ average received power at the base station;

$\mathbf{Y}^{(b)}$ received signal at subarray b, $\mathbf{Y}^{(b)} \subset \mathbb{C}^{M_b \times \tau_p}$;

$\mathbf{N}^{(b)}$ receiver noise at subarray b, $\mathbf{N}^{(b)} \subset \mathbb{C}^{M_b \times \tau_p}$;

$\mathbf{y}_t^{(b)}$ correlated received signal at subarray b with normalized pilot sequence $\mathbf{s}_t$;

$\mathbf{n}_t$ effective receiver noise associated with the t-th pilot sequence;

σ^2 noise variance

α_t sum of signal gains associated with pilot sequence $\mathbf{s}_t$;

$\mathbf{V}^{(b)}$ orthogonal precoded downlink pilot by subarray b, $\mathbf{V}^{(b)} \subset \mathbb{C}^{M_b \times \tau_p}$;

q downlink transmit power;

$\mathbf{v}_k$ received downlink signal by user equipment k, $\mathbf{v}_k \subset \mathbb{C}^{\tau_p \times 1}$;

$\boldsymbol{\eta}_k$ receiver noise at user equipment k;

v_k correlated received signal at user equipment k;

η_k effective receiver noise at user equipment k;

$\mathbf{V}_{XL}$ SUCRe-XL protocol precoded downlink pilot;

$\mathbf{z}_k$ received downlink signal by user equipment k, $\mathbf{z}_k \subset \mathbb{C}^{\tau_p \times 1}$;

z_k correlated received signal at user equipment k;

ϵ_k bias term at user equipment k;

δ adjustable scale factor;

P_{no} probability of the contending users' visibility regions not overlapping;

ξ average number of accepted user equipments per resolved collision;

λ normalized number of accepted users equipments;

Λ total number of accepted user equipments in the random access blocks.

List of Figures

List of Tables

Contents

1 Introduction

This chapter presents an overview of the 5G system features, extra-large MIMO systems, random access protocols, the grant-based scheme, and the state of the art of these technologies. Moreover, we present the goals and motivation for carrying out the study developed in this Dissertation, identifying opportunities to contribute to the communication technology advances.

1.1 5G Wireless Systems

As stated by the International Communication Union (ITU) (International Telecommunication Union - Development Sector, 2020), there is a predicted increase in the percentage of Internet users, and consequently network access and data traffic for the next few years coming. To enable such requirement the fifth generation of wireless networks (5G) is expected to provide three main services: enhanced Mobile Broadband (eMBB), Ultra-Reliable Low-Latency Communication (URLLC), and massive Machine-Type Communication (mMTC). Another awaited scenario is crowded Mobile Broadband (cMMB), where the number of UEs surpasses those of available pilot sequences and a very high data rate is demanded.

At the moment, crowded communication scenarios, as in mMTC and cMBB modes, pose pertinent challenges related to the unpredictable uncoordinated massive number of simultaneous accesses. Random access with massive MIMO is a promising method to conduct this growing transmission demand. The main idea is to explore massive MIMO properties such as channel hardening and favorable propagation, to provide low complexity decoding in an uncoordinated operation. Several approaches have presented suitable results and the technique still is a broad area of research. Open challenges include the adaptation of these protocols in novel systems as extra-large aperture arrays and intelligent massive MIMO (BJÖRNSON et al., 2019).

Massive MIMO for 5G cellular networks became a reality and beyond 5G deployment is taking place as many new architectures are being developed. One example is the so-called "User-Centric Cell-Free Massive MIMO", where BS antennas are spread along a certain area, causing a *user-centric* approach (UEs surrounded by BS antennas) and not the opposite (BSs surrounded by terminals). Fig. 1.1 illustrates in the left a conventional cellular network, where each UE is connected to only one BS, and in the right, a cell-free massive MIMO network, configuring a user-centric approach. Recent works explore different ways to implement applicable algorithms for attaining substantial, higher system performance compared to the conventional cellular massive MIMO and small-cell networks. Industrial implementation is also taking its way, as *radio stripes* from Ericsson provide a

low-cost integrated system with a single radio frequency (RF) antenna cable (Interdonato et al., 2019).

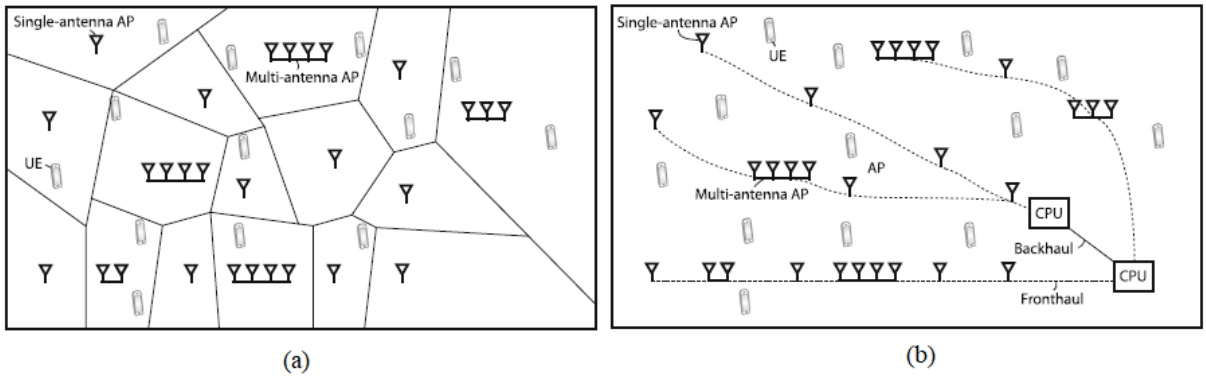

Figure 1.1 – Representation of a conventional cellular network (left) and a cell-free massive MIMO network (right). AP stands for access point (Adapted from (Interdonato et al., 2019)).

Another main area of research is the operation of massive MIMO systems at millimeter-wave (mmWave). Although conventional massive MIMO assumes frequencies of sub-6 GHz levels, the system also functions ideally at 30-300 GHz frequency levels, also known as mmWave. These frequency bands have some similarities, however, the employment is radically distinct. In summary, Tables 1.1 and 1.2 present the different use cases and propagation scenarios, and the suitability and feasibility of each operation (Bjornson et al., 2019), (Larsson et al., 2018).

Machine learning (ML) is another huge field to be explored in the 5G and beyond wireless communications. ML has vast possibilities of applications, such as regression, dimensionality reduction, classification, and clustering among others. Fig. 1.2 presents overall existing ML techniques being divided into three major categories: supervised, unsupervised, and reinforcement learning. Shortly, supervised learning requires labeled training data and unsupervised does not, although the latter is more complex than the former. While reinforcement learning deals with data on a cyclic basis using environment of states, actions, observations, and rewards. The survey in (Sharma; Wang, 2020) recognizes ML as a suitable enabler of ultra-dense IoT network issues and also shows new challenges and future research directions for ML-assisted solutions. Besides, it presents the Q-learning technique to minimize random access congestion. The authors in (Hussain et al., 2020) identify paramount limitations of the conventional resource management techniques in dealing with IoT networks. Furthermore, it introduces ML and deep learning resource management approaches, allowing Heterogeneous Networks (HetNets), Device-to-Device (D2D), mMIMO, and Non-Orthogonal Multiple Access (NOMA) technologies to be implemented. Moreover, it discusses distinct items related to resource management such as power allocation, traffic classification and prediction, cell selection, resource allocation,

Use case	**mMIMO in sub-6 GHz**	**mMIMO in mmWave**
Broadband access	Uniformly good quality-of-service and high data rates in most propagation scenarios (∼100 Mbit/s/user with 40 MHz of bandwidth).	Huge data rates in some scenarios, (∼10 Gbit/s/user with many GHz of bandwidth).
IoT, mMTC	Better power efficiency and coverage than traditional networks.	Requires significant power overhead for low data rate cases.
URLLC	Better reliability than traditional networks through channel hardening.	Unreliable propagation because of blockage.
Mobility support	Equally satisfactory as traditional networks.	Possible in theory, however challenging.
High throughput fixed link	100 antennas at the BS suffice for narrow beamforming with 20 dB gain. Limited by array size.	Admits more antennas, probably providing higher beamforming gain than at sub-6 GHz, however the gain per antenna is lower.
High user density	Spatial multiplexing of tens of UEs is achievable.	In practice, limited by hybrid cases. Equal performance of the 6 GHz, in theory.

Table 1.1 – Feasibility and suitability of mMIMO in different use cases (Adapted from (Bjornson et al., 2019)).

Propagation scenario	**mMIMO in sub-6 GHz**	**mMIMO in mmWave**
Outdoor-to-outdoor, indoor-to-indoor communication	Great data rates and reliability in LoS and NLoS scenarios.	High data rates in LoS hotspots, however unreliable due to blockage.
Outdoor-to-indoor communication	High data rates and reliability.	Increased propagation losses.
Backhaul/fronthaul links	Relatively modest data rates per multiplexed links.	Great for LoS links with fixed antennas.
Operational regime	High SNR and inter-user interference cause limitations.	Noise-limited in indoor scenarios and can be interference-limited outdoors.

Table 1.2 – Feasibility and suitability of mMIMO in different propagation scenarios (Adapted from (Bjornson et al., 2019)).

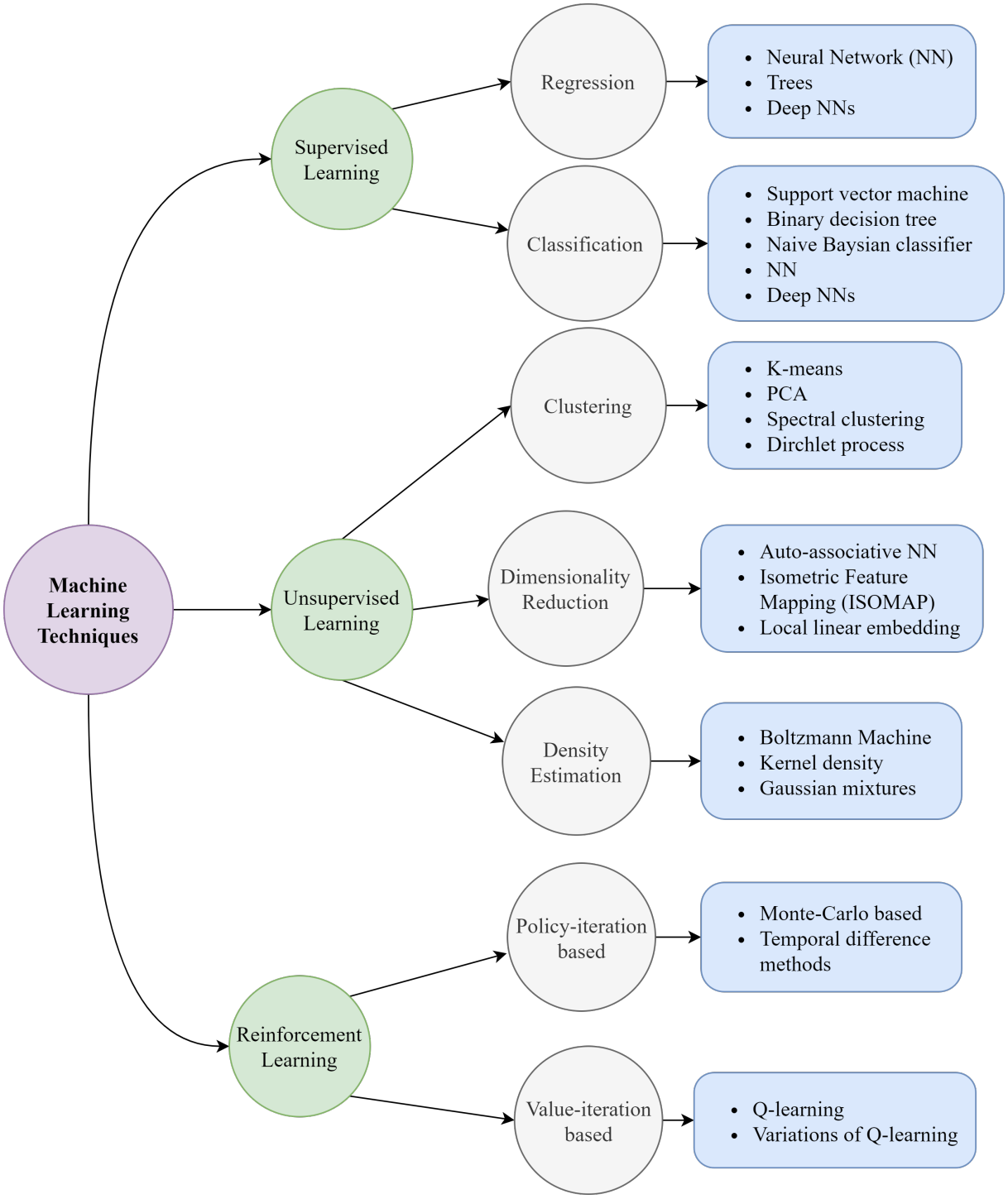

Figure 1.2 – Classification of existing ML techniques (Adapted from (Sharma; Wang, 2020)).

among others. It also presents future challenges for ML and deep learning techniques characterizing as a promising area of research.

Another promising physical-layer technology for beyond 5G systems is the so-called reconfigurable intelligent surfaces (RIS), which are passive configurable thin surfaces composed of scatters that are capable of beamforming transmitted signals to the receiver. Since it is a brand new technology, (Björnson et al., 2020) debunks three misunderstandings

while inspiring future analysis in the matter. Paper (Huang et al., 2019) provides the first contribution of resource allocation in cellular systems utilizing RIS architectures. It presents two energy efficiency (EE) maximization algorithms and indicates 300% increase in EE comparing with relay-assisted communication. Likewise, many other articles are already contributing to the progress of RIS structures, as (Di Renzo et al., 2020) and (Liaskos et al., 2018).

One last current big area of research, the extra-large massive MIMO systems (XL-MIMO) is a promising architecture for 5G and beyond scenarios. XL-MIMO has many challenges ahead, being the main scenario focus on this Dissertation. Basically, the idea is to increase the number of antenna-elements of the BS array to the extreme aiming to attain better coverage and other advantages. XL-arrays can be implemented in large walls of buildings, shopping malls, stadiums, and other infrastructures. These XL-arrays cause the so-called spatial non-stationarity effects when the BS experiences different signal powers along the array antennas coming from different UEs. This feature is created by the near-field transmissions propagation and it must not be neglected, since many attributes differ from the conventional stationary massive MIMO (Carvalho et al., 2020). More information can be found in Section 1.3.

1.2 Random Access

Channel state information (CSI) is necessary to provide coherent communication and this is implemented by using orthogonal pilots. However, the number of UEs in crowded scenarios is much greater than the available pilot sequences, causing an unfeasible situation to schedule. There are different methods of RA, which can be classified in two types: random access to pilots (RAP) and random access to pilots and data transmission (RAPiD) (Carvalho et al., 2017). The second approach is a grant-free RA and uses pilot hopping in multiple time slot transmissions, managing pilot collisions and interference with massive MIMO (mMIMO) properties (de Carvalho et al., 2016), (Sorensen et al., 2018). RAP and RAPiD methods are better known as grant-based and grant-free RA respectively. Furthermore, the first one requires an assignment step before connection of the transmitting device, and the second one allows immediate data transmission without assignment (Carvalho et al., 2017), (Senel; Larsson, 2018).

This work focuses on RAP, a grant-based RA; herein the transmissions happen in an RA pilot domain and several UEs are trying to acquire a payload data pilot for a collision-free connection. In this approach, there is a pool of available RA pilots, which are used only for RA attempts and are transmitted through specific RA blocks. The mentioned payload data pilots are used in resource blocks different from those RA blocks. A promising protocol to handle many sporadic access attempts is the Strongest-User-Collision Resolution (SUCRe) (Björnson et al., 2017). In general, it resolves RA pilot

collisions, in a totally distributed way, choosing the strongest colliding user and it is well settled in a crowded mMIMO system.

Since mMIMO is already an essential enabler for 5G networks, in (BJÖRNSON et al., 2019) five challenges for this technique have been discussed. One of them is to establish how the several conventional mMIMO approaches will be structured in extra-large arrays. These arrays can be implemented under several types of infrastructures, as buildings, stadiums, or shopping malls, where UEs are mainly placed near the panels generating non-stationary visibility regions (VRs).

This Dissertation contribution consists of proposing a grant-based RA protocol to operate advantageously in XL-MIMO systems, in which the large array size and the proximity with the users give rise to spatial non-stationarities across the array. In such configuration, it is possible to take advantage of UEs distinct VRs as an additional degree of freedom in order to improve the system performance while reducing the latency in the pilot allocation step.

1.2.1 Grant-free Random Access

Grant-free RA protocols transmit both pilots and data already from the first connection attempt. These methods provide simplicity, and coding is used to recover small packets of information, being a more suitable approach for mMTC systems. In this scenario, massive intermittent short payload data is transmitted from machine-type devices, causing an assignment step inefficient. There are mainly two kinds of grant-free RA based on multiple slots transmission: pilot RA (de Carvalho et al., 2017) and coded RA (Sorensen et al., 2018). The first one relies on the average value of pilot collisions through the slots with a determined transmission rate. This is possible due to the pilot hopping, an additional degree of freedom, across these numerous time slots. The second one implements a coded random access procedure exploiting properties of massive MIMO. It also uses pilot hopping across time slots. By generating bipartite graphs, it realizes successive interference cancellation (SIC) between colliding data using previously collected channel state information. Therefore, a probability of activation optimizes collision-free transmissions.

In order to better comprehend a grant-free RA protocol, coded pilot RA (Sorensen et al., 2018) is taken as an example and described below. Firstly, with a predefined number of time slots, active UEs select a seed of a specific sequence to notify the BS which slots will be used. In these different intervals, each UE chooses pilot sequences randomly, providing an additional degree of freedom called pilot hopping, reducing the probability of pilot collisions. Simultaneously, in these time slots repeated UL and optional DL data are transmitted after each pilot. With this configuration, the BS is able to generate a bipartite graph acquiring non-collided data and use this stored information to realize a SIC technique to clear the remaining conflict data. Fig. 1.3 illustrates a diagram example

of two arbitrary UEs using different seeds to transmit their signals in four time-slots. Since it is a grant-free RA protocol, there is no need for an assignment process.

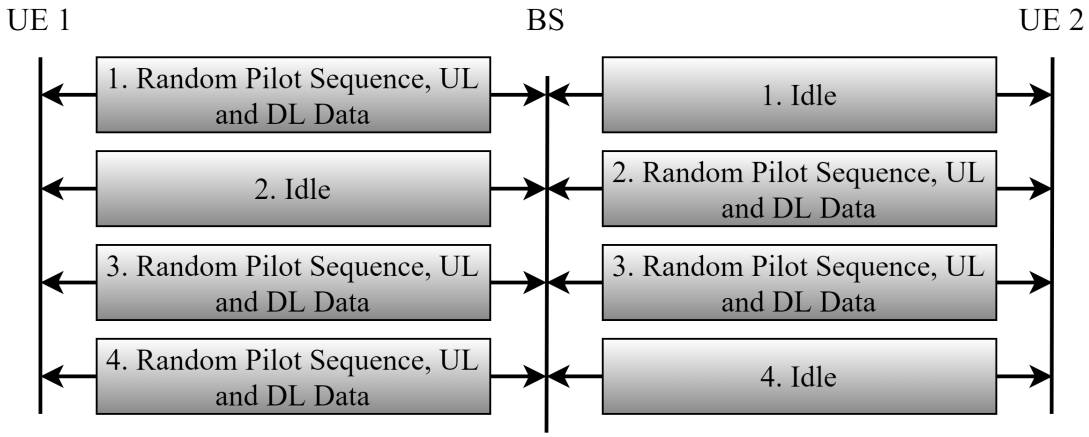

Figure 1.3 – Simplified diagram of the coded pilot RA protocol with two arbitrary UEs.

Intermittent transmissions also bring sparsity to the system, allowing compressed sensing (CS) techniques. Differently from previous concepts, in CS schemes each device has a pseudo-orthogonal pilot sequence. Since there is a large number of users and the non-orthogonality, coherent communication is not efficient. The problem is handled by an approximate message passing (AMP) algorithm with an MMSE denoiser function (Chen et al., 2018). This solution has an extension with massive MIMO in (Liu; Yu, 2018a), (Liu; Yu, 2018b). Recently, non-coherent communication is showing a higher performance than coherent communication (Senel; Larsson, 2018), being a promising candidate for the upcoming crowded scenarios.

1.2.2 Grant-based Random Access

Different from grant-free, grant-based techniques are more suitable for cMBB scenarios, where a large amount of information per transmission is needed. For this case, a huge number of devices also realize intermittent access attempts, but the data size per transmission is long enough to justify an assignment process before connection. To enable such methods, orthogonal pilot sequences are usually implemented to provide coherent communication, and since the number of this kind of pilots are limited, their allocation is essential. Grant-based RA protocols allocate dedicated collision-free pilots in an RA pilot domain process. The SUCRe protocol is an example, it resolves a large number of pilot collisions in a decentralized and uncoordinated fashion. It basically works as follows, each contending device resolves a pilot collision comparing the contending users' channel gain with its own. SUCRe presents a great performance in crowded massive MIMO systems (Björnson et al., 2017) surpassing a classical RA protocol, which deals pilot collision by retransmission. The protocol has already presented many improvements. Soft decision retransmission proposed by (Marinello; Abrão, 2019) is one of the new features

providing a reduced assignment delay for a greater number of devices. Other approaches as SUCR-IPA (SUCRe combined idle pilots access) (Han et al., 2017a) and SUCR-GBPA (SUCRe combined graph-based pilots access) (Han et al., 2017b) implement pilot reuse in different steps of the conventional protocol. There is also the decentralized pilot power allocation ACBPC (access class barring with power control) (Marinello et al., 2020), which accomplished a uniform efficiency of user connections along the cell. It is evident that grant-based RA is still being developed and presenting satisfactory results.

To better understand the functionality of the conventional SUCRe protocol, a brief explanation of the four steps is described as follows. In the first step, each UE that wants to establish a connection with the BS randomly chooses its RA pilot from a set in an uncoordinated fashion. Then these UEs transmit their UL RA pilot with a predefined power. The BS estimates the channels associated with the transmitted pilots, incapable to determine if a collision occurred. In the second step, the BS responds with those DL pilots precoded with the channels obtained in step 1, which leads to spatial directed signals. In the third step, all UEs can estimate the sum of signal gains from their selected pilot and realize a decision rule: only the UE that considers itself the winner (with the strongest signal gain) can repeat its pilot. The remaining contending UEs are instructed to wait for a random period before another attempt. In the fourth step, there is the allocation of the dedicated payload pilots for the winners with a DL signal from the BS. A simplified diagram of the protocol is presented in Fig. 1.4, with an arbitrary UE on the left and the BS on the right side.

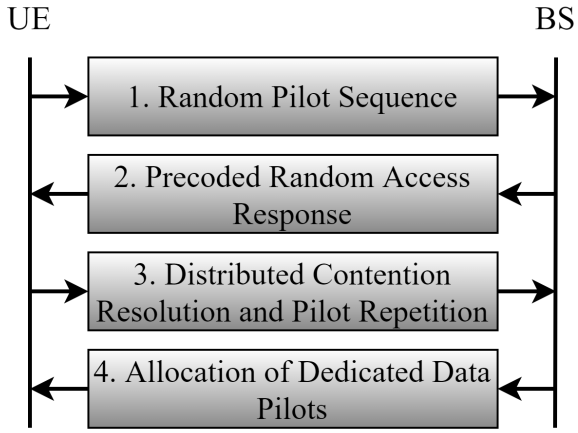

Figure 1.4 – Simplified diagram of the conventional SUCRe protocol (Adapted from (Björnson et al., 2017)).

1.3 Extra-Large Arrays

Massive MIMO is already a key enabler for 5G wireless systems to provide its services. With a massive number of antennas, the technology shows satisfactory results in

several typical scenarios. Additionally, relying on spatial dimensions benefits that afford fundamental properties such as channel hardening and asymptotic favorable propagation, it remains efficient and requires low cost for implementation.

However, it is possible to improve this technology by increasing its dimension on a large structure scale, such as stadiums, large shopping malls, airports, buildings, not increasing cost or compromising efficiency. In this manner, the distribution of arrays can provide better coverage and high data rates for a higher number of devices in a much greater area. This new concept is called extra-large scale massive MIMO (XL-MIMO) and it is bringing new opportunities and challenges to research.

One of the main characteristics of XL-MIMO is the spatial non-stationary properties generated by the large array. Each part of the array can receive or transmit different signals due to the wide environment. Since the array is much bigger and UEs are in a near field, it is also possible that different parts of the array receive distinct signal powers in a segment called the visibility region (VR). In this case, the operation of each UE is limited by its VR, but this property can be treated as a new degree of freedom, giving several benefits for the system and increasing the cost efficiency, managing a greater number of UEs in overcrowded scenarios (Carvalho et al., 2020). Fig. 1.5(a) presents an example of a uniform planar extra-large MIMO array (UPA) with five different VRs in its structure. These VRs constitute only a portion of antennas that each UE sees according to their near positions obstructions (physical obstacles) and specific channel conditions. These VRs are subject to overlapping and non-overlapping situations, which can be considered as an advantage to develop new random access techniques in (over)crowded scenarios.

Stationary regimes like massive MIMO and Large scale MIMO have limited size arrays and experience the same scatterers. This is not the case for XL-arrays that see different scatterers in different regions of the array. Therefore VRs of subarrays (SAs) are used to represent spatial non-stationarities (Ali et al., 2019), (Amiri et al., 2018), (Cheng et al., 2019). A simple example for these cases is illustrated in Fig. 1.5, where Fig. 1.5(a) depicts a UPA XL-array with arbitrary UEs and their respective VRs. The near-field feature causes each portion of the XL-array to have a specific reception, some group of antennas may receive overlapping, non-overlapping, or no signals. In contrast, Fig. 1.5(b) presents the stationary massive MIMO, where UEs are distant enough and are able to visualize the entire array. Naturally, UPA is not the only available option for XL-arrays. Indeed, Fig. 1.6 shows three simplified types of uniform arrays for cellular systems: Fig. 1.6(a) is a linear, Fig. 1.6(b) is a planar and Fig. 1.6(c) is a volumetric XL-array. In this order, there is an increase in degree-of-freedom for signal reception, and also complexity of implementation issues. Each one has a particular reception capability and structure design can vary.

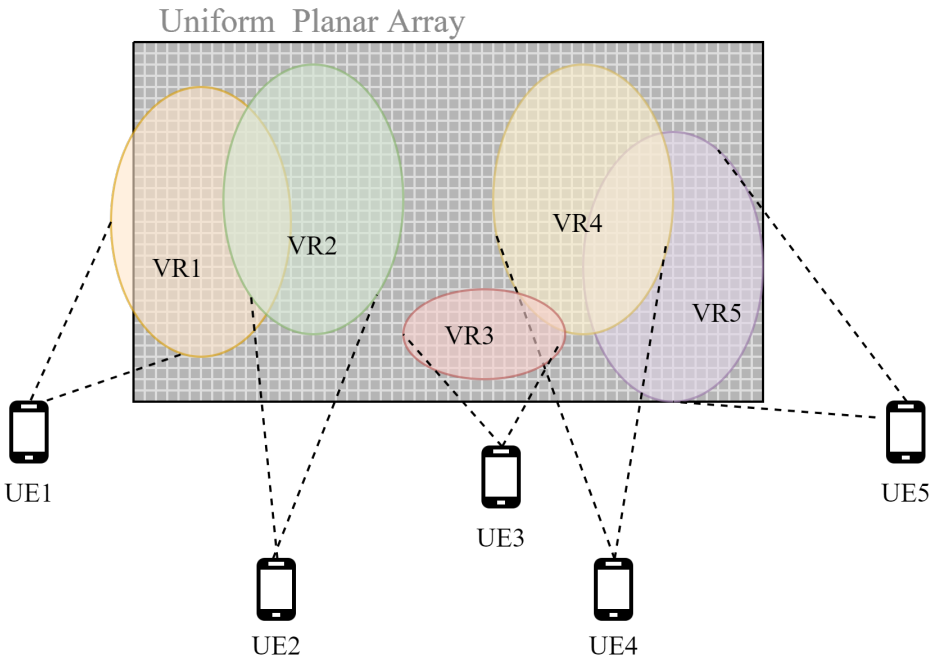

(a) UPA XL-MIMO

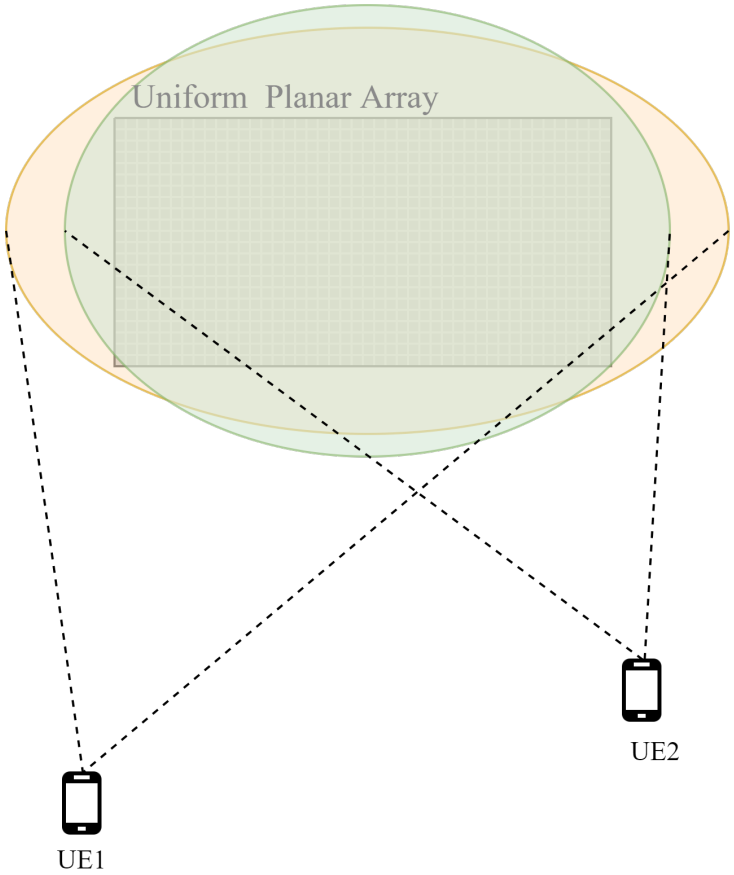

(b) UPA Stationary Massive-MIMO

Figure 1.5 – Illustration of Uniform Planar Arrays for two different cases. (a) Example of an XL-MIMO array with five UEs and their respective VRs. (b) Example of stationary massive MIMO with two UEs.

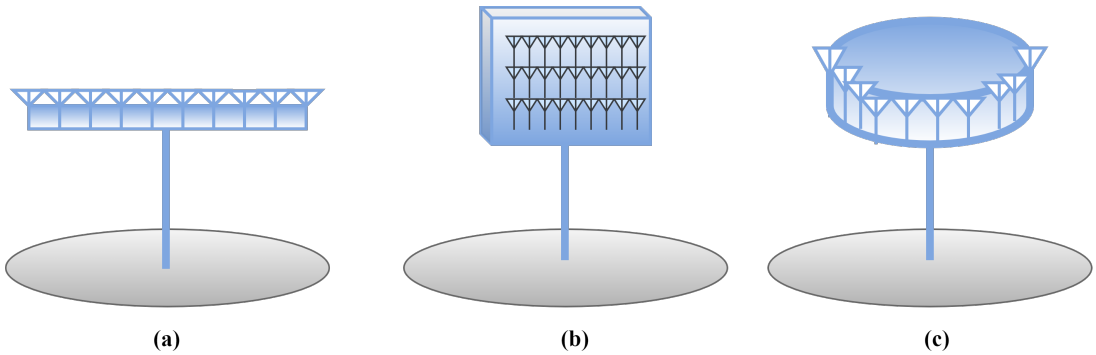

Figure 1.6 – Example of uniform arrays. (a) Linear; (b) Planar; (c) Volumetric.

1.4 Channel Modeling in XL-MIMO

Channel model is another challenge for XL-MIMO since near-field propagation differs from far-field propagation. This feature causes wavefronts spherical instead of planar, generating different power levels along the entire array (Zhou et al., 2015), (Yin et al., 2017), (CALVEZ et al., 2018), (Han et al., 2020). Many pieces of research as the ones cited herein are proposing several channel model approaches for XL-MIMO considering different scenarios. For example, in Fig. 1.7, we have a rectangular cell with several UEs, obstacles, and a BS ULA divided by four subarrays. In this scenario, UE $k = 4$ does not have any obstacle between the BS and itself. However, due to distance from SAs 3 and 4, signal powers received by the BS at these SAs can be considered insignificant comparing to those at SAs 1 and 2. Therefore, the near-field propagation causes different antennas of the XL-array to experience several variations from a single user. In other words, different portions of the XL-array experience distinct scatterers and vice versa. Herein scatterers are the representation of random geometrical dispersions, experienced by a transmitted signal also causing signal power variations. A mathematical model is given in the following.

A more realistic XL-MIMO channel model should include the near-field propagation effects and the spatial non-stationarity features (Han et al., 2020). Let (x, y) be the Cartesian coordinates represented by Fig 1.8(a), where an XL ULA with M antennas is standing at the y-axis and two scatterers are seen by the single UE. In this case, to simulate the near-field attribute, each BS antenna $m = 1, \ldots, M$, is exposed by different responses $\mathbf{a}_s \in \mathbb{C}^{M\times 1}$ from scatterer s, which each element is given by

$$[\mathbf{a}_s]_m = \frac{d_{so}}{d_{sm}} \exp(j2\pi d_{sm}), \tag{1.1}$$

where $d_{so} = x$ is the distance between scatterer s and the BS extreme-large uniform linear array, and d_{sm} is the distance between the same scatterer and the m-th BS antenna-element, Fig. 1.8(a). Therefore, the farther scatterer s is from antenna element m the lower is its response stimulation.

Moreover, to consider blockages and spatial non-stationarities, let ω_s be the subset

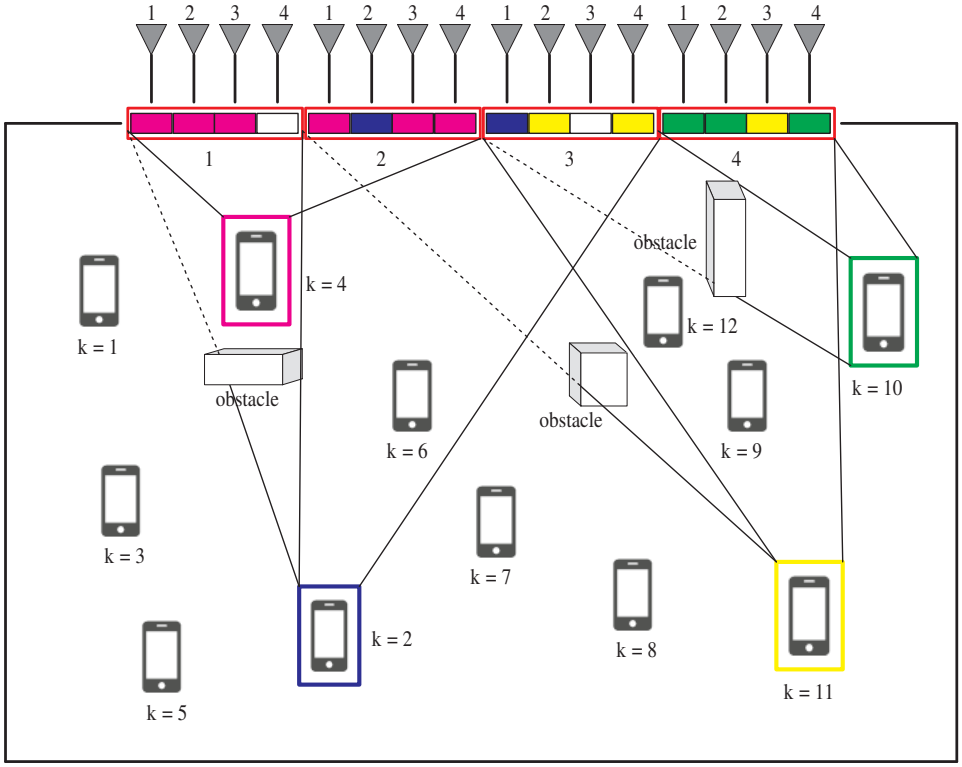

Figure 1.7 – Example of an XL ULA with four SAs, each with four antennas. UEs have different VRs and consequently distinct associated SAs and channel gains to establish communication (Nishimura et al., 2020).

of subarrays that scatterer s can see and $\mathbf{p}(\omega_s) \in \mathbb{Z}^{M\times 1}$ be the overall vector that selects the subarrays visible for scatterer s. As an example, Fig.1.8(b) indicates the following configuration: $\omega_1 = \{1, 2\}$, $\omega_2 = \{2, 3\}$ and $\omega_S = \{B-1, B\}$. Therefore,

$$[\mathbf{p}(\omega_s)]_m = \begin{cases} 1, & \text{if } \lceil \frac{mB}{M} \rceil \in \omega_s; \\ 0, & \text{else,} \end{cases} \tag{1.2}$$

where B is the number of subarrays and $\lceil \cdot \rceil$ rounds the number to its nearest higher integer. Furthermore, the channel between the UE and the BS is given by

$$\mathbf{h} = \sum_{s=1}^{S} g_s \mathbf{a}_s \odot \mathbf{p}(\omega_s), \tag{1.3}$$

where g_s is the path-loss related to scatterer s and $\odot$ is the Hadamard product.

In summary, different subarrays see different scatterers and vice versa; besides, each UE explores distinct scatterers. Additionally, the path-loss attenuation due to distance also must be considered, since the large dimension of the XL-arrays can produce reception discrepancies along its antenna-elements. This is a relatively simple approach to deal with channel modeling in a uniform linear XL-array scenario. Realistic and very accurate channel models for XL-MIMO systems require further analyses and designs, representing a huge area of research, but it is not the focus of this Dissertation.

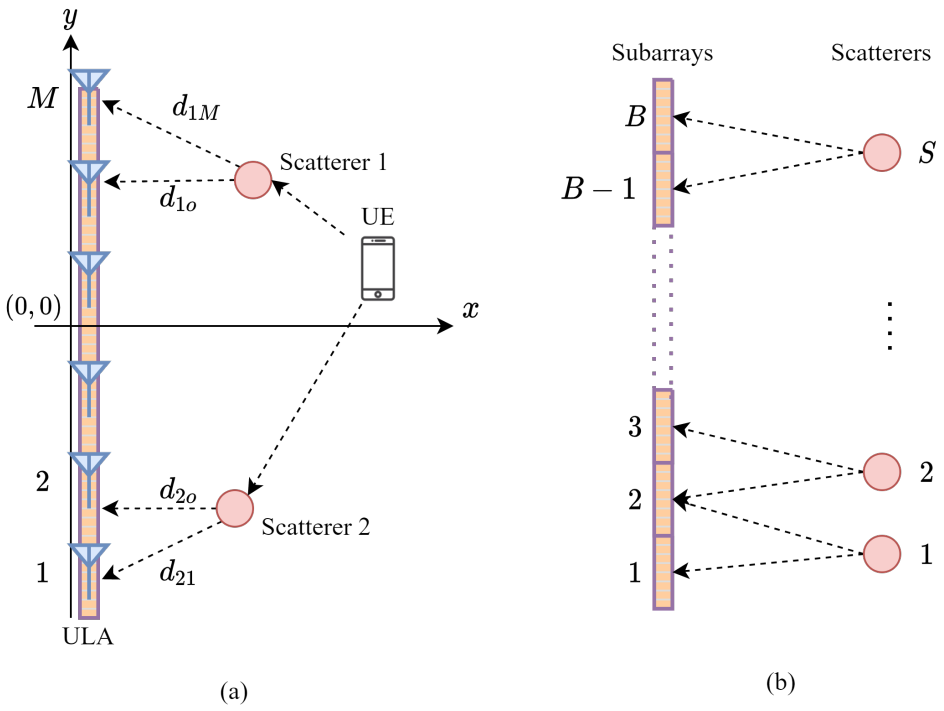

Figure 1.8 – Simplified XL-MIMO scenario. (a) XL ULA on the y-axis, two scatterers and one UE, (b) XL ULA divided into equally sized subarrays and the representation of each scatterer visibility region (VR). (Adapted from (Han et al., 2020)).

1.5 Motivation

ITU-R, 3GPP and METIS state that the 5G wireless systems must be able to establish three main services or modes: eMBB, URLLC, and mMTC. Each service has its own features and focus, such as high data throughput, extremely low-latency, and ultra-high reliability, or massive intermittent machine access characteristics. These communication modes can be deployed under different scenarios and distinct combinations, one of which is cMBB, which is expected to manage a massive number of access attempts combined with high-data throughput. Such application scenarios and transmission mode are the main focus of this work. Since the number of UEs, and importantly the UEs density is increasing rapidly in urban, industrial, and metropolitan scenarios due to the development of communication technologies such as IoT, or M2M; hence, this issue is timely, highly contemporary, and relevant. Furthermore, this Dissertation proposes technological innovations to improve the performance of grant-based RA protocols for overcrowded cellular XL-MIMO systems.

Moreover, analyzing how RA protocols can be deployed in conjunction with massive MIMO topology is an interesting alternative to the conventional techniques for dealing with crowded random access situations. This work has proposed adaptations on the random access protocols for M-MIMO to the new XL-MIMO concept and scenarios, motivated by searching for new feasible and promising solutions, contributing scientifically to the advance

in the research field. Our numerical results indicate performance improvements of the adapted/proposed protocols using a small number of subarrays in overcrowded scenarios. With more evaluations, more challenges can be opened for designing new grant-based RA protocols operating in this new system configuration posed by the XL-MIMO crowded Mobile Broadband scenarios.

1.6 Goals

This Dissertation chased the following objectives:

1. Extensive literature review and defining the state-of-art in fifth-generation (5G) mobile communication systems, specifically mMTC and cMBB services;
2. Proposition, including modifications, analyses, and comparison of grant-based RA protocols for XL-MIMO systems;
3. Statistical and numerical analyses of the proposed schemes, by developing Monte-Carlo simulations (MCS) to corroborate the theoretical formulation and desirable figures of merit;
4. Attempt to extend the analyses and comparison aiming at verifying consistency and applicability of the proposed RA protocols modifications; such extensions were developed analytically and/or numerically;
5. Publication goals: generate at least three papers for the results dissemination purpose.

1.7 Organization

The succeeding chapters are organized as follows:

Chapter 2: a detailed description of the traditional SUCRe protocol is given as the starting point since the proposed protocols are grant-based adaptations of the same scenario with similar parameters.

Chapter 3: a brief explanation of the propositions is presented, each with its most important numerical result.

Chapter 4: conclusions and future directions for the considered scenario are shown to bring perspective for further research.

Appendix: the three paper styled propositions are displayed:

[A] Nishimura, O. S.; Marinello, J. C.; Abrão, T. A Grant-based Random Access Protocol in Extra-Large Massive MIMO System. IEEE Communications Letters,
DOI: 10.1109/LCOMM.2020.3012586, p. 1–5, 2020.

[B] Nishimura, O. S.; Marinello, J. C.; Souza, R. D; Abrão, T. Fairness in a Class Barring Power Control Random Access Protocol for Crowded XL-MIMO Systems. Submitted to AEUE - International Journal of Electronics and Communications on March, 6th, 2021.

[C] Nishimura, O. S.; Marinello, J. C.; Abrão, T. A Graph-Based Random Access Protocol for Extra-Large Massive MIMO Systems. Under development.

2 System Model For Grant-Based Random Access Protocols

In this chapter, an overview of the system model for grant-based random access (RA) protocols, and conventional SUCRe RA protocol are presented. SUCRe protocol is defined as our starting point, since in the next chapter our contributions are developed in the form of RA protocols for massive MIMO systems, including a) the SUCRe-XL protocol for XL-MIMO systems, which is an extension and adapted version of the conventional SUCRe for XL-MIMO systems; b) an improved grant-base RA protocols in terms of delivered user-rate fairness.

In the following sections a detailed description of the deployed system model is provided, as well as a comprehensive explanation of the conventional SUCRe protocol (Björnson et al., 2017).

2.1 SUCRe Protocol

SUCRe is an RA protocol for crowded massive MIMO systems. It avoids intra-cell pilot contamination, exploiting channel hardening and favorable propagation. Utilizing the channel reciprocity in time-division-duplexing (TDD) operation, a user can estimate, in a distributed way, the sum of the contending UEs (UEs that chose the same RA pilot) signal gains and compare with its own. Thus, if the UE judges that its signal is the strongest, it decides to repeat the pilot.

The SUCRe protocol consists of four main steps plus step 0, where the BS maintains a control signal in broadcasting. Briefly, in the first step, in a group of inactive users, each UE that wants to become active randomly selects and sends a UL pilot sequence. In the second, the BS responds with DL precoded pilots using previously calculated channel estimates. In this step, each UE estimates the sum of the signal gains of the other contending UEs and compare them with their own. With this data, in step 3, each user performs a decision rule, where only the UE with the highest signal gain should repeat the pilot sequence. In the last step, there is the allocation of resources and assignment of pilot sequences to the winning users, or, in case of a remaining collision, a new contention resolution is applied.

All the equations of this Dissertation adopt the notations from the List of Notations, repeated below. The conjugate, transpose and conjugate-transpose of a matrix $\mathbf{A}$ are represented by $\mathbf{A}^*$, $\mathbf{A}^T$ and $\mathbf{A}^H$, respectively. $\mathbf{I}_M$ is the $M \times M$ identity matrix, $|\cdot|$ and $\|\cdot\|$ represent the cardinality of a set and the Euclidean norm of a vector, respectively. $\mathbb{E}\{\cdot\}$, and $\mathbb{V}\{\cdot\}$ denote the expectation and the variance of a random variable. $\mathcal{N}(.,.)$ denotes

a Gaussian distribution, $\mathcal{CN}(.,.)$ represents a circularly-symmetric complex Gaussian distribution, and $B(.,.)$ represents a binomial distribution. $\mathbb{C}$ and $\mathbb{R}$ denote spaces of complex and real-valued numbers, while $\Gamma(\cdot)$ represents the Gamma function, where $\Gamma(n) = (n-1)!$.

It is considered an arbitrary cell 0, with the set of inactive UEs $\mathcal{K}_0 = \mathcal{U}_0 \backslash \mathcal{A}_0$ in an arbitrary RA block, where $\mathcal{U}_0$ is the set of UEs in cell 0, and $\mathcal{A}_0$ is a subset $\mathcal{A}_0 \subset \mathcal{U}_0$, representing the active users on the regular payload data blocks. The scenarios herein consider a TDD operation and equally sized coherence blocks, where the channel is time-invariant and frequency-flat. Active UEs utilize payload data pilots in the majority of these blocks (resource blocks), and some of these blocks are reserved for RA attempts (RA blocks), where inactive UEs that want to become active use RA pilots. There are $K_0 = |\mathcal{K}_0|$ inactive UEs in cell 0. Let τ_p be the number of mutually orthogonal pilot sequences $\boldsymbol{\psi}_1, ..., \boldsymbol{\psi}_{\tau_p} \in \mathbb{C}^{\tau_p}$, with length τ_p. In this case, the expression $\|\boldsymbol{\psi}_t\|^2 = \tau_p$ is valid.

It is adopted $\mathbf{h}_k \in \mathbb{C}^M$ as the channel vector between the UE $k \in \mathcal{K}_0$ and its BS with M antennas. The channel model assumed for the proposed simulation follows an uncorrelated Rayleigh fading, which is

$$\mathbf{h}_k \sim \mathcal{CN}(0, \beta_k \mathbf{I}_M), \tag{2.1}$$

for all users equipments $k = 1, 2, ..., \mathcal{K}_0$, each with a large scale fading coefficient β_k.

In step 1, each UE k selects one RA pilot $c(k) \in \{1, 2, ..., \tau_p\}$ uniformly. Each user would like to become active with probability $P_a \leq 1$. Then, a UL pilot sequence $\boldsymbol{\psi}_{c(k)}$ will be transmitted by a UE k with power $\rho_k > 0$. Additionally, inactive UEs that do not want to become active remain with $\rho = 0$. It follows that each inactive user chooses a specific $\boldsymbol{\psi}_t$ with probability P_a/τ_p. The set composed by the UEs indices transmitting pilot t is represented by $S_t = \{k : c(k) = t, \rho_k > 0\}$. Therefore, the number of UEs that selected pilot t in the first attempt follows a binomial distribution

$$|S_t| \sim B\left(K_0, \frac{P_a}{\tau_p}\right). \tag{2.2}$$

SUCRe protocol strongly relies on massive MIMO channel hardening and asymptotic favorable propagation:

$$\frac{\|\mathbf{h}_k\|^2}{M} \xrightarrow{M\to\infty} \beta_k, \quad \forall k, \tag{2.3}$$

$$\frac{\mathbf{h}_k^H \mathbf{h}_i}{M} \xrightarrow{M\to\infty} 0, \quad \forall k, i, k \neq i. \tag{2.4}$$

For the next steps of the SUCRe protocol, as represented in Fig. 1.4, channels are assumed to satisfy conditions in equations (2.3) and (2.4).

Fig. 2.1 depicts the four steps of the SUCRe protocol with the respective variables obtained by each side of communication. The protocol details can be described in four steps as follows.

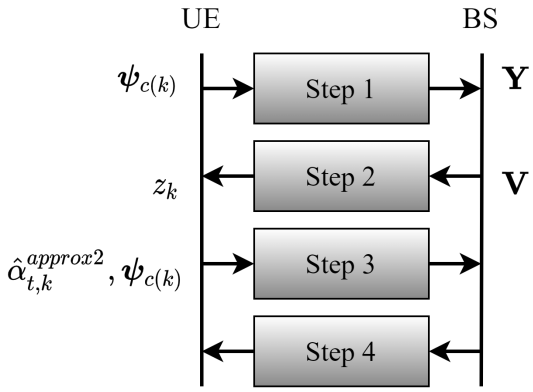

Figure 2.1 – Simplified diagram of the conventional SUCRe protocol with notable variables.

Step 1: In this step, a signal $\mathbf{Y} \in \mathbb{C}^{M \times \tau_p}$ is received by the BS:

$$\mathbf{Y} = \sum_{k \in \mathcal{K}_0} \sqrt{\rho_k} \mathbf{h}_k \boldsymbol{\psi}_{c(k)}^T + \mathbf{W} + \mathbf{N}, \tag{2.5}$$

where $\mathbf{N} \in \mathbb{C}^{M \times \tau_p}$ is the independent receiver noise with each element following a distribution $\mathcal{CN}(0, \sigma^2)$, and $\mathbf{W} \in \mathbb{C}^{M \times \tau_p}$ is interference from other cells. Then, the BS correlates the transmitted RA pilot with an arbitrary normalized pilot sequence ψ_t,

$$\mathbf{y}_t = \mathbf{Y} \frac{\boldsymbol{\psi}_t^*}{\|\boldsymbol{\psi}_t\|} = \sum_{i \in S_t} \sqrt{\rho_i \tau_p} \mathbf{h}_i + \mathbf{W} \frac{\boldsymbol{\psi}_t^*}{\|\boldsymbol{\psi}_t\|} + \mathbf{n}_t. \tag{2.6}$$

where $\mathbf{n}_t = \mathbf{N} \frac{\boldsymbol{\psi}_t^*}{\|\boldsymbol{\psi}_t\|} \sim \mathcal{CN}(0, \sigma^2 \mathbf{I}_M)$ is the effective receiver noise. In the equation, it is visible that $\|\boldsymbol{\psi}_t\| = \sqrt{\tau_p}$.

The inter-cell interference is given by two summations in equation 2.7. The first one is interfering data transmissions coming from neighboring cells with different time-frequency locations for RA blocks than cell 0, which is represented by the lth interferer channel $\mathbf{w}_l \in \mathbb{C}^M$, with some random data $\mathbf{d}_l \in \mathbb{C}^{\tau_p}$. The second summation stands for the other cells interferers (same time-frequency locations for random access blocks),

$$\mathbf{W} = \sum_l \mathbf{w}_l \mathbf{d}_l^T + \sum_{t=1}^{\tau_p} \sum_{k \in S_t^{interf}} \sqrt{\rho_{t,k}} \mathbf{g}_{t,k} \boldsymbol{\psi}_t^T. \tag{2.7}$$

Each interferer k that uses the pilot $\boldsymbol{\psi}_t$ is an element of the set S_t^{interf}. The interferer has the channel $\mathbf{g}_{t,k}$ to the base station in cell 0, with a transmit power $\rho_{t,k}$. Correlating equation 2.7, with the same normalized pilot, makes

$$\mathbf{W} \frac{\boldsymbol{\psi}_t^*}{\|\boldsymbol{\psi}_t\|} = \sum_l \mathbf{w}_l \frac{\mathbf{d}_l^T \boldsymbol{\psi}_t^*}{\|\boldsymbol{\psi}_t\|} + \sum_{k \in S_t^{interf}} \sqrt{\rho_{t,k} \tau_p} \mathbf{g}_{t,k}. \tag{2.8}$$

According to the conditions 2.3 and 2.4, it is possible to assume $\|\mathbf{w}_l\|^2/M \to \beta_{w,l}$ and $\|\mathbf{g}_{t,k}\|^2/M \to \beta_{t,k}$. It follows that

$$\frac{\left|\mathbf{W}\frac{\boldsymbol{\psi}_t^*}{\|\boldsymbol{\psi}_t\|}\right|^2}{M} \xrightarrow{M\to\infty} \sum_l \beta_{w,l}\frac{|\mathbf{d}_l^T\boldsymbol{\psi}_t^*|^2}{\|\boldsymbol{\psi}_t\|^2} + \sum_{k\in S_t^{interf}} \rho_{t,k}\tau_p\beta_{t,k} = \omega_t. \tag{2.9}$$

Using this result and again according to the two conditions, 2.3 and 2.4, equation 2.6 becomes

$$\frac{\|\mathbf{y}_t\|^2}{M} \xrightarrow{M\to\infty} \sum_{i\in S_t} \rho_i\beta_i\tau_p + \omega_t + \sigma^2. \tag{2.10}$$

Step 2: In the second step, an orthogonal precoded DL pilot, $\mathbf{V} \in \mathbb{C}^{M\times\tau_p}$, is sent as a response for the corresponding uplink RA pilot at step 1. The precoding vector is conjugate beamforming, which is made by utilizing the normalized conjugate of $\mathbf{y}_t$, thus

$$\mathbf{V} = \sqrt{q}\sum_{t=1}^{\tau_p}\frac{\mathbf{y}_t^*}{\|\mathbf{y}_t\|}\boldsymbol{\phi}_t^T. \tag{2.11}$$

The DL pilot sequence is represented by $\boldsymbol{\phi}_t \in \mathbb{C}^{\tau_p}$, where $\boldsymbol{\phi}_1, ..., \boldsymbol{\phi}_{\tau_p} \in \mathbb{C}^{\tau_p}$ are mutually orthogonal pilot sequences and satisfy $\|\boldsymbol{\phi}_t\|^2 = \tau_p$. The predefined DL transmit power is q. The UE $k \in S_t$ then receives the signal $\mathbf{z}_k^T \in \mathbb{C}^{\tau_p}$ given by

$$\mathbf{z}_k^T = \mathbf{h}_k^T\mathbf{V} + \mathbf{v}_k^T + \boldsymbol{\eta}_k^T, \tag{2.12}$$

where $\boldsymbol{\eta}_k \sim \mathcal{CN}(0, \sigma^2\mathbf{I}_{\tau_p})$ is the receiver noise, $\mathbf{v}_k \in \mathbb{C}^{\tau_p}$ is the inter-cell interference, and $\mathbf{h}_k^T$ is the reciprocal DL channel. Correlating the received signal with normalized conjugated DL pilot sequence, equation 2.12 becomes

$$z_k = \mathbf{z}_k^T\frac{\boldsymbol{\phi}_t^*}{\|\boldsymbol{\phi}_t\|} = \sqrt{q\tau_p}\mathbf{h}_k^T\frac{\mathbf{y}_t^*}{\|\mathbf{y}_t\|} + \mathbf{v}_k^T\frac{\boldsymbol{\phi}_t^*}{\|\boldsymbol{\phi}_t\|} + \eta_k. \tag{2.13}$$

The effective receiver noise is given by $\eta_k = \boldsymbol{\eta}_k^T\frac{\phi_t^*}{\|\phi_t\|} \sim \mathcal{CN}(0, \sigma^2)$. Dividing the equation by $\sqrt{M}$, considering the asymptotic favorable propagation and the convergence in 2.10, it follows that

$$\frac{z_k}{\sqrt{M}} = \sqrt{q\tau_p}\frac{(\mathbf{h}_k^H\mathbf{y}_t)^*}{M}\frac{1}{\sqrt{\frac{1}{M}\|\mathbf{y}_t\|^2}} + \frac{\mathbf{v}_k^T\boldsymbol{\phi}_t^*}{\sqrt{M}\|\boldsymbol{\phi}_t\|} + \frac{\eta_k}{\sqrt{M}} \xrightarrow{M\to\infty} \frac{\sqrt{\rho_k q}\beta_k\tau_p}{\sqrt{\sum_{i\in S_t}\rho_i\beta_i\tau_p + \omega_t + \sigma^2}}. \tag{2.14}$$

The signal and interference gains summation is defined as

$$\alpha_t = \sum_{i\in S_t}\rho_i\beta_i\tau_p + \omega_t. \tag{2.15}$$

These gains were received by the BS in the UL transmission of step 1. Thus, noise, interference and estimation errors in the imaginary part are removed from equation 2.14,

$$\frac{\Re(z_k)}{\sqrt{M}} \approx \frac{\sqrt{\rho_k q}\beta_k\tau_p}{\sqrt{\alpha_t + \sigma^2}}. \tag{2.16}$$

User equipment k can now estimate α_t by isolating it,

$$\hat{\alpha}_{t,k}^{\text{approx}_1} = \max\left(\frac{Mq\rho_k\beta_k^2\tau_p^2}{(\Re(z_k))^2} - \sigma^2, \rho_k\beta_k\tau_p\right). \tag{2.17}$$

The article (Björnson et al., 2017) compares three different estimators for $\hat{\alpha}_t$. The more appropriate choice for the purpose is the estimation $\hat{\alpha}_{t,k}^{\text{approx}_2}$, which is given by

$$\hat{\alpha}_{t,k}^{\text{approx}_2} = \max\left(\left(\frac{\Gamma(M+1/2)}{\Gamma(M)}\right)^2 \frac{q\rho_k\beta_k^2\tau_p^2}{(\Re(z_k))^2} - \sigma^2, \rho_k\beta_k\tau_p\right), \tag{2.18}$$

and it is also adopted in this work.

In this step, the main objective of the SUCRe protocol is performed. To resolve the contentions in a distributed and not coordinated method, each user has an estimate $\hat{\alpha}_{t,k}$, which is the contending UEs signal gains summation (plus inter-cell interference), and its average signal gain $\rho_k\beta_k\tau_p$, which is included in $\hat{\alpha}_{t,k}$. In this way, each user is capable of confirming if a pilot collision has occurred, $\hat{\alpha}_{t,k} > \rho_k\beta_k\tau_p$, and how strong is its signal in relation to the sum of the contenders, $\rho_k\beta_k\tau_p/\hat{\alpha}_{t,k}$. The number of contenders $|S_t|$ is, a priory, unknown by the users, leading to the only possibility, the comparison of his own signal gain with the sum of the contenders signal gains.

There are three basic definitions in order to resolve a contention.

D1. The UE $k \in S_t$ is the contention winner, or strongest user, if its average gain $\rho_k\beta_k\tau_p$ is the largest one. It follows that the contender satisfying $\rho_k\beta_k\tau_p > \hat{\alpha}_{t,k} - \rho_k\beta_k\tau_p$ will be the strongest user and may repeat the pilot transmission. As stated in the third definition below, the contention winner may not exist.

D2. A collision is resolved if a single UE considers itself the strongest user.

D3. A false positive occurs when more than one user appoints itself as the contention winner. A false negative is when none of the users appoints itself as the contention winner.

User equipments using the SUCRe protocol will obey the following decision rule:

$$\mathcal{R}_k: \quad \rho_k\beta_k\tau_p > \hat{\alpha}_{t,k}/2 + \epsilon_k \quad (repeat), \tag{2.19}$$

$$\mathcal{I}_k: \quad \rho_k\beta_k\tau_p \leq \hat{\alpha}_{t,k}/2 + \epsilon_k \quad (inactive). \tag{2.20}$$

In the decision rule, there is a optimization bias term, ϵ_k, that will be given by

$$\epsilon_k = -\beta_k/\sqrt{M} - \overline{\omega}/2. \tag{2.21}$$

Article (Björnson et al., 2017) varies the bias term to find an optimal operation point. In this work, the bias term will be fixed as in equation 2.21, where $\overline{\omega} = \mathbb{E}\{\|\mathbf{W}\frac{\psi_t^*}{\|\psi_t\|}\|^2/M\}$ is the average UL interference that is assumed to be known by the UEs.

Step 4: After the BS reception of the repeated UL pilot transmissions from step 3, it tries to decode the message with new channel estimates from the repeated pilots. If the decoding goes well, the BS can allocate pilot sequences in the payload data blocks to the contention winners, followed by a replying DL message informing the successful addition and possibly more information if necessary. If the decoding fails, the protocol has failed to resolve the collision and the unsuccessful user is instructed to try after a stipulated time or/and using another RA pilot sequence.

As a representative finding, Fig. 2.2 presents the *average number of access attempts* (ANAA) for different numbers of inactive UEs (iUEs). This simulation considers a UE activation probability equal to $P_a = 0.1\%$ and 10 available RA pilots; hence, fundamentally overcrowded scenarios are established when one available RA pilot per UE (that wants to become active) is achieved, thus starting from 10000 inactive UEs. The Baseline represents an ALOHA-like protocol which resolves contentions by pilot retransmission, *i.e.*, contending UEs retransmit RA pilots after a random time period. SUCRe surpasses the Baseline in several numbers of iUEs; at 8000 iUEs the SUCRe protocol reduces the ANAA approximately in 90%. When the scenario becomes overcrowded, SUCRe still can manage access attempts with some delay, while for the Baseline it becomes impractical.

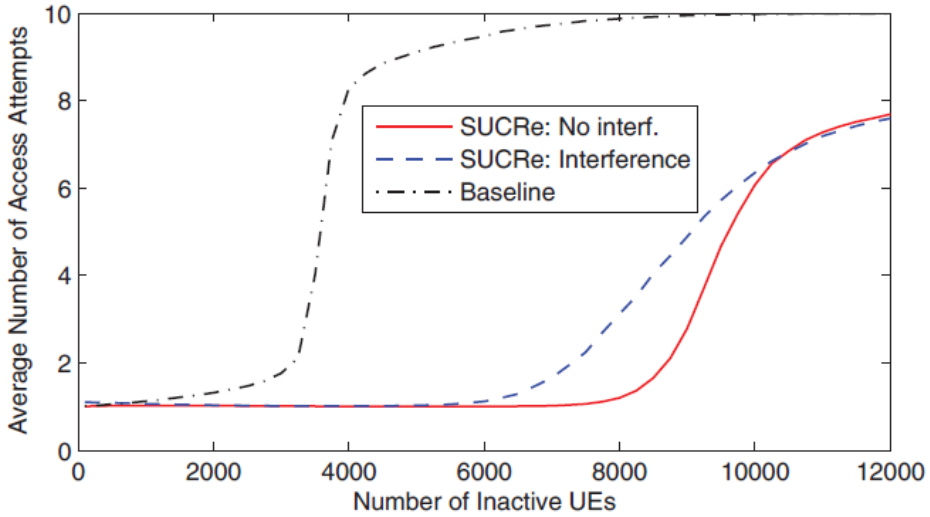

Figure 2.2 – Average number of access attempts *vs.* number of inactive UEs (Björnson et al., 2017).

2.2 Conclusions

The SUCRe random access protocol offers efficient management of RA pilots for data transmission and presents satisfactory results for crowded urban scenarios. The protocol utilizes massive MIMO properties to advantageously provide distributed pilot resolution and uncoordinated processing, without significantly increasing computational complexity. However, the protocol still has possible improvements in overcrowded scenarios,

where only a subset of UEs are admitted. Besides, only one BS structure is presented and its hard decision rule causes a disadvantage for UEs located at the edge of the cell.

In the next chapter, some SUCRe extensions are proposed and analyzed with a brief presentation of such extensions.

3 Extending SUCRe RA Protocol for Extra-Large MIMO Systems

This chapter summarizes the main contributions proposed in this Dissertation, in terms of SUCRe-based RA protocols extensions considering new XL-MIMO scenarios. We have extended and adapted new features to the conventional SUCRe aiming at providing useful and promising RA solutions for M-MIMO and XL-MIMO systems. Hence, in section 3.1 we briefly describe the proposed SUCRe RA Protocol suitable for XL-MIMO system scenarios. Section 3.2 briefly describes the proposed adaptation of ACBPC for XL-MIMO systems. Finally, section 3.3 sketches the third extension proposed in this Dissertation.

3.1 SUCRe RA Protocol for XL-MIMO

We have proposed adaptations of the conventional SUCRe to deal with the new features of the XL-MIMO system (Appendix A). The proposed SUCRe-XL protocol maintains the overall structure of the conventional one, as well as the decentralized and uncoordinated processing. As the conventional protocol, SUCRe-XL is also composed of four steps, as indicated in Fig. 3.1. The overall method remains the same, each UE needs to win a contention to acquire a dedicated data pilot. However, since the BS is an XL-array, the transmitted signals are scattered with different power levels in distinct subarrays. In that case, the BS must gather all signals related to the RA pilots to provide the equivalent *sum of signal gains* for the contending UEs. The protocol presents adaptability and with an insignificant increase in computational complexity. Results show an increase in performance, reducing access latency for different number of subarrays at the base station. Fig. 3.2 presents the *average number of access attempts* (ANAA) as a function of the number of inactive UEs. Notice that when the number of SAs increase, $B \in \{1; 5; 20\}$, the ANAA of the SUCRe-XL improves slightly, and its performance remains significantly better than the considered Baseline. For a deep analysis and more numerical results, see Appendix A.

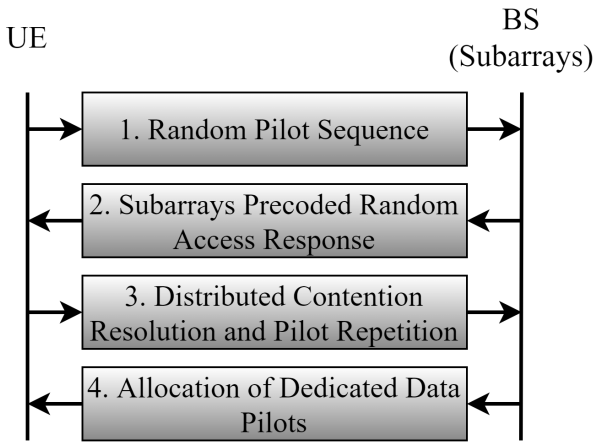

Figure 3.1 – Simplified SUCRe-XL diagram.

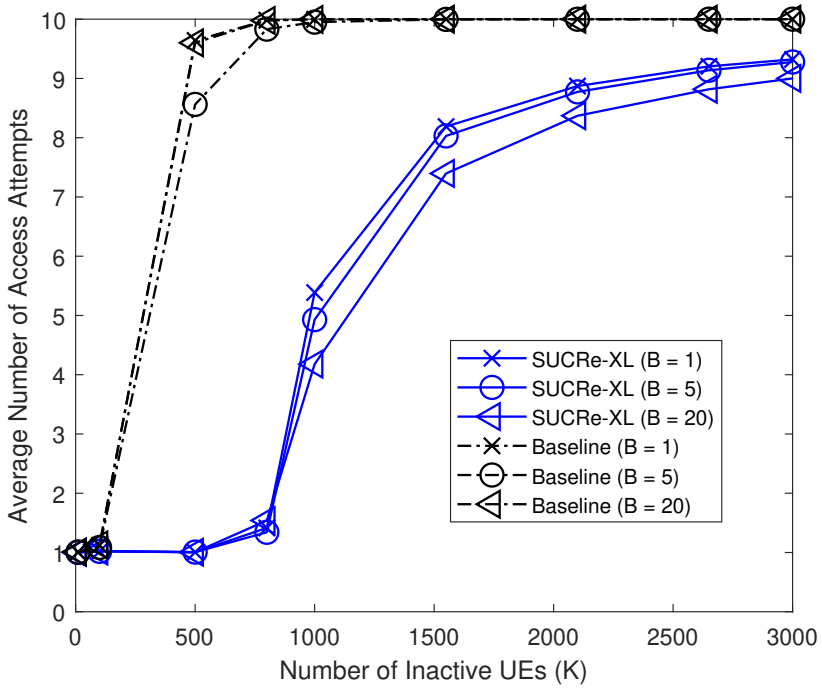

Figure 3.2 – Average number of access attempts *vs.* number of inactive UEs, corroborating the better performance of the SUCRe-XL when the number of SAs increases.

3.2 Improving Fairness of a Grant-Based RA Protocol in XL-MIMO Systems

In this section, an overview of the second RA protocol extension for crowded XL-MIMO systems is presented, while Appendix B extends the analysis and details of the proposed RA protocol for XL-MIMO. The motivation for proposing such extension base on UEs fairness access is clear: the conventional SUCRe and also the previous SUCRe-XL protocol extension proposed in section 3.1 are considered selective; hence, UEs near the BS have a greater chance of connection than those on the edge of the cell, creating unfairness. Additionally, these protocols still have their limitations in managing overcrowded scenarios and great numbers of access attempts. Therefore to generate fairness and explore other advantages or benefits, such as the increase of spectral efficiency and a greater number of accepted UEs in the new crowded XL-MIMO systems, the following proposal is presented.

To solve the conventional SUCRe problem, (Marinello et al., 2020) proposes a power control strategy to give chance for more distant UEs. In this work, such protocol is named Access Class Barring with Power Control (ACBPC), and a simplified diagram is illustrated in Fig. 3.3. Notice that the steps are similar to those of the conventional SUCRe, only modifying steps 1 and 3. Basically, UEs transmit their selected RA pilots with a limiting power control policy in step 1. In other words, UEs with high large scale fading coefficients reduce their transmit power to give a chance for unfavorable UEs. Therefore, in the second step, UEs realize a decision rule-based on an estimated number of contending UEs, that is an ACB factor. With this technique, the system presents several benefits, as fairness and improved spectral efficiency.

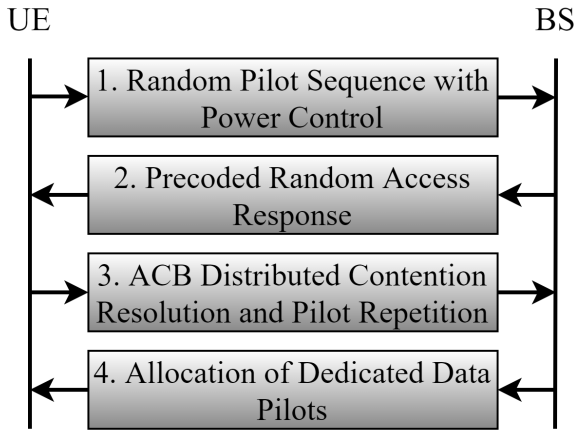

Figure 3.3 – Simplified diagram of the ACBPC protocol for crowded massive MIMO systems.

Furthermore, to improve fairness in the SUCRe-XL protocol, in this second proposition it is demonstrated how to adapt the ACBPC protocol for an XL-MIMO system.

Results show an increase in performance for overcrowded scenarios and a capability to provide almost equal chances of connection for all UEs along the cell.

3.2.1 Access Class Barring with Power Control for Extra-Large Massive MIMO Systems

To implement this new protocol, named ACBPC-XL, the modification is applied in the transmit powers of each UE in step 1 (eqs. (A.8) and (A.9)), and in the decision rule (eq. (A.20)) of step 3 of the SUCRe-XL. As in (Marinello et al., 2020), the transmit power of UE k is determined: $\rho_k^{pc} = \min\left\{\frac{\bar{\rho}}{\sum_{b\in\mathcal{V}_k}\beta_k^{(b)}}, \rho^{max}\right\}$, where ρ^{max} is the maximum transmit power and $\bar{\rho}$ is the average received power at the BS. Which modifies the *sum of the signal gains* as follows,

$$\alpha_t = \sum_{i\in\mathcal{S}_t}\left(\rho_i^{pc}\sum_{b\in\mathcal{V}_i}\beta_i^{(b)}\tau_p\right) = \bar{\rho}\tau_p|\mathcal{S}_t|. \tag{3.1}$$

Now, each UE can take an estimate of the number of the contending UEs using pilot t:

$$|\hat{\mathcal{S}}_t|_k = \frac{\hat{\alpha}_{t,k}}{\bar{\rho}\tau_p}. \tag{3.2}$$

Then, it is defined an ACB factor $\zeta_k = |\hat{\mathcal{S}}_t|_k^{-1}$, which UE k realizes a decision with probability ζ_k instead of using eq. (A.20). Notice that the additional computation is insignificant since each UE needs to generate a random value in the interval (0;1) and compare it with ζ_k.

Fig. 3.4 shows the *average number of access attempts* (ANAA) as a function of the distance between iUEs and the BS for $K = 900$, 1000, 2000 and 2600 iUEs. Notice that for the SUCRe-XL protocol the performance diminishes as the distance grows, indicating the disadvantage in providing access to the cell-edge users. On the other hand, for the ACBPC-XL the ANAA remains almost constant throughout the entire cell area, which represents nearly equal chances for all iUEs uniformly distributed along the entire cell area. Furthermore, we can see the degradation caused by the increase of iUEs in the cell. For the SUCRe-XL, curves shift left, and for the ACBPC-XL, curves shift up. But the proportion of iUEs that benefited with better access probability grows with K under the proposed ACBPC-XL protocol. Table 3.1 presents the distance of the ANAA crossing points of the ACBPC-XL and SUCRe-XL, and the percentage of benefited iUEs for the specific number of SAs. That confirms the increase of benefited iUEs when their number rise, being able to achieve even 91% of them.

In conclusion, the proposed ACBPC-XL procedure was able to provide improved access fairness and performance in the new XL-MIMO system scenarios. In other words, the adapted protocol provides almost equal chances of connection for UEs localized in the entire cell, mainly benefiting those ones at the cell-edge.

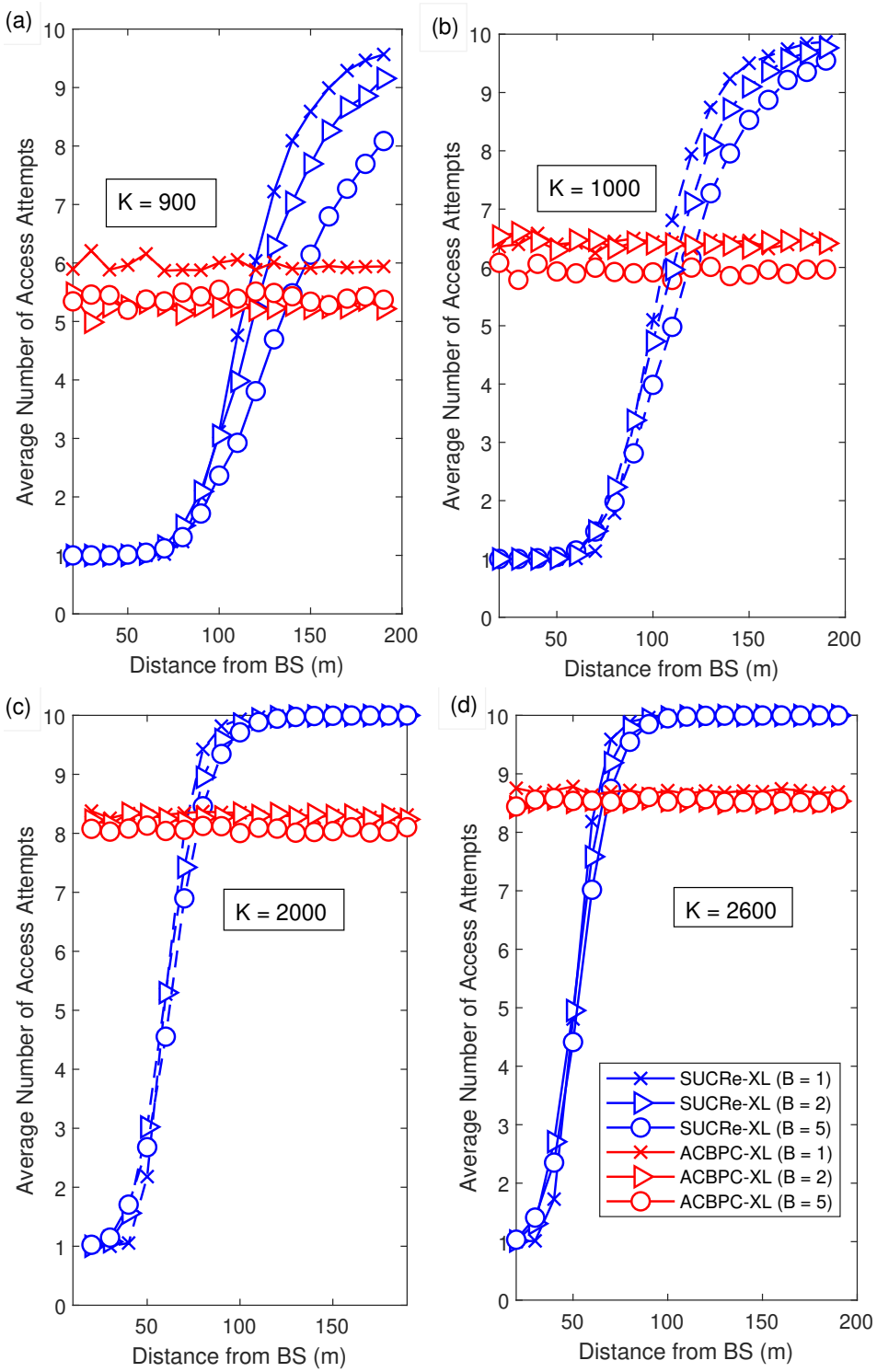

Figure 3.4 – ACBPC-XL and SUCRe-XL performance. Average number of access attempts *vs.* distance from the BS for (a) $K = 900$; (b) $K = 1000$; (c) $K = 2000$; (d) $K = 2600$ iUEs.

Table 3.1 – Distance [meters] and % of Benefited Users when the ANAA metric for ACBPC-XL becomes smaller than SUCRe-XL, Fig.3.4.

B	**1**		**2**		**5**	
$K = 900$	119	65%	120	65%	140	52%
$K = 1000$	108	72%	115	68%	120	65%
$K = 2000$	70	89%	75	87%	80	85%
$K = 2600$	63	91%	65	90%	70	89%

3.3 A Graph-Based Random Access Protocol for Extra-Large Massive MIMO Systems

This RA protocol is in development, being suggested as future work. Nevertheless, its structure and idea are already organized. Additionally, some preliminary results are discussed in Appendix C to give a clear perspective for its future development.

The main concept utilized in this work is the adaptation of the GBPA protocol (Han et al., 2017b) in the new extra-large massive MIMO systems. Furthermore, an overview of the conventional SUCR-GBPA protocol is presented below.

3.3.1 SUCR-GBPA Protocol

The SUCR-GBPA is a grant-based RA protocol that explores the standard features of the conventional SUCRe protocol, adding the usage of idle pilots and successive interference cancellation (SIC). SUCR-GBPA shows satisfactory results surpassing the SUCRe in UL data throughput.

Fig. 3.5 displays a diagram representing the four steps of the SUCR-GBPA:

Step 1: All inactive UEs that want to become active select one UL RA pilot from a pool of mutually orthogonal pilots. Then each of these UEs transmits their pilots to the BS.

Step 2: From the collected channel responses, correlating the signals with the available RA pilots, the BS is able to recognize which pilots were not selected (idle pilots). Therefore, the BS transmits precoded DL signals with the collected channels (contending UEs) from each RA pilot and the available idle pilots.

Step 3: UEs in the process now realize the SUCRe decision rule to determine which one is the strongest contending UE. All UEs that consider themselves winners repeat their RA pilots and the remaining UEs reselect their pilots from the idle pool. Furthermore, every UE that wants to be active retransmits a UL signal.

Step 4: The BS estimates the channel response again and starts a SIC algorithm. As an example, Fig. 3.6 shows a SIC process realized by the BS. Circles are the variable nodes and represent UEs that want to become active. Squares are the factor nodes representing the selected pilots. In this case, there are five UEs and four RA pilots selected, where $\{1, 2, 3, 4\}$ are the pilots indexes at *Step 1* and $\{1', 2', 3', 4'\}$ are the same pilots at step 3.

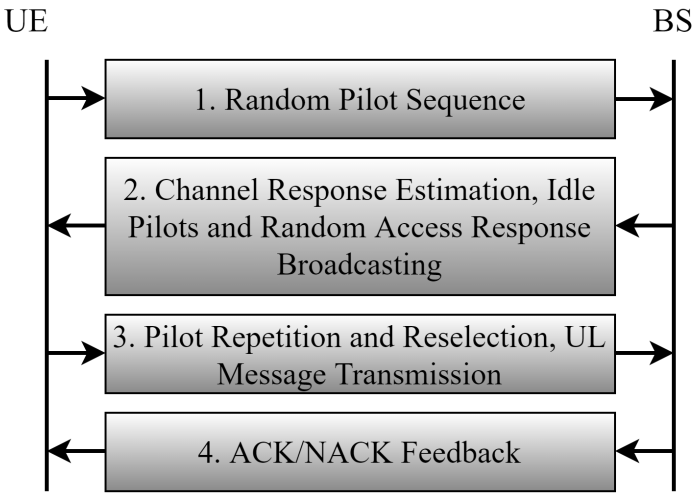

Figure 3.5 – Diagram of the SUCR-GBPA protocol for crowded massive MIMO systems (Adapted from (Han et al., 2017b)).

Let $\mathbf{h}_k$ denote the channel response of UE k, and $\mathcal{F}_i^j$ be the channel response of factor node j at iteration i (SIC). Fig. 3.6(a) is a resulting arrangement of the three first steps of the protocol. Therefore, in *Step 1*, UEs 1-2 select pilot 1, and UEs 3-4-5, pilot 3. In *Step 2*, only UE1 wins the contention and repeats pilot 1, the other UEs now select idle pilots: UEs 2-3 choose pilot 2 and UEs 4-5, pilot 4. With that arrangement, the BS starts the SIC process searching for degree-one factor nodes. After finding it, the BS eliminates its interference from other factor nodes as demonstrated in Fig. 3.6(b). This strategy is repeated until there are no more degree-one factor nodes, as in Fig. 3.6(d). Thus, in this example, UEs 4-5 fail to establish a connection and they are instructed to restart the attempt from *Step 1*. The successful UEs receive a DL acknowledge and are able to access the network.

Different from the SUCR-GBPA, the proposed GBPA-XL protocol is composed of three steps and does not use idle pilots. Fig. 3.7 depicts a simplified diagram of the GBPA-XL and its steps are briefly described in the following:

Step 1: Each iUE that wants to become active selects at random a pair of available RA pilots and transmits the first one with a message, which contains the pilot indexes information

Step 2: All the iUEs in the process now transmits the second selected RA pilot and also the same message containing the pilots' indexes;

Step 3: The BS starts searching and decoding non-overlapping, non-colliding received signals (degree-one factor nodes) from each subarray in the BS of an XL-MIMO structure. From the acquired information the BS continues with a successive interference cancellation (SIC) algorithm until there are no more decodable messages. Each subarray contributes with a SIC process, which may lead to significant growth in computational complexity when the number of SAs increases. Finally, the BS admits the UEs with successful estimated

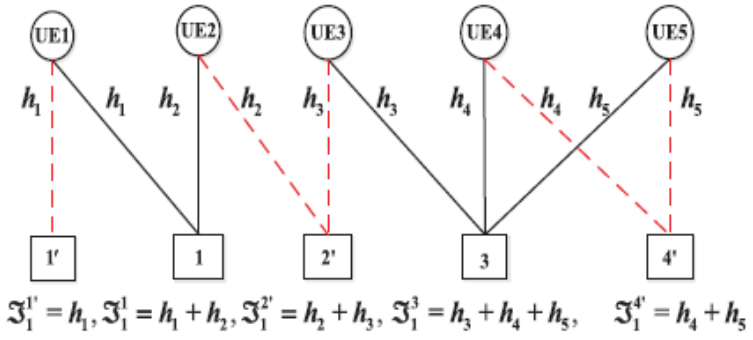

(a)

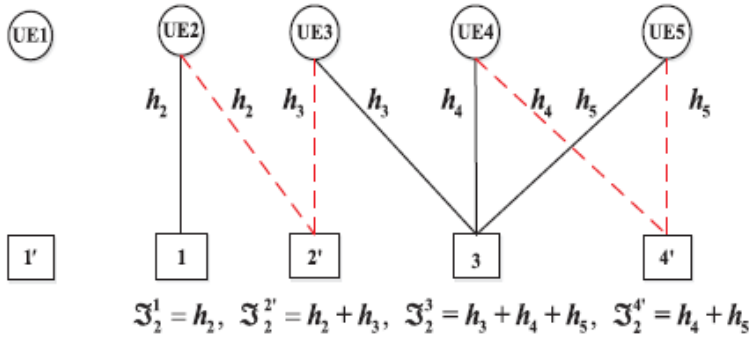

(b)

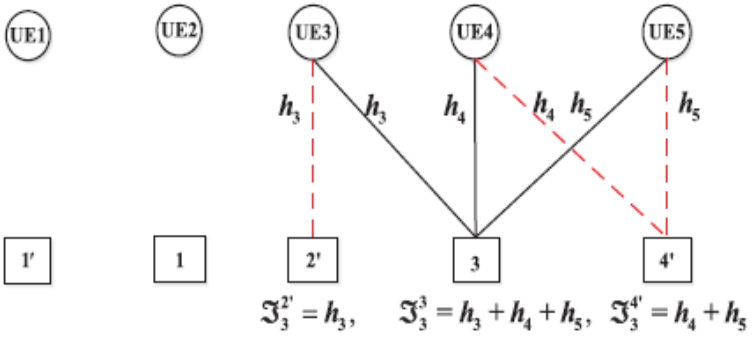

(c)

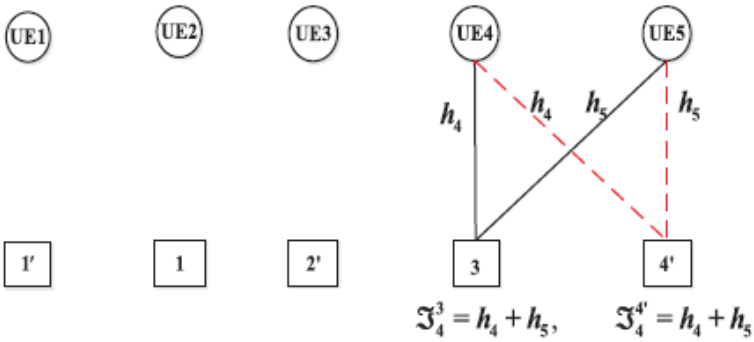

(d)

Figure 3.6 – Example of the SIC algorithm (*Step 4*) of the SUCR-GBPA protocol (Han et al., 2017b)

channels, keeping communication with their respective SAs, where their channels were obtained.

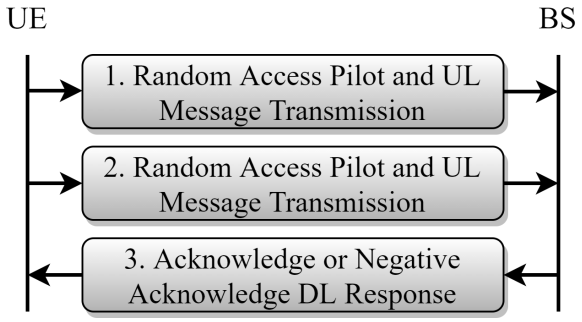

Figure 3.7 – Simplified GBPA-XL protocol diagram.

The proposed GBPA-XL protocol uses pilot hopping methodology, interference cancellation principle, and spatially non-stationarities XL-MIMO channel feature to increase the probability of successful connections in a crowded scenario. Preliminary results indicate almost a binary behavior, where performance remains satisfactory until a specific number of inactive UEs be supported. Fig. 3.8 shows the *average number of access attempts* as a function of the number of iUEs for the GBPA-XL, DCE-XL, and SUCRe-XL protocols. The named *Direct Channel Estimation for XL-MIMO* (DCE-XL) differs from the GBPA-XL not applying the SIC algorithm, only functioning with degree-one factor nodes. While the GBPA-XL still can generate degree-one factor nodes as the SIC process unfolds. When the number of inactive UEs increases, GBPA-XL and DCE-XL performances degrade abruptly, presenting unpractical results under over-crowded scenarios, indicating that with a certain number of access attempts, there are no more degree-one factor nodes and/or the SIC algorithm can no longer generate these nodes.

As a recommendation, a hybrid approach can be easily conceived by combining the GBPA-XL until its worse operation point and then switching it to another suitable XL RA protocol for overcrowded scenarios, as the proposed SUCRe-XL or ACBPC-XL strategies. As a result, a better performance, including the ANAA, are attainable with a hybrid approach at the cost of increasing the computational complexity.

3.4 Conclusions

Two complete grant-based RA protocols for XL-MIMO crowded systems have been proposed, indicating adaptability, similarities, and new behaviors from their configurations. The SUCRe-XL offers very similar curves from the conventional protocol maintaining its uncoordinated and decentralized advantages, without significantly increasing computational complexity. Increasing the number of SAs at the BS, the performance was affected favorably, diminishing access latency and failed access attempts. However, SUCRe-XL also realizes the strongest-user decision criterion to resolve pilot collisions, which degrades the probability

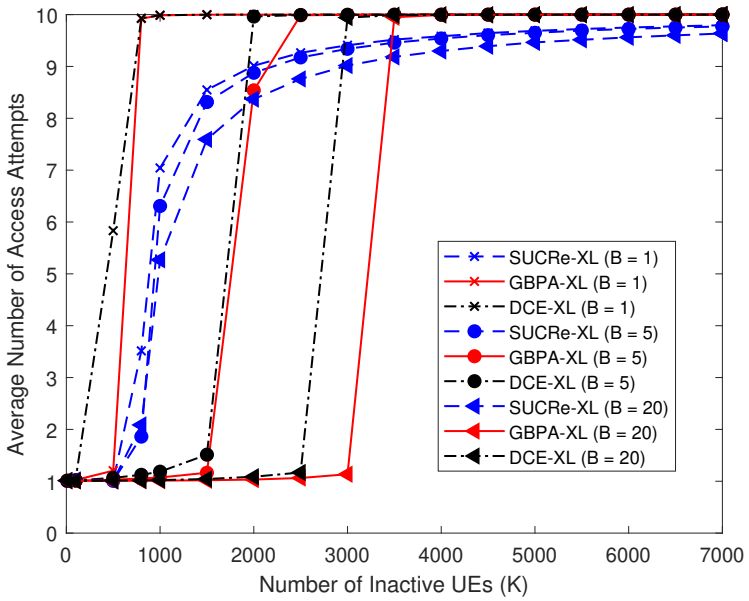

Figure 3.8 – Average number of access attempts (ANAA) *vs.* number of inactive UEs (K) in the cell, for different numbers of subarrays (B).

of edge UEs to successfully access the network. One solution for this issue was successfully proposed with ACBPC-XL, representing an evolution for the ACBPC under conventional massive MIMO.

The proposed protocol also demonstrates similarities with the conventional ACBPC and successfully provides almost equal access probability and delay for all UEs in the entire cell. Moreover, the proposed ACBPC-XL also does not indicate any considerable increase in computational complexity, since its modification is relatively simple and does not require additional overhead. Nonetheless, in the ACBPC-XL operation, delay inevitably becomes larger for UEs closer to the BS, which have to compensate for the uniform access probability across the cell provided by the ACBPC-XL protocol.

4 Conclusions and Future Directions

Extra-large massive MIMO systems is a new promising structure, presenting interesting and satisfactory results. The application also presents results achieving the 5G requirements and new challenges ahead. Therefore, this work contributes to the grant-based random access protocols field, showing new methods to handle the conventional RA protocols and it also provides future work perspectives to continue the development and research. The proposed protocols herein prove to be applicable and well suitable for cMBB scenarios, when high data throughput and massive access must be managed. The overall results indicate improvements, specifically in access delay reduction, regarding the number of subarrays at the base station and the number of inactive user equipment in the cell. Three new protocols are proposed: SUCRe-XL, ACBPC-XL, and GBPA-XL. The SUCRe-XL presents a higher capacity to manage overcrowded scenarios, reducing failed access attempts and latency, maintaining the original uncoordinated and decentralized features, with no significant increase of computational complexity. The ACBPC-XL improves performance from that of the SUCRe-XL and provides a higher user access fairness along the entire cell, also keeping the important decentralized and uncoordinated processing. The GBPA-XL, still in development, currently shows almost optimal performance for a lower number of UEs in the cell, paying with increased computational complexity at the BS. For a higher number of inactive UEs the immediate solution would be a hybrid approach, selecting between the existing protocols. The choice of the protocol must be taken by evaluating the trade-off between performance and complexity.

4.1 Future Directions in RA Protocols for 5G & 6G

Random access protocols with conventional massive MIMO indicates satisfactory performance to fulfill the 5G wireless system requirements. However, the combination of these protocols with novel physical layer structures, such as extreme-large massive MIMO, has revealed promising features and performance to justify further research and development efforts. Since many attributes change from one structure to another, unexpected and beneficial features can be found in these implementations. This is a way to explore new challenges in the perspective of the next generation of wireless systems, 6G. Overcrowded scenarios with required high data throughput and massive access attempts are predicted to grow rapidly as the number of UEs increases and new technologies advance. Furthermore, RA protocols in XL-MIMO systems have demonstrated themselves to be a suitable configuration to handle such cases. More specifically, it is suggested for future

works a richer performance analysis and also an adaptation of the current channel models to a more realistic one, with LoS and spherical wavefronts, since the considered model is rather simplified in the proposed protocols Another recommendation is the implementation of new techniques or structures to handle the assumed cMBB scenario, such as machine learning, or cell-free mMIMO systems.

Bibliography

3GPP. *The 5G Evolution*. [S.l.], 2020. Releases 16-17. Cited on page 76.

3rd Generation Partnership Project. *Spatial channel model for Multiple Input Multiple Output (MIMO) simulations*. [S.l.], 2018. Version 15.0.0. Cited 3 times on page(s) 61, 77, and 90.

Ali, A.; Carvalho, E. D.; Heath, R. W. Linear receivers in non-stationary massive MIMO channels with visibility regions. *IEEE Wireless Communications Letters*, v. 8, n. 3, p. 885–888, 2019. Cited on page 28.

Amiri, A.; Angjelichinoski, M.; de Carvalho, E.; Heath, R. W. Extremely large aperture massive MIMO: Low complexity receiver architectures. In: *2018 IEEE Globecom Workshops (GC Wkshps)*. [S.l.: s.n.], 2018. p. 1–6. Cited 4 times on page(s) 28, 59, 77, and 89.

Bjornson, E.; Van der Perre, L.; Buzzi, S.; Larsson, E. G. Massive mimo in sub-6 ghz and mmwave: Physical, practical, and use-case differences. *IEEE Wireless Communications*, v. 26, n. 2, p. 100–108, 2019. Cited 3 times on page(s) 17, 21, and 22.

BJÖRNSON, E.; SANGUINETTI, L.; WYMEERSCH, H.; HOYDIS, J.; MARZETTA, T. L. Massive MIMO is a reality – what is next? five promising research directions for antenna arrays. *arXiv:1902.07678*, 2019. Cited 4 times on page(s) 20, 25, 59, and 76.

Björnson, E.; de Carvalho, E.; Sørensen, J. H.; Larsson, E. G.; Popovski, P. A random access protocol for pilot allocation in crowded massive MIMO systems. *IEEE Transactions on Wireless Communications*, v. 16, n. 4, p. 2220–2234, April 2017. Cited 17 times on page(s) 14, 24, 26, 27, 35, 39, 40, 59, 61, 64, 65, 66, 73, 74, 78, 80, and 82.

Björnson, E.; Ozdogan, O.; Larsson, E. G. Reconfigurable intelligent surfaces: Three myths and two critical questions. *IEEE Communications Magazine*, v. 58, n. 12, p. 90–96, 2020. Cited on page 23.

CALVEZ, A. L.; MAGOAROU, L. L.; PAQUELET, S. Massive MIMO channel estimation taking into account spherical waves. *CoRR*, abs/1811.05669, 2018. Cited on page 30.

Carvalho, E. D.; Ali, A.; Amiri, A.; Angjelichinoski, M.; Heath, R. W. Non-stationarities in extra-large-scale massive mimo. *IEEE Wireless Communications*, v. 27, n. 4, p. 74–80, 2020. Cited 3 times on page(s) 24, 28, and 74.

Carvalho, E. d.; Bjornson, E.; Sorensen, J. H.; Popovski, P.; Larsson, E. G. Random access protocols for massive MIMO. *IEEE Communications Magazine*, v. 55, n. 5, p. 216–222, May 2017. Cited 3 times on page(s) 24, 58, and 88.

Chen, Z.; Sohrabi, F.; Yu, W. Sparse activity detection for massive connectivity in cellular networks: Multi-cell cooperation vs large-scale antenna arrays. In: *2018 IEEE International Conference on Acoustics, Speech and Signal Processing (ICASSP)*. [S.l.: s.n.], 2018. p. 6618–6622. Cited on page 26.

Cheng, X.; Xu, K.; Sun, J.; Li, S. Adaptive grouping sparse bayesian learning for channel estimation in non-stationary uplink massive MIMO systems. *IEEE Transactions on Wireless Communications*, v. 18, n. 8, p. 4184–4198, 2019. Cited on page 28.

de Carvalho, E.; Björnson, E.; Larsson, E. G.; Popovski, P. Random access for massive MIMO systems with intra-cell pilot contamination. In: *2016 IEEE International Conference on Acoustics, Speech and Signal Processing (ICASSP)*. [S.l.: s.n.], 2016. p. 3361–3365. Cited 2 times on page(s) 24 and 59.

de Carvalho, E.; Björnson, E.; Sørensen, J. H.; Larsson, E. G.; Popovski, P. Random pilot and data access in massive MIMO for machine-type communications. *IEEE Transactions on Wireless Communications*, v. 16, n. 12, p. 7703–7717, Dec 2017. Cited on page 25.

Di Renzo, M.; Zappone, A.; Debbah, M.; Alouini, M. S.; Yuen, C.; de Rosny, J.; Tretyakov, S. Smart radio environments empowered by reconfigurable intelligent surfaces: How it works, state of research, and the road ahead. *IEEE Journal on Selected Areas in Communications*, v. 38, n. 11, p. 2450–2525, 2020. Cited on page 24.

Fallgren, M.; AL, B. T. et. Deliverable D1.1: Scenarios, requirements and KPIs for 5G mobile and wireless system. n. ICT-317669-METIS, 2013. Disponível em: <https://www.metis2020.com/>. Cited 3 times on page(s) 58, 72, and 88.

Han, H.; Guo, X.; Li, Y. A high throughput pilot allocation for M2M communication in crowded massive MIMO systems. *IEEE Transactions on Vehicular Technology*, v. 66, n. 10, p. 9572–9576, Oct 2017. Cited 3 times on page(s) 27, 73, and 74.

Han, H.; Li, Y.; Guo, X. A graph-based random access protocol for crowded massive MIMO systems. *IEEE Transactions on Wireless Communications*, v. 16, n. 11, p. 7348–7361, Nov 2017. Cited 9 times on page(s) 14, 15, 27, 47, 48, 49, 73, 74, and 90.

Han, Y.; Jin, S.; Wen, C.; Ma, X. Channel estimation for extremely large-scale massive MIMO systems. *IEEE Wireless Communications Letters*, v. 9, n. 5, p. 633–637, 2020. Cited 3 times on page(s) 14, 30, and 32.

Huang, C.; Zappone, A.; Alexandropoulos, G. C.; Debbah, M.; Yuen, C. Reconfigurable intelligent surfaces for energy efficiency in wireless communication. *IEEE Transactions on Wireless Communications*, v. 18, n. 8, p. 4157–4170, 2019. Cited on page 24.

Hussain, F.; Hassan, S. A.; Hussain, R.; Hossain, E. Machine learning for resource management in cellular and iot networks: Potentials, current solutions, and open challenges. *IEEE Communications Surveys Tutorials*, v. 22, n. 2, p. 1251–1275, 2020. Cited on page 21.

Interdonato, G.; Bjornson, E.; Quoc Ngo, H.; Frenger, P.; Larsson, E. G. Ubiquitous cell-free massive MIMO communications. *Journal on Wireless Communications and Network*, n. 197, 2019. Cited 2 times on page(s) 14 and 21.

International Telecommunication Union - Development Sector. *Measuring digital development - Facts and Figures*. [S.l.], 2020. Cited on page 20.

Larsson, E. G.; Marzetta, T. L.; Ngo, H. Q.; Yang, H. Antenna count for massive mimo: 1.9 ghz vs. 60 ghz. *IEEE Communications Magazine*, v. 56, n. 9, p. 132–137, 2018. Cited on page 21.

Liaskos, C.; Nie, S.; Tsioliaridou, A.; Pitsillides, A.; Ioannidis, S.; Akyildiz, I. A new wireless communication paradigm through software-controlled metasurfaces. *IEEE Communications Magazine*, v. 56, n. 9, p. 162–169, 2018. Cited on page 24.

Liu, L.; Yu, W. Massive connectivity with massive MIMO - part i: Device activity detection and channel estimation. *IEEE Transactions on Signal Processing*, v. 66, n. 11, p. 2933–2946, June 2018. Cited on page 26.

Liu, L.; Yu, W. Massive connectivity with massive MIMO - part ii: Achievable rate characterization. *IEEE Transactions on Signal Processing*, v. 66, n. 11, p. 2947–2959, June 2018. Cited on page 26.

Marinello, J. C.; Abrão, T. Collision resolution protocol via soft decision retransmission criterion. *IEEE Transactions on Vehicular Technology*, v. 68, n. 4, p. 4094–4097, April 2019. Cited 4 times on page(s) 26, 73, 74, and 81.

Marinello, J. C.; Abrão, T.; Souza, R. D.; de Carvalho, E.; Popovski, P. Achieving fair random access performance in massive MIMO crowded machine-type networks. *IEEE Wireless Communications Letters*, v. 9, n. 4, p. 503–507, 2020. Cited 8 times on page(s) 27, 44, 45, 73, 74, 78, 80, and 81.

Martinez, A. O.; Eggers, P.; De Carvalho, E. Geometry-based stochastic channel models for 5g: Extending key features for massive mimo. In: *2016 IEEE 27th Annual International Symposium on Personal, Indoor, and Mobile Radio Communications (PIMRC)*. [S.l.: s.n.], 2016. p. 1–6. Cited 2 times on page(s) 74 and 75.

Martínez, O.; De Carvalho, E.; Nielsen, J. Ø. Towards very large aperture massive mimo: A measurement based study. In: *2014 IEEE Globecom Workshops (GC Wkshps)*. [S.l.: s.n.], 2014. p. 281–286. Cited on page 88.

Nishimura, O. S.; Filho, J. C. M.; Abrão, T. A Grant-based Random Access Protocol in Extra-Large Massive MIMO System. *IEEE Communications Letters*, v. 10.1109/LCOMM.2020.3012586, p. 1–5, 2020. Cited 12 times on page(s) 14, 31, 75, 76, 77, 79, 80, 81, 82, 83, 90, and 92.

Senel, K.; Larsson, E. G. Grant-free massive MTC-enabled massive MIMO: A compressive sensing approach. *IEEE Transactions on Communications*, v. 66, n. 12, p. 6164–6175, Dec 2018. Cited 2 times on page(s) 24 and 26.

Sharma, S. K.; Wang, X. Toward massive machine type communications in ultra-dense cellular iot networks: Current issues and machine learning-assisted solutions. *IEEE Communications Surveys Tutorials*, v. 22, n. 1, p. 426–471, 2020. Cited 3 times on page(s) 14, 21, and 23.

Sorensen, J. H.; de Carvalho, E.; Stefanovic, C.; Popovski, P. Coded pilot random access for massive MIMO systems. *IEEE Transactions on Wireless Communications*, v. 17, n. 12, p. 8035–8046, Dec 2018. Cited 4 times on page(s) 24, 25, 59, and 90.

Yin, X.; Wang, S.; Zhang, N.; Ai, B. Scatterer localization using large-scale antenna arrays based on a spherical wave-front parametric model. *IEEE Transactions on Wireless Communications*, v. 16, n. 10, p. 6543–6556, 2017. Cited on page 30.

Zhou, Z.; Gao, X.; Fang, J.; Chen, Z. Spherical wave channel and analysis for large linear array in LoS conditions. In: *2015 IEEE Globecom Workshops (GC Wkshps)*. [S.l.: s.n.], 2015. p. 1–6. Cited on page 30.

Appendix

APPENDIX A – A Grant-based Random Access Protocol in Extra-Large Massive MIMO System

Otávio Seidi Nishimura, José Carlos Marinello Filho, Taufik Abrão

Abstract

Extra-large massive multiple-input multiple-output (XL-MIMO) systems is a new concept, where spatial non-stationarities allow activate a high number of user equipments (UEs). This paper focuses on a grant-based random access (RA) approach in the novel XL-MIMO channel scenarios. Modifications in the classical Strongest User Collision Resolution (SUCRe) protocol have been aggregated to explore the visibility regions (VRs) overlapping in XL-MIMO. The proposed grant-based RA protocol takes advantage of this new degree of freedom for improving the number of access attempts and accepted UEs. As a result, the proposed grant-based protocol for XL-MIMO systems is capable of reducing latency in the pilot allocation step.

Keywords: Random access protocol, Grant-based, massive MIMO, XL-MIMO, non-stationarity, visibility region (VR).

A.1 Introduction

As stated by the METIS (mobile enablers twenty-twenty society) project (Fallgren; AL, 2013), there is a predicted rapidly increase in the demand of network access and data traffic for the next few years coming. To enable such requirement the fifth generation of wireless networks (5G) is expected to provide three main services: enhanced Mobile Broadband (eMBB), Ultra Reliable Low-Latency Communication (URLLC) and massive Machine Type Communication (mMTC). Another awaited scenario is crowded Mobile Broadband (cMMB), where the number of UEs surpasses those of available pilot sequences and very high data rate is demanding.

Channel state information (CSI) is necessary to provide coherent communication and this is implemented by using orthogonal pilots. However, the number of UEs in crowded scenarios is much greater than the available pilot sequences, causing an unfeasible situation to schedule. There are different methods of RA, which can be classified in two types: random access to pilots (RAP) and random access to pilots and data transmission (RAPiD) (Carvalho et al., 2017). The second approach is a grant-free RA and uses pilot

hopping in multiple time slot transmissions, managing pilot collisions and interference with massive MIMO (mMIMO) properties (de Carvalho et al., 2016), (Sorensen et al., 2018).

This paper focuses in RAP, a grant-based RA; herein the transmissions happen in an RA pilot domain and several UEs are trying to acquire a dedicated pilot for a collision free connection. A promising protocol to handle many sporadic access attempts is the SUCRe (Björnson et al., 2017). In general, it resolves RA pilot collisions, in a totally distributed way, choosing the strongest colliding user and it is well settled in a crowded mMIMO system.

Since mMIMO is already an essential enabler for 5G networks, in (BJÖRNSON et al., 2019) five challenges for this technique have been discussed. One of them is to establish how the several conventional mMIMO approaches will be structured in extra large arrays. These arrays can be implemented under several types of infrastructures, as buildings, stadiums, or shopping malls, where UEs are mainly placed near the panels generating non-stationary VRs.

The paper *contribution* consists in proposing a grant-based RA protocol to operate advantageously in XL-MIMO systems, in which the large array size and the proximity with the users give rise to spatial non-stationarities across the array. In such configuration, it is possible to take advantage of UEs distinct VRs as an additional degree of freedom in order to improve the system performance while reducing the latency in the pilot allocation step.

Notation: The conjugate, transpose and conjugate-transpose of a matrix $\mathbf{A}$ are represented by $\mathbf{A}^*$, $\mathbf{A}^T$ and $\mathbf{A}^H$, respectively. $\mathbf{I}_M$ is the $M \times M$ identity matrix, $|\cdot|$ and $\|\cdot\|$ represent the cardinality of a set and the Euclidean norm of a vector, respectively. Operators $\mathbb{E}\{\cdot\}$, and $\mathbb{V}\{\cdot\}$ denote the expectation and the variance of a random variable. $\mathcal{N}(.,.)$ denotes a Gaussian distribution, $\mathcal{CN}(.,.)$ represents a circularly-symmetric complex Gaussian distribution, and $\mathcal{B}(.,.)$ represents a binomial distribution. $\mathbb{C}$ and $\mathbb{R}$ denote spaces of complex and real-valued numbers, while $\Gamma(\cdot)$ represents a Gamma function. The operator that gives the real part of its argument is $\Re(.)$

A.2 System model

For simplicity, the adopted XL-array is a uniform linear array (ULA, Fig. A.1), operating in time-division-duplexing (TDD). Since channel modeling is not the focus of this work, it is assumed a simplified bipartite graph model in XL-MIMO, as the one used in (Amiri et al., 2018). Accordingly, the system is divided into B SAs, each composed by a fixed number of $M_b = M/B$ antennas. Let $\mathcal{M}$ be the set composed by $1, .., B$, and $\mathcal{V}_k \subset \mathcal{M}$ be the subset of visible SAs associated to user k. To model the VR set $\mathcal{V}_k$ at random, each SA is independent and identically distributed (i.i.d.) following a Bernoulli

distribution with success probability P_b. Then, every UE has a binary vector of size B to indicate if each SA is visible (1) or not (0). For simulation purposes, $|\mathcal{V}_k| > 0,\ \forall\ k$.

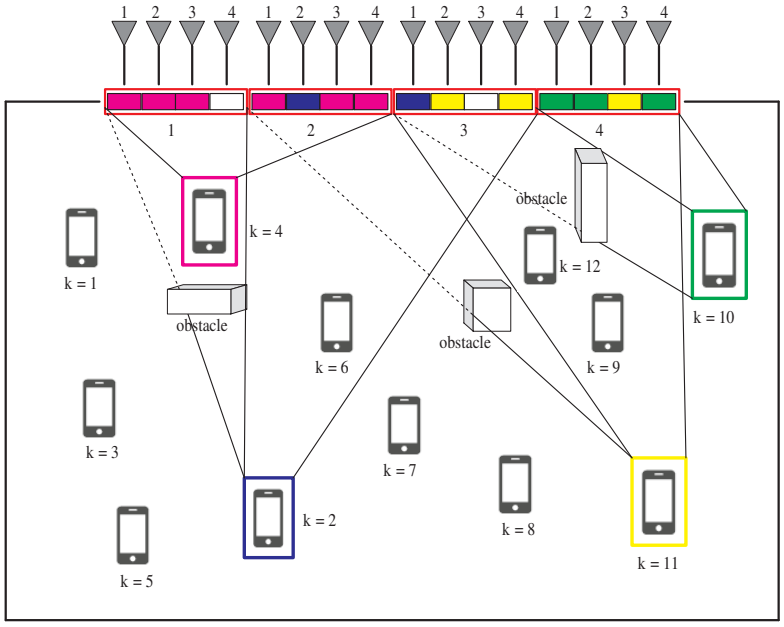

Figure A.1 – Example of a uniform linear extra large array with $B = 4$ SAs, each with $M_b = 4$ antennas. UEs have different VRs and consequently distinct associated SAs and channel gains to establish communication. There are $K = 12$ iUEs, but only UEs $k = 2, 4, 10, 11$ want to become active.

Let $\mathcal{K} = \mathcal{U} \backslash \mathcal{A}$ be the set of inactive UEs (iUEs), where $\mathcal{U}$ is the set of UEs in the entire cell, and $\mathcal{A} \subset \mathcal{U}$ is the subset of active users, each with their dedicated payload pilot. Thus, $K = |\mathcal{K}|$ represents the number of iUEs. Let τ_p denote the number of mutually orthogonal pilot sequences $\boldsymbol{s}_1, ..., \boldsymbol{s}_{\tau_p} \in \mathbb{C}^{\tau_p \times 1}$. In this case, each pilot has length τ_p and $\|\boldsymbol{s}_t\|^2 = \tau_p$.

In this work, it is considered a sliced channel vector $\mathbf{h}_k^{(b)} \in \mathbb{C}^{M_b \times 1}$ between the UE $k \in \mathcal{K}$ and the b-th SA with M_b antennas. The vector follows a Rayleigh fading channel model

$$\mathbf{h}_k^{(b)} \sim \mathcal{CN}(0, \beta_k^{(b)} \mathbf{R}_k^{(b)}), \tag{A.1}$$

for all users $k = 1, 2, ..., K$, each with a large scale fading coefficient $\beta_k^{(b)}$. When assuming i.i.d. fading channel, $\mathbf{R}_k^{(b)} = \mathbf{I}_{M_b}$, while for correlated fading channels

$$[\mathbf{R}_k^{(b)}]_{i,\ell} = r^{-|\ell - i|} e^{j\theta_k^{(b)}(\ell - i)}, \tag{A.2}$$

where $\theta_k^{(b)}$ is the angle between the k-th UE and the b-th SA, and $r \in (0; 1)$ is the correlation index. Actually, a UE has one coefficient per antenna, since the BS is an extra large array. To simplify, $\beta_k^{(b)}$ assumes the mean value considering all antennas of SA b, $\beta_k^{(b)} = \frac{1}{M_b} \sum_{m=1}^{M_b} \beta_{k,m}^{(b)}$, where $\beta_{k,m}^{(b)}$ is the coefficient between UE k and antenna m ($m = 1, ..., M_b$) at the b-th SA. In addition, invisible SAs for the kth UE, $b \notin \mathcal{V}_k$, are

assumed to have $\beta_k^{(b)} = 0$. Moreover, herein, a urban micro scenario model (3rd Generation Partnership Project, 2018) is considered:

$$\beta_{k,m}^{(b)} = 10^{-\kappa \log(d_{k,m}^{(b)}) + \frac{g+\varphi}{10}}, \tag{A.3}$$

where $d_{k,m}^{(b)}$ represents the distance between UE k and antenna m ($m = 1, ..., M_b$) at the b-th SA, $g = -34.53$ dB is the pathloss at the reference distance, the pathloss exponent $\kappa = 3.8$, and $\varphi \sim \mathcal{N}(0, \sigma_{sf}^2)$ is the shadow fading, a log-normal random variable with standard deviation $\sigma_{sf} = 10$ dB.

Each iUE realizes an RA attempt with probability $P_a \leq 1$. User $k \in \mathcal{K}$ uniformly selects an uplink RA pilot sequence $\boldsymbol{s}_{r(k)} \in \mathbb{C}^{\tau_p \times 1}$, where $r(k) \in \{1, 2, ..., \tau_p\}$. Since transmission is uncoordinated, it is possible and usual that more than one UE choose the same pilot sequence $\boldsymbol{s}_t$. Therefore, let $\mathcal{S}_t = \{k : r(k) = t, \rho_k > 0\}$ represent the set of iUEs indices transmitting pilot t, with power ρ_k. The cardinality of this set follows a binomial distribution (Björnson et al., 2017):

$$|\mathcal{S}_t| \sim \mathcal{B}\left(K, \frac{P_a}{\tau_p}\right). \tag{A.4}$$

Fig. A.2 depicts an arbitrary uplink RA arrangement with $K = 3$, $B = 4$, $\tau_p = 1$ and $P_a = 1$. In this case, there are collisions in SAs 1, 3 and 4 between users 1 and 2, and 2 and 3, but no collisions between users 1 and 3.

	Subarray 1	Subarray 2	Subarray 3	Subarray 4
User 1	$\boldsymbol{s}_t$		$\boldsymbol{s}_t$	
User 2	$\boldsymbol{s}_t$		$\boldsymbol{s}_t$	$\boldsymbol{s}_t$
User 3		$\boldsymbol{s}_t$		$\boldsymbol{s}_t$

Figure A.2 – An example of the proposed UL arrangement with a probability $P_a = 1$, $K = 3$ users, $B = 4$ subarrays and $\tau_p = 1$ available pilot sequence.

SUCRe protocol relies on mMIMO properties, as channel hardening and asymptotic favorable propagation:

$$\frac{\|\mathbf{h}_k^{(b)}\|^2}{M_b} \xrightarrow{M_b \to \infty} \beta_k^{(b)}, \quad \forall k, b \tag{A.5}$$

$$\frac{\mathbf{h}_k^{(b)H} \mathbf{h}_{k'}^{(b')}}{M_b} \xrightarrow{M_b \to \infty} 0, \quad \forall (k, b) \neq (k', b'), \tag{A.6}$$

respectively. From eq. (A.5), it follows that

$$\sum_{j \in \mathcal{V}_k} \frac{\|\mathbf{h}_k^{(j)}\|^2}{M_b} \xrightarrow{M_b \to \infty} \sum_{j \in \mathcal{V}_k} \beta_k^{(j)}, \quad \forall k \tag{A.7}$$

which represents the overall channel gain over the visible SAs for k-th UE. Notice that the number of antennas per SA, M_b, does not always remain large, since VRs represent just a

portion of antennas available for each user in a specific time. Nevertheless, the proposed protocol, named SUCRe-XL (SUCRe in extra-large systems), still present a satisfying performance even under certain reduced number of antennas per SA.

A.3 Proposed SUCRe-XL protocol

It is first described how a straightforward adaptation of the conventional SUCRe protocol to the XL-MIMO scenario would be, demonstrating why it does not work. Then, it is proposed the SUCRe-XL protocol employing the necessary modifications to operate in the XL-MIMO regime in step 2. Next, there are the definition of the contention resolution rules and allocation strategy for the dedicated payload pilots.

***Step 1**: Random UL Pilot Sequence.* All UEs that want to be active send RA pilot sequences. In the BS, the bth SA receives signal $\mathbf{Y}^{(b)} \in \mathbb{C}^{M_b \times \tau_p}$:

$$\mathbf{Y}^{(b)} = \sum_{k \in \mathcal{K}} \sqrt{\rho_k} \mathbf{h}_k^{(b)} \boldsymbol{s}_{r(k)}^T + \mathbf{N}^{(b)}, \tag{A.8}$$

where $\mathbf{N}^{(b)} \in \mathbb{C}^{M_b \times \tau_p}$ is the receiver noise, with i.i.d. elements distributed as $\mathcal{CN}(0, \sigma^2)$. To estimate the channel of UEs $k \in \mathcal{S}_t$ $(t = 1, ..., \tau_p)$, the BS correlates $\mathbf{Y}^{(b)}$ for each sub-array b with each normalized pilot sequence $\boldsymbol{s}_t$,

$$\mathbf{y}_t^{(b)} = \mathbf{Y}^{(b)} \frac{\boldsymbol{s}_t^*}{\|\boldsymbol{s}_t\|} = \sum_{i \in \mathcal{S}_t} \sqrt{\rho_i \tau_p} \mathbf{h}_i^{(b)} + \mathbf{n}_t, \quad b = 1, \ldots, B. \tag{A.9}$$

where $\mathbf{n}_t = \mathbf{N} \frac{\boldsymbol{s}_t^*}{\|\boldsymbol{s}_t\|} \sim \mathcal{CN}(0, \sigma^2 \mathbf{I}_{M_b})$ is the effective receiver noise. With eq. (A.5) and (A.6), respectively, the following approximation holds:

$$\frac{\|\sum_{b \in \mathcal{M}} \mathbf{y}_t^{(b)}\|^2}{M_b} \xrightarrow{M_b \to \infty} \underbrace{\sum_{b \in \mathcal{M}} \sum_{i \in \mathcal{S}_t} \rho_i \tau_p \, \beta_i^{(b)}}_{\alpha_t} + B\sigma^2. \tag{A.10}$$

Hence, the *sum of the signal gains*, α_t, received at the BS for each RA pilot in step 1 is readily identified as the first term in (A.10). The proof of property (A.10) is demonstrated as follows. For simplicity, let ρ_i be the same for all i; then we have:

$$\left(\sum_{b \in \mathcal{M}} \mathbf{y}_t^{(b)} \right)^H = \sum_{b \in \mathcal{M}} \sum_{i \in S_t} \sqrt{\rho_i \tau_p} \mathbf{h}_i^{(b)H} + \mathbf{n}_t^{(b)H}.$$

To obtain $\|\cdot\|^2$ we calculate:

$$\begin{aligned}\left\|\sum_{b\in\mathcal{M}}\mathbf{y}_t^{(b)}\right\|^2 &= \left(\sum_{b\in\mathcal{M}}\mathbf{y}_t^{(b)}\right)^H\cdot\left(\sum_{b\in\mathcal{M}}\mathbf{y}_t^{(b)}\right)\\ &= \rho_i\tau_p\sum_{b\in\mathcal{M}}\sum_{i\in S_t}\|\mathbf{h}_i^{(b)}\|^2+2\rho_i\tau_p\sum_{b\in\mathcal{M}}\sum_{\substack{i,j\in S_t\\ i\neq j}}\mathbf{h}_i^{(b)H}\mathbf{h}_j^{(b)}\\ &+2\rho_i\tau_p\sum_{\substack{m,b\in\mathcal{M}\\ m\neq b}}\sum_{i,j\in S_t}\mathbf{h}_i^{(m)H}\mathbf{h}_j^{(b)}+2\sqrt{\rho_i\tau_p}\sum_{m,b\in\mathcal{M}}\sum_{i\in S_t}\mathbf{h}_i^{(m)H}\mathbf{n}_t^{(b)}\\ &+2\sum_{\substack{m,b\in\mathcal{M}\\ m\neq b}}\mathbf{n}_t^{(m)H}\mathbf{n}_t^{(b)}+\sum_{b\in\mathcal{M}}\|\mathbf{n}_t^{(b)}\|^2.\end{aligned}\tag{A.11}$$

Dividing $\left\|\sum_{b\in\mathcal{M}}\mathbf{y}_t^{(b)}\right\|^2$ by $M_b\to\infty$, components with different indices, as the second to the fifth, become zero, following property in eq. (A.6). Furthermore, the first component obeys approximation (A.5), resulting in β_i. The last term becomes noise variance, validating approximation (A.10).

***Step 2**: Precoded Random Access DL Response.* In the second step of the SUCRe procedure, each SA responds with an orthogonal precoded DL pilot $\mathbf{V}^{(b)}\in\mathbb{C}^{M_b\times\tau_p}$. Using a normalized conjugate of $\mathbf{y}_t^{(b)}$, results:

$$\mathbf{V}^{(b)}=\sqrt{\frac{q}{B}}\sum_{t=1}^{\tau_p}\frac{\mathbf{y}_t^{(b)*}}{\|\mathbf{y}_t^{(b)}\|}\boldsymbol{s}_t^H,\quad b=1,\ldots,B,\tag{A.12}$$

where q is the predefined DL transmit power. Then, UE $k\in\mathcal{S}_t$ receives signal $\mathbf{v}_k^T\in\mathbb{C}^{1\times\tau_p}$ given by

$$\mathbf{v}_k^T=\sum_{m\in\mathcal{V}_k}\mathbf{h}_k^{(m)T}\mathbf{V}^{(m)}+\boldsymbol{\eta}_k^T,\tag{A.13}$$

where $\boldsymbol{\eta}_k\sim\mathcal{CN}(0,\sigma^2\mathbf{I}_{\tau_p})$ is the receiver noise. Next, each UE correlates the received signal in eq. (A.13) with RA pilot $\boldsymbol{s}_t$:

$$v_k=\mathbf{v}_k^T\frac{\boldsymbol{s}_t}{\|\boldsymbol{s}_t\|}=\sqrt{\frac{q\tau_p}{B}}\sum_{m\in\mathcal{V}_k}\mathbf{h}_k^{(m)T}\frac{\mathbf{y}_t^{(m)*}}{\|\mathbf{y}_t^{(m)}\|}+\eta_k,\tag{A.14}$$

where $\eta_k=\boldsymbol{\eta}_k^T\frac{\boldsymbol{s}_t}{\|\boldsymbol{s}_t\|}\sim\mathcal{CN}(0,\sigma^2)$ is the effective receiver noise. Dividing the equation by $\sqrt{M_b}$, and considering that asymptotic conditions of eq. (A.5) and (A.6) hold, it follows that:

$$\frac{v_k}{\sqrt{M_b}}=\sqrt{\frac{q\tau_p}{B}}\sum_{m\in\mathcal{V}_k}\frac{\left(\mathbf{h}_k^{(m)H}\mathbf{y}_t^{(m)}\right)^*}{M_b\sqrt{\frac{1}{M_b}\left\|\mathbf{y}_t^{(m)}\right\|^2}}+\frac{\eta_k}{\sqrt{M_b}}\xrightarrow{M_b\to\infty}\sum_{m\in\mathcal{V}_k}\frac{\sqrt{\rho_k q/B}\tau_p\beta_k^{(m)}}{\sqrt{\sum_{i\in\mathcal{S}_t}\rho_i\beta_i^{(m)}\tau_p+\sigma^2}}.$$

Notice that the magnitude α_t received at the BS, as in eq. (A.10), cannot be mathematically separated, due to the sum of different denominators. Since the users

cannot obtain this information, the application of the *strongest user* criterion becomes difficult. For this reason, the following SUCRe for XL-MIMO protocol is proposed.

SUCRe-XL Precoded DL Response. In the second step of the SUCRe-XL protocol, instead of employing conjugate-$\mathbf{y}_t^{(b)}$ precoding as in eq. (A.12), all SAs use the same precoding vector $\sum_{b\in\mathcal{M}} \mathbf{y}_t^{(b)}$. Thus, each SA responds with the same signal $\mathbf{V}_{\text{XL}} \in \mathbb{C}^{M_b\times\tau_p}$:

$$\mathbf{V}_{\text{XL}} = \sqrt{\frac{q}{B}} \sum_{t=1}^{\tau_p} \frac{\sum_{b\in\mathcal{M}} \mathbf{y}_t^{(b)*}}{\|\sum_{b\in\mathcal{M}} \mathbf{y}_t^{(b)}\|} \boldsymbol{s}_t^H. \tag{A.15}$$

Then, the UE $k \in \mathcal{S}_t$ receives signal $\mathbf{z}_k^T \in \mathbb{C}^{1\times\tau_p}$,

$$\mathbf{z}_k^T = \sum_{m\in\mathcal{V}_k} \mathbf{h}_k^{(m)T} \mathbf{V}_{\text{XL}} + \boldsymbol{\eta}_k^T, \tag{A.16}$$

and correlates it with RA pilot $\boldsymbol{s}_t$:

$$z_k = \mathbf{z}_k^T \frac{\boldsymbol{s}_t}{\|\boldsymbol{s}_t\|} = \sqrt{\frac{q\tau_p}{B}} \sum_{m\in\mathcal{V}_k} \mathbf{h}_k^{(m)T} \frac{\sum_{b\in\mathcal{M}} \mathbf{y}_t^{(b)*}}{\|\sum_{b\in\mathcal{M}} \mathbf{y}_t^{(b)}\|} + \eta_k. \tag{A.17}$$

In the same way of eq. (A.3), it follows that:

$$\frac{z_k}{\sqrt{M_b}} = \sqrt{\frac{q\tau_p}{B}} \frac{\left(\sum_{m\in\mathcal{V}_k} \mathbf{h}_k^{(m)H} \sum_{b\in\mathcal{M}} \mathbf{y}_t^{(b)}\right)^*}{M_b \sqrt{\frac{1}{M_b}\left\|\sum_{b\in\mathcal{M}} \mathbf{y}_t^{(b)}\right\|^2}} + \frac{\eta_k}{\sqrt{M_b}} \xrightarrow{M_b\to\infty} \frac{\sqrt{\rho_k q/B}\tau_p \sum_{m\in\mathcal{V}_k} \beta_k^{(m)}}{\sqrt{\sum_{b\in\mathcal{M}} \sum_{i\in\mathcal{S}_t} \rho_i \beta_i^{(b)} \tau_p + B\sigma^2}}.$$

Thus, noise and estimation errors in the imaginary part are removed from eq. (A.17), resulting

$$\frac{\Re(z_k)}{\sqrt{M_b}} \approx \frac{\sqrt{\rho_k q/B}\sum_{m\in\mathcal{V}_k} \beta_k^{(m)}\tau_p}{\sqrt{\alpha_t + B\sigma^2}}. \tag{A.18}$$

Hence, the kth UE can now have an estimate by isolating α_t. The estimator of (Björnson et al., 2017) can be readily adapted to our RA XL-MIMO scenario as

$$\widehat{\alpha}_{t,k} = \max\left[\rho_k \sum_{m\in\mathcal{V}_k} \beta_k^{(m)}\tau_p \ , \quad \left(\frac{\Gamma(M_b+1/2)}{\Gamma(M_b)}\right)^2 \frac{\rho_k q\tau_p^2 \left(\sum_{m\in\mathcal{V}_k} \beta_k^{(m)}\right)^2}{B[\Re(z_k)]^2} - B\sigma^2\right]. \tag{A.19}$$

It is proved that changing the precoding as in eq. (A.15) and adapting the $\widehat{\alpha}_{t,k}$ estimator as in eq. (A.19) are sufficient to implement the proposed RA protocol in XL-MIMO scenarios. Such procedure does not cause any additional overhead or sum rate loss in comparison with the original SUCRe protocol (Björnson et al., 2017).

***Step 3**: Contention Resolution and Pilot Repetition.* To resolve contentions distributively and uncoordinately, the k-th UE now has $\widehat{\alpha}_{t,k}$, which is the summation of the contending UEs signal gains with its own $\rho_k \sum_{m\in\mathcal{V}_k} \beta_k^{(m)}\tau_p$. However, the number of contenders $|\mathcal{S}_t|$ as well as the VRs of each UE are unknown by the users, leading to the only possibility of

comparing its own overall gain with $\widehat{\alpha}_{t,k}$, by computing $\frac{\rho_k}{\widehat{\alpha}_{t,k}} \sum_{m \in \mathcal{V}_k} \beta_k^{(m)} \tau_p$. Hence, UEs using the SUCRe-XL protocol apply the following decision rule:

$$\begin{cases} \mathcal{R}_k : & \sum_{m \in \mathcal{V}_k} \rho_k \beta_k^{(m)} \tau_p > \widehat{\alpha}_{t,k}/2 + \epsilon_k \quad (repeat), \\ \mathcal{I}_k : & \sum_{m \in \mathcal{V}_k} \rho_k \beta_k^{(m)} \tau_p \leq \widehat{\alpha}_{t,k}/2 + \epsilon_k \quad (inactive). \end{cases} \tag{A.20}$$

In this decision rule, the bias term ϵ_k is given by

$$\epsilon_k = \frac{\delta}{\sqrt{M_b}} \sum_{b \in \mathcal{V}_k} \beta_k^{(b)} \tag{A.21}$$

where δ is an adjustable scale factor for finding a suitable operation point. As in (Björnson et al., 2017), we adopt a satisfactory value of $\delta = -1$.

There are four possible cases in a contention process:

1. Non-overlapping UEs win (false positive). Ex.: from Fig. A.2 if users 1 and 3 win.
2. Only one UE wins.
3. None of the UEs win (false negative).
4. Overlapping UEs win (false positive). Ex.: from Fig. A.2, users 1 and 2 or 2 and 3 win.

Although case 1 is a false positive, there is no pilot collision. Therefore, cases 1 and 2 are successful attempts and there is the allocation of the RA pilot. Case 4 is considered a pilot collision; *i.e.*, a pilot collision occurs if more than one UE in $\mathcal{S}_t$ retransmit in step 3 and have overlapping VRs.

***Step 4**: Allocation of Dedicated Payload Pilots* After the BS receives the repeated UL pilot transmissions from step 3, it tries to decode the message with new channel estimates from the repeated pilots. If the decoding is successful, the BS can allocate pilot sequences in the payload data blocks to the non-overlapping contention winners, followed by a replying DL message informing the successful connection and, if necessary, more information. If the decoding fails, the protocol failed to resolve that collision and the unsuccessful UE is instructed to try again after a random interval.

SUCRe-XL Complexity is equivalent to that of conventional SUCRe protocol. Although the computation of the precoding vector increases marginally at the BS with the number of SAs B, due to the sum of all different estimated channels in (A.15), the same precoding vector is used for all SAs, different than the precoding in (A.12) for the original SUCRe. While the original SUCRe has to compute B different vector inner products in (A.12), the proposed SUCRe-XL protocol has to compute a sum of B vectors followed by a single vector inner product in (A.15). Also, each UE $k \in \mathcal{S}_t, \forall t$ has to estimate the sum of its large scale fading coefficients in SUCRe-XL protocol, which can be evaluated as the

average received power of a beacon signal in a step 0, similarly as assumed in (Björnson et al., 2017).

A.4 Numerical Results

It is assumed a 100 meter ULA with $M = 500$ antennas in a 200×200 m^2 square cell with $K = 1000$ uniformly distributed iUEs (crowded scenario) as illustrated in Fig. A.1, each user wants to become active with probability $P_a = 0.01$. It is considered $\tau_p = 10$ pilots, and transmit powers $\rho_k = q = 1$. Two channel models were deployed: ***i***) uncorrelated Rayleigh fading, as in eq. (A.1), with $\mathbf{R}_k^{(b)} = \mathbf{I}_{M_b}$; ***ii***) correlated Rayleigh fading model, following eq. (A.2), with $r = 0.7$.

A baseline ALOHA-like (Björnson et al., 2017) performance has been included for comparison purpose, which treats pilot collision by retransmission after a random waiting time period, hence, contending users retransmit their pilots at random if collision occurs.

The ***Probability to Resolve Collision*** (PRC) is calculated numerically taking all resolved collisions per total number of collisions occurred. Simulations were carried out in sequential RA blocks fashion, where iUEs try to access the channel in each iteration. For each parameter value of the x-axis (B or P_b in Figs. A.4, A.5, A.6, A.7, A.8 and A.9), it is simulated 10^4 sequential RA blocks. If an attempt fails, UE makes another attempt with probability 0.5 in the subsequent blocks. It is given a limit of 10 RA attempts per UE, after which a failed access attempt is declared.

Fig. A.3 depicts the normalized mean square error (NMSE), given by $\mathbb{E}\{|\widehat{\alpha}_{t,k} - \alpha_t|^2\}/\alpha_t$. It shows that increasing the number of SAs B, which means reducing the number of antennas per SA M_b, since $M/B = M_b$, causes a progressive discrepancy on α_t estimation due to (A.5) and (A.6) do not hold when M_b decreases. Indeed, NMSE levels for the SUCRe-XL protocol deteriorate steadily when $B > 50$ for both channel models. To simplify this simulation (Fig. A.3), all subarrays are visible, *i.e.*, $|\mathcal{V}_k| = B$, $\forall k$.

Fig. A.4 presents the PRC *vs.* the number of subarrays (B). This performance indicator, for the SUCRe-XL, increases until $B = 25$ for the uncorrelated Rayleigh fading. Besides, it is worth to note that the case $B = 1$ corresponds to a spatial stationary regime. The initial PRC increase is due to the SUCRe-XL decision rule associated with the possibility of users retransmitting the same RA pilot having non overlapping VRs, but then the reduced number of antennas per SA diminishes the channel hardening and favourable propagation effects, as well as the quality of the $\widehat{\alpha}_{t,k}$ estimates and, consequently, the PRC. Channel correlation highlights this effect, making the PRC starts to decrease with a lower B value.

Fig. A.5 depicts the PRC for different probabilities of each SA being visible for a given UE, P_b. Notice that P_b is inversely proportional to the density of obstacles affecting transmitted signals. The probability of the VRs of $|\mathcal{S}_t|$ UEs in (A.4) not overlapping, given

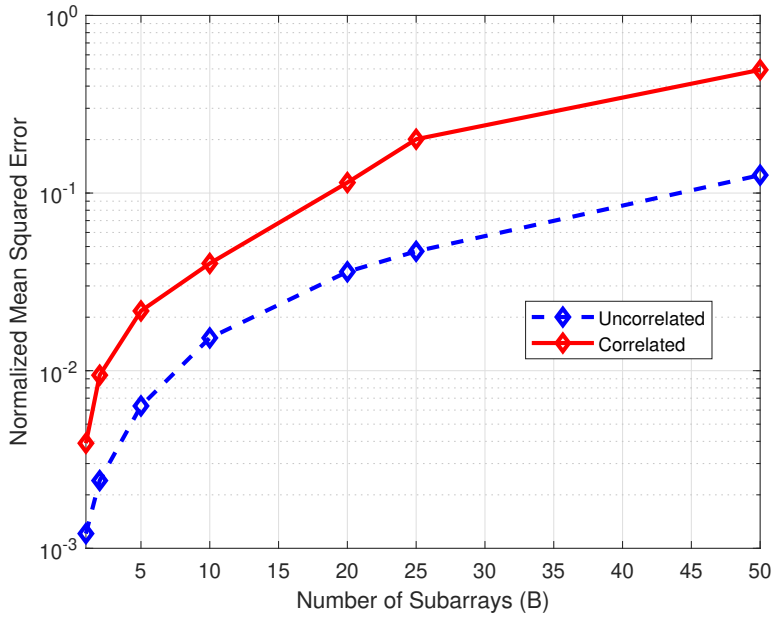

Figure A.3 – NMSE *vs.* the number of subarrays (B) to verify the α_t estimation for the correlated and uncorrelated Rayleigh fading models for the SUCRe-XL protocol. All SAs are considered visible ($P_b = 1$).

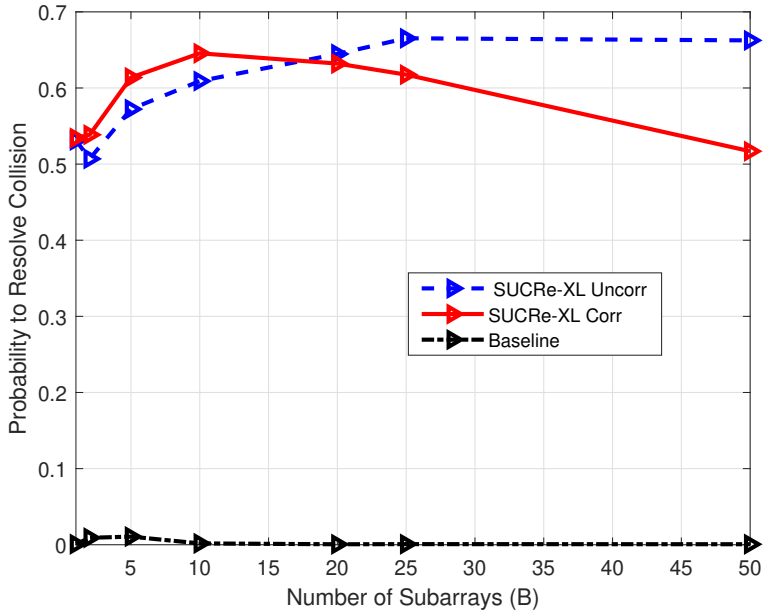

Figure A.4 – PRC *vs.* the number of subarrays (B) for the SUCRe-XL and Baseline ($K = 1000$ iUEs).

by

$$P_{no} = ((1 - P_b)^{|\mathcal{S}_t|} + |\mathcal{S}_t| P_b (1 - P_b)^{|\mathcal{S}_t|-1})^B, \tag{A.22}$$

decreases with increasing B and/or P_b. Thus, decreasing P_b causes $|\mathcal{V}_k| \; \forall \; k$ to diminish at the BS side. Hence, the probability of pilot collisions in overlapping areas reduces when probability P_b decreases, improving the SUCRe-XL PRC for $B = 20$, as well for the Baseline performance. However, this could not be seen for the the SUCRe-XL for $B = 5$, since the effect of the imposed constraint [1] $|\mathcal{V}_k| \geq 1$ is more noticeable when $P_b \leq 1/B$. Thus, when decreasing P_b below the threshold $1/B$, the expected value of visible subarrays would decrease below 1, in such a way that the additional constraint $|\mathcal{V}_k| \geq 1$ turns to intervene more frequently, breaking the trend of the presented result in increasing the PRC with the decrease of P_b, as expected according to the P_{no} expression. Besides, this does not occur for $B = 1$ (stationary case), since the only SA existent is the entire linear array. Furthermore, the Baseline success probability grows abruptly comparing with the proposed protocol with P_b reduction. This behavior might come from non-overlapping cases, when the decision rule would be unnecessary: the Baseline recognizes non-overlapping pilot collisions as successful attempts, while UEs in the SUCRe-XL protocol still have to decide to repeat the RA pilot, even when they are not overlapping.

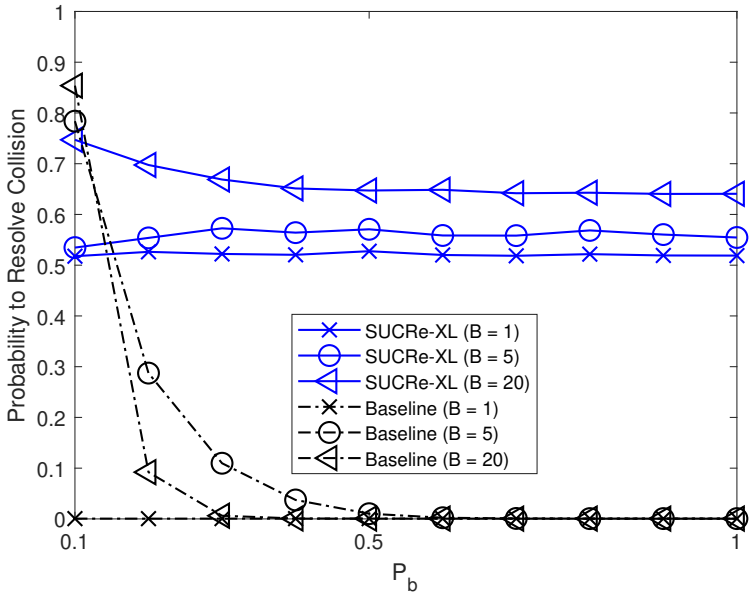

Figure A.5 – PRC *vs.* the Bernoulli probability (P_b), which determines the VRs. It is considered the uncorrelated Rayleigh fading model ($K = 1000$).

Average Number of Access Attempts. Numerical results in Fig. A.6 shows the average number of RA attempts as a function of the number of iUEs, for the stationary ($B = 1$) and non-stationary SUCRe-XL protocol. The fraction of UEs that could not access the network, *i.e.*, the portion that is unsuccessful in the maximum number of

[1] To avoid the possibility of a given user do not see any subarray, while the average number of visible subarrays per user follows $\mathbb{E}[|\mathcal{V}_k|] = B \cdot P_b$.

10 RA attempts, is illustrated in Fig. A.7. There is a clear advantage of SUCRe-XL in reducing the failed access attempts when exploiting the channel non-stationarity features, supporting a higher number of machine type UEs.

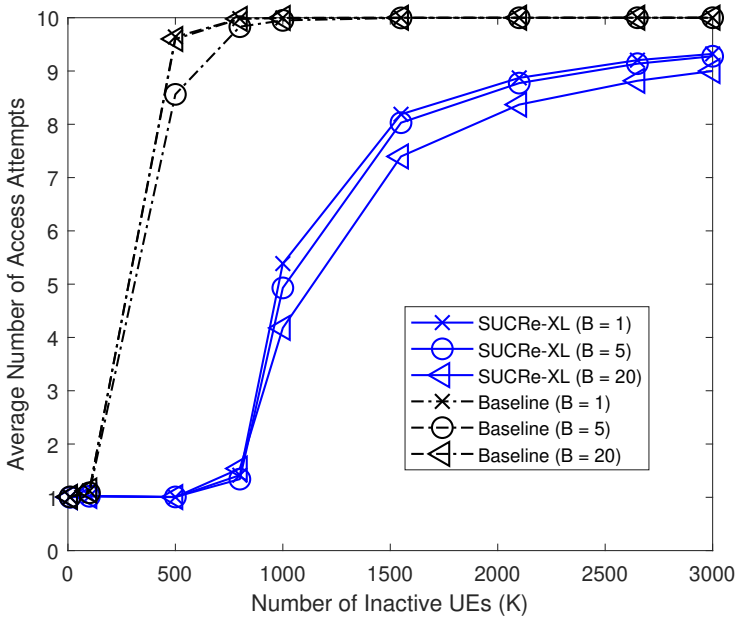

Figure A.6 – Average number of access attempts *vs.* the number of inactive UEs (K), for the SUCRe-XL and Baseline protocols for different numbers of subarrays (B), considering the uncorrelated Rayleigh fading model.

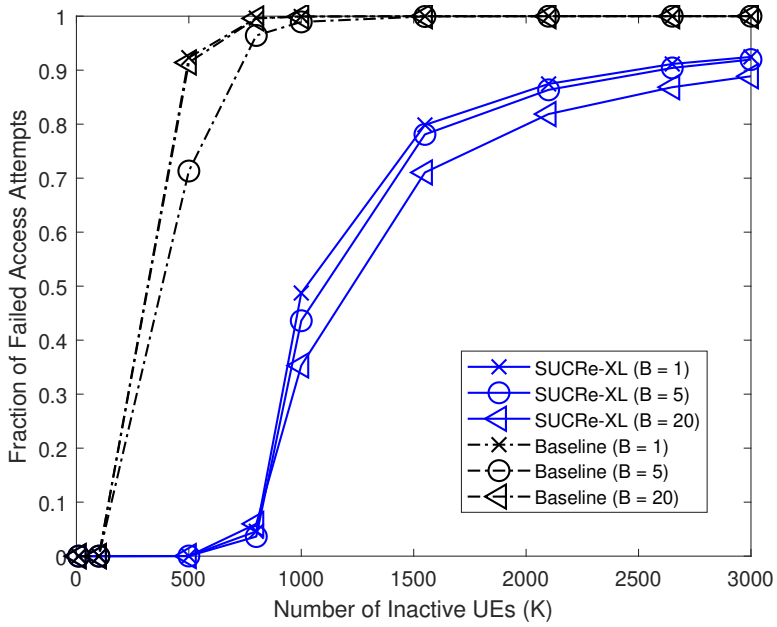

Figure A.7 – Probability of failed access attempt *vs.* the number of iUEs (K), for the SUCRe-XL and Baseline protocols for different numbers of subarrays (B), considering the uncorrelated Rayleigh fading model ($P_b = 0.5$).

Fig. A.8 presents the *average number of accepted UEs per resolved collision* (ξ), showing that ξ remains around one with increasing number of subarrays. Although ξ is

slightly higher for the Baseline scheme, the resolved collisions are much rarer in this simple scheme, as shown in Fig. A.4. In the same scenario, Fig. A.9 indicates the *normalized number of accepted UEs* (λ) that realized successful attempts. Hence, in average, the total number of admitted UEs along the 10^4 RA blocks is given by $\Lambda = \lambda \cdot K \cdot P_a \cdot 10^4$. Indeed, non-stationary cases surpasses the stationary one, specially in overcrowded mMTC scenarios, being able to manage a greater number of UEs. In addition, the fair approach provides a greater capability dealing with a larger number of inactive UEs.

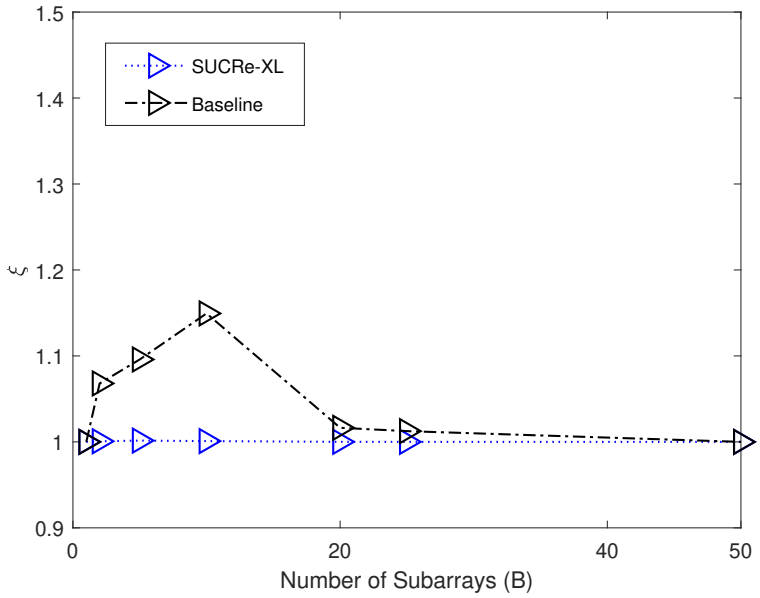

Figure A.8 – Average number of UEs per resolved collision (ξ) *vs.* the number of subarrays (B), for the SUCRe-XL and Baseline protocols, considering the uncorrelated Rayleigh fading model.

A.5 Final Remarks

Grant-based RA operating under massive extra-large ULA has demonstrated satisfactory performance to handle multiple access attempts under (over)crowded scenarios, typically present in cMMB. Additionally, the conventional SUCRe protocol is one promising method to manage these crowded scenarios in massive MIMO systems, already with many extensions and developments. Furthermore, XL-MIMO is a promising concept to surpass the performance of conventional antenna arrangements. These extra-large arrays are also predicted to provide low cost materials, keeping low energy consumption and computational complexity. Hence, to take advantage of channel non-stationarities, adapted SUCRe protocols for XL-MIMO has been proposed and compared. Numerical results show that the proposed protocol can support a higher number of active UEs, since it attains a reduced fraction of failed access attempts and reduced access latency. Besides,

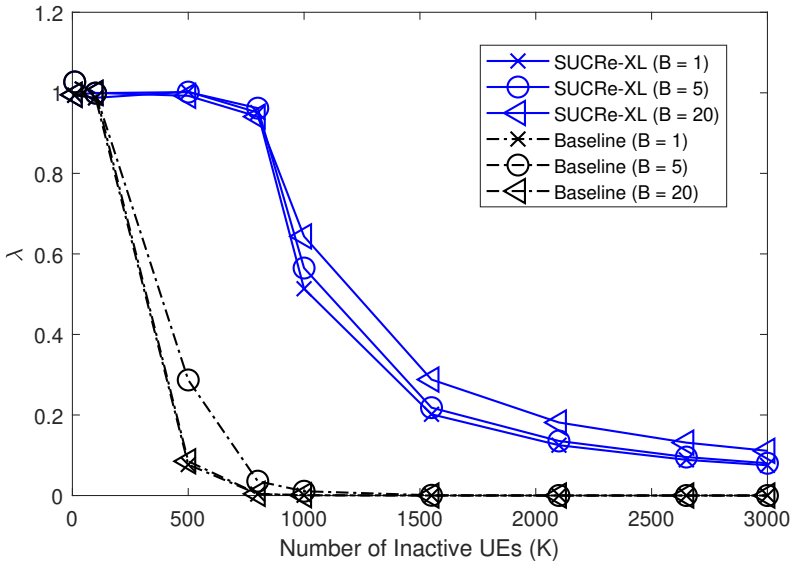

Figure A.9 – Normalized number of accepted UEs (λ) *vs.* the number of inactive UEs (K) for different numbers of subarray (B), for the SUCRe-XL and Baseline protocols, considering the uncorrelated Rayleigh fading model ($P_b = 0.5$).

the SUCRe-XL still provide the uncoordinated and decentralized features of the original technique, not significantly increasing computational complexity.

APPENDIX B – Improving Fairness of a Grant-Based Random Access Protocol for Extra-Large Massive MIMO Systems

Otávio Seidi Nishimura, José Carlos Marinello Filho, Taufik Abrão, Richard Demo Souza

Abstract

This paper focuses on conceiving a random access (RA) protocol able to provide connection for a very large number of devices covered by a uniform linear/planar array (ULA/UPA) in an extra-large massive multiple-input multiple-output (XL-MIMO) system at the base station (BS). Recently, the strongest user collision resolution (SUCRe) protocol has been adapted to the XL-MIMO scenario, in the so called SUCRe-XL protocol. However, the protocol has a bias, since devices closer to the BS are favored in detriment of the farther ones. This leads to a poor connectivity performance and excessive access delays to most users which are not very close to the BS, as we show herein. In this letter, we propose a fairer RA protocol to the XL-MIMO scenario, namely the access class barring with power control (ACBPC) protocol. Exploring the visibility regions (VRs) which naturally arise in XL-MIMO scenarios as a new degree of freedom, the proposed grant-based RA protocol can improve the probability of resolving pilot collisions. Numerical results indicate that the proposed ACBPC-XL protocol is able to manage a higher number of users, diminishing the access delay while improving fairness along the entire cell, since the achieved connectivity performance does not depend on the distance between users and BS. Typical XL-MIMO scenarios indicate that $\approx 85\%$ of users have their RA performance improved when employing the ACBPC-XL instead of SUCRe-XL protocol.

Keywords: Random access protocol, grant-based protocols, massive MIMO, XL-MIMO, non-stationarity, visibility region (VR), fairness, ACBPC.

B.1 Introduction

Fundamental services within the fifth generation of wireless networks (5G), as massive Machine Type Communication (mMTC) and crowded Mobile Broadband (cMBB) use cases, demand a highly efficient procedures to deal with massive user equipment (UE) access attempts (Fallgren; AL, 2013). In such scenarios, it is usual that the number

of available pilot sequences is lower than the number of UEs. Therefore, implementing collision resolution protocols becomes essential to allow coherent communication.

One widely-known grant-based random access (RA) protocol for crowded massive MIMO systems is the strongest user collision resolution (SUCRe) (Björnson et al., 2017). The protocol resolves RA pilot collisions by selecting the UE with the strongest signal gain to repeat its pilot, in a completely decentralized and uncoordinated fashion. However, SUCRe is selective non-uniform treatment to provide user access, offering, a higher connection probability for UEs near the BS and lower chances for UEs located at the cell edge. To alleviate this problem, extensions of SUCRe protocol have been proposed (Marinello; Abrão, 2019; Marinello et al., 2020; Han et al., 2017a; Han et al., 2017b), for instance, a *soft SUCRe* version and an *access class barring with power control* (ACBPC) method were proposed in (Marinello; Abrão, 2019) and (Marinello et al., 2020), respectively. The first one only softens the average number of RA attempts along the cell, still bringing lower connection probabilities for UEs far from the BS, while (Marinello et al., 2020) provides *connectivity fairness* in a massive MIMO system, *i.e.*, uniform chances of connection for all UEs, independent of their distances to the BS equipped with hundreds of antennas.

Massive multiple-input multiple-output(MIMO) techniques can be successfully used to improve the performance of random access (RA) in such crowded networks (Björnson et al., 2017; Marinello et al., 2020; Han et al., 2017a; Han et al., 2017b; Marinello; Abrão, 2019). Indeed the seminal work was explored in strongest-user collision resolution (SUCRe) protocol (Björnson et al., 2017), where the intrinsic properties of favorable propagation in massive MIMO allows exploration of a distributed RA solution that is able to resolve up to 90% of collisions, while serving a large number of users.

The SUCRe variants (Han et al., 2017a; Han et al., 2017b; Marinello; Abrão, 2019) following the same structure of the original SUCRe, composed by four steps. In the first step the UEs transmit pilots randomly selected. In SUCRe concept, only the UE with the larger average channel gain (*strongest* UE) in a collision is allowed access to the select pilot and retransmits it in the third step. The other UEs in the collision wait until the next access attempt. In another SUCRe variant, the SUCRe protocol is combined with the idea of idle pilots access (SUCR-IPA) (Han et al., 2017a); hence, the BS detects the set of pilots that are unused in step 1 and transmits their indices with an access class barring (ACB) factor in the second step, hence creating an opportunity for the weakest UEs to access those unused pilots in the third step. SUCR-IPA outperforms the original SUCRe at the cost of increased control overhead. Besides, the SUCRe combined with graph-based pilot access (SUCR-GBPA) (Han et al., 2017b) also announces the indices of non-used pilots in the second step, but not an ACB factor. Then, those UEs not apt to transmit data with the original selected pilot, randomly select another from the non-used pilots broadcasted by the BS. A bipartite graph can be constructed by setting the active UEs as the variable nodes and the chosen pilots as the factor nodes. A successive interference

cancellation (SIC) is used to estimate the channel of each UE.

Deploying the idea of retransmission probability, a soft decision rule for SUCRe in overcrowded scenarios is developed in (Marinello; Abrão, 2019). A retransmission from the k-th UE depends on the probability of it being the strongest contender for a pilot. The UE is able to compute this probability itself by knowing some parameters of the network, like the path-loss exponent and the number of inactive UEs in the cell. Such soft SUCRe variant achieves a better RA performance in terms of average number of access attempts and probability of failed access attempts than original SUCRe protocol, without requiring additional coordination or centralized processing.

When a pilot collision occurs in SUCRe, the UEs that are closer to the BS, and therefore have the strongest channels, are favored in the collision resolution process. In the case of very crowded networks, this may considerably increase the probability of failed access attempts for the other UEs, leading to an unfair performance (Marinello et al., 2020). Notice that similar effects occurs with their variants SUCR-IPA, SUCR-GBPA, and *Soft*-SUCRe. This is a a direct consequence of selecting the *strongest* UE in the collision resolution process disregarding the distance of the UE to the BS (Han et al., 2017a; Han et al., 2017b; Marinello et al., 2020) and in the original SUCRe (Björnson et al., 2017).

Against these previous scenario, herein, we have considered a new MIMO system configuration, with extreme large number of antennas at BS, typically thousands of antennas, characterized by the spatial non-stationaries and the respective visibility regions (Martinez et al., 2016; Carvalho et al., 2020). Massive MIMO is a reality and although its performance is already mature and several pieces of research have shown satisfactory performance. Traditional massive MIMO structures are usually compact, thus not presenting large dimensions., despite equipped with tens or even hundred of antennas. To bring better coverage and possibly enjoy other benefits, one can extend the array dimension to the extreme, increasing and distributing its thousand of antennas through an entire wall building. Hence, the BS can provide the essential massive MIMO properties, such as channel hardening, asymptotic favorable propagation, and high array gains in each sub-array defined by the respective visibility region of a UE, being a cost-efficient way to provide adequate signaling for extremely crowded scenarios.

Such method is the so called extra-large massive multiple-input multiple-output (XL-MIMO), a new concept where extremely large arrays are built in several types of infrastructures, such as buildings, stadiums, or shopping malls (Carvalho et al., 2020). The extreme large number of antennas and dimension of array cause near-field communication scenarios, where UEs present spatial non-stationaries, overlapping, and visibility regions (VRs). The *concept of VR* can be understood as a terminal geographical area; hence, when the terminal is located in such area, it sees a given set of clusters. There is a correspondence between set of clusters associated with a specific VR. As a result, when the moves out of the VR, it sees a different set of clusters. The VR concept also denotes a portion of

the array of a XL-MIMO from which a given set of clusters is visible. Finally, VRs can be distinguished from the point-of-view of the UE domain, and from the array domain (Martinez et al., 2016).

Due to the spherical propagation, different portions of the extra-large array experience distinct level of signals. Furthermore, different UEs have different scatterers and thus different VRs. Therefore, from the BS point of view, some sets of antennas may receive interference from several transmissions, where the overlapping event occurs. While other portions may receive non-overlapping signals. Fig B.1 depicts an overview of the XL-MIMO system scenario equipped with a uniform linear array (ULA) at the BS, and, where UEs experience one scatterer each, which causes different VRs at the BS, *i.e.*, the UEs may see distinct subarrays (SAs). Additionally, due to the obstacle, some SAs may not be visible by these UEs. How to efficiently exploit the VRs in such XL arrays domain aiming to improve RA is an open problem.

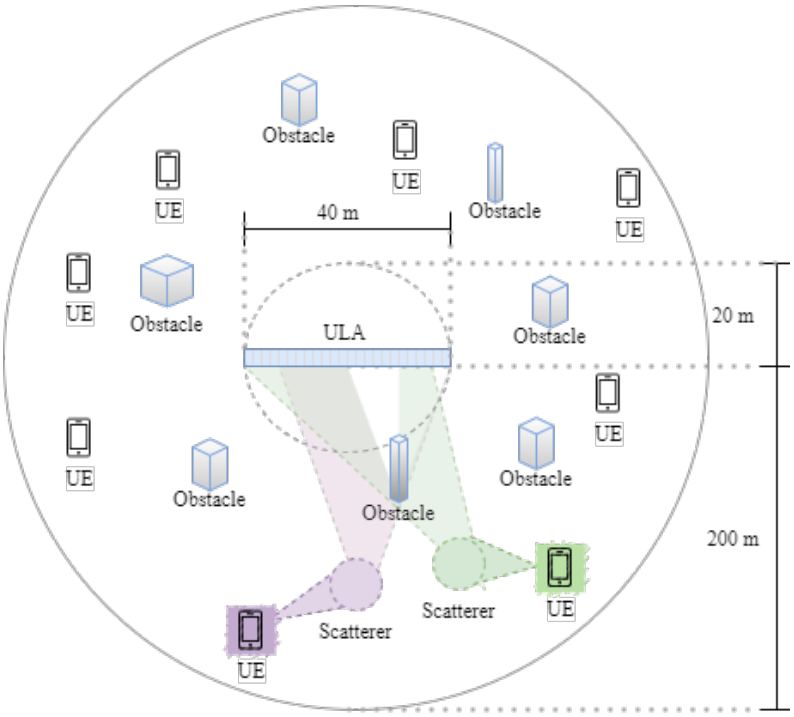

Figure B.1 – Crowded XL-MIMO scenario composed by an XL ULA and uniformly distributed UEs in a ring area $\pi \cdot (r_{ext}^2 - r_{int}^2)$ $[m^2]$, with their respective VRs. In our model, VRs at ULA are the result of non-line-of-sight (NLoS) propagation channels.

In (Nishimura et al., 2020), the grant-based SUCRe RA protocol has been extended to the XL-MIMO systems, in which the large array size and the proximity with the users give rise to spatial non-stationarities across the array. In such scenarios, it is possible to take advantage of distinct VRs from different UEs as an additional degree of freedom in order to improve the system performance, *i.e.*, increasing the probability of collision resolution and reduction of average number of access attempts, while reducing the latency

in the pilot allocation step.

Recently, the 3rd Generation Partnership Project (3GPP) finished its Release 16 with new features and improvements (3GPP, 2020). One important feature is the Two-step Random Access Channel (2-steps RACH), in contrast with the traditional 4-steps method. This enhancement has the purpose of reducing latency and optimize signal transmissions, hence, significantly shorting the overhead. Its functionality consists of the UE transmitting the UL preamble and the message in a single step, which would be the combination of steps 1 and 3 of the conventional 4-steps method. The second step is the DL message from the next-generation Node B (gNB), admitting the UE if the payload message were successfully decoded (3GPP, 2020).

For sake of simplicity, and due to a lack of XL-MIMO RA protocols available in the literature for comparison, in this work, we do not consider the 2-steps RACH approach introduced very recently in the 3GPP Release 16. As a consequence, in the numerical results section, we have opted to compare with a version of conventional SUCRe protocol adapted to the XL-MIMO system available in the recent literature (Nishimura et al., 2020). Notice that the SUCRe protocol and the majority of its extensions, operating in 4 steps, are well-known to be decentralized and uncoordinated, which brings lower computational complexity in the BS.

Contribution: A challenge for 5G and beyond systems is how conventional techniques can be adapted to new concepts such as ultra-reliability and very short end-to-end latency, and structures as XL arrays (BJÖRNSON et al., 2019). Against this background, this work proposes a novel ACBPC protocol specifically to operate in crowded XL-MIMO systems, namely the ACBPC-XL protocol. The main feature of the proposed protocol is to provide fair access alongside the entire cell area while reducing the RA delay as an alternative for the unfair approach of SUCRe-XL (Nishimura et al., 2020). Extending the traditional massive MIMO protocols to operate in a new XL array structures may result in unexpected behavior. This work aggregate comprehensive analyses to characterize such new behaviors, advantages, and drawbacks associated by such new XL-MIMO configuration and associated scenarios. The proposed XL arrays-based RA protocol explores the VRs advantageously as an additional degree of freedom for improving users' connectivity performance across the cell coverage in overcrowded extra-large MIMO scenarios, reducing the average access delay of edge users substantially. As a result, for typical crowded XL-MIMO scenarios, approximately 85% of the users have attained improved connectivity performance when employing the proposed ACBPC-XL protocol compared with SUCRe-XL.

The main differences compared to (Nishimura et al., 2020) lie in ***a***) the massive antenna regime, *i.e.* XL array defined by the spatial non-stationaries against stationary massive MIMO arrays; ***b***) in the Step 3 ("*ACB Distributed Contention Resolution and Pilot Repetition*") and Step 1 of the RA protocol; in Section B.3, Table B.1 depicts such differences and specifics of both protocols.

Notation: The conjugate, transpose and conjugate-transpose of a matrix $\mathbf{A}$ are represented by $\mathbf{A}^*$, $\mathbf{A}^T$ and $\mathbf{A}^H$, respectively. $\mathbf{I}_M$ is the $M \times M$ identity matrix, $|\cdot|$ and $\|\cdot\|$ represent the cardinality of a set and the Euclidean norm of a vector, respectively. $\mathcal{N}(.,.)$ denotes a Gaussian distribution, $\mathcal{CN}(.,.)$ represents a circularly-symmetric complex Gaussian distribution, and $\mathcal{B}(.,.)$ represents a binomial distribution. $\mathbb{C}$ denotes spaces of complex -valued numbers, while $\Gamma(\cdot)$ represents a Gamma function. The real part operator is $\Re(.)$.

B.2 System model

We consider an extra-large uniform linear array (ULA) at the BS, which operates in a time-division-duplexing (TDD) method. In the considered simplified bipartite graph model, as in (Amiri et al., 2018), the array is divided into B subarrays (SAs), each with $M_b = M/B$ antennas. Let $\mathcal{M}$ be the set of SAs and $\mathcal{V}_k \subset \mathcal{M}$ the subset of SAs visible to UE k. The subset $\mathcal{V}_k$ is generated at random, where each SA is visible with probability P_b by UE k. This probability reproduces the effect of random obstacles in the environment, blocking the VRs. The subset of SAs visible to each UE are assumed to be independent from each other. For simulation purposes, $|\mathcal{V}_k| > 0,\ \forall\ k$.

Let $\mathcal{U}$ be the set of UEs in the cell, $\mathcal{A} \subset \mathcal{U}$ the active UEs, where each UE has its dedicated pilot, and $\mathcal{K} = \mathcal{U} \backslash \mathcal{A}$ the inactive UEs (iUEs), where UEs do not have dedicated pilots and need to be assigned if they want to be active. Hence, $K = |\mathcal{K}|$ is the number of iUEs in the cell. We define τ_p as the number of available RA pilot sequences $\boldsymbol{s}_1, ..., \boldsymbol{s}_{\tau_p} \in \mathbb{C}^{\tau_p \times 1}$. Each pilot has length τ_p and $\|\boldsymbol{s}_t\|^2 = \tau_p$, since we are considering mutually orthogonal pilot sequences.

The large scale fading models a urban micro scenario (3rd Generation Partnership Project, 2018),

$$\beta_{k,m}^{(b)} = 10^{-\kappa \log(d_{k,m}^{(b)}) + \frac{g+\varphi}{10}}, \tag{B.1}$$

where $d_{k,m}^{(b)}$ is the distance between UE k and antenna m ($m = 1, ..., M_b$) of SA b, $\varphi \sim \mathcal{N}(0, \sigma_{sf}^2)$ is the shadow fading, with standard deviation $\sigma_{sf} = 10$ dB, $\kappa = 3.8$ is the pathloss exponent, and $g = -34.53$ dB is the pathloss at the reference distance. As in (Nishimura et al., 2020), we adopt the simplification $\beta_k^{(b)} = \frac{1}{M_b} \sum_{m=1}^{M_b} \beta_{k,m}^{(b)}$, and $\beta_k^{(b)} = 0$ for blocked SAs. Moreover, let $\mathbf{h}_k^{(b)} \in \mathbb{C}^{M_b \times 1}$ be the Rayleigh fading channel vector between UE $k \in \mathcal{K}$ and SA b, where $\mathbf{h}_k^{(b)} \sim \mathcal{CN}(0, \beta_k^{(b)} \mathbf{I}_{M_b})$. Notice that all UEs are subject to pathloss and Rayleigh channel fading.

In the first step, all iUEs make a RA attempt with probability $P_a \leq 1$. Each UE chooses uniformly at random one RA pilot sequence $\boldsymbol{s}_t$, $t = 1, \ldots, \tau_p$, and transmits with power $\rho_k > 0$. Therefore, let $\mathcal{S}_t \in \mathcal{K}$ be the set of UEs indices that selected pilot t. As in

(Björnson et al., 2017), it follows that:

$$|\mathcal{S}_t| \sim \mathcal{B}\left(K, \frac{P_a}{\tau_p}\right). \tag{B.2}$$

Fig. B.2 depicts an arbitrary arrangement of VRs and the UL pilots with $K = 3$, $B = 4$, $\tau_p = 5$ and $P_a = 1$. Suppose, without loss of generality, that the SAs can be ordered left to right and UEs up to down. Hence, since all UEs selected the same RA pilot, collisions occur in SA 1, 3 and 4 between users 1-2, and 2-3, but no collisions between users 1-3.

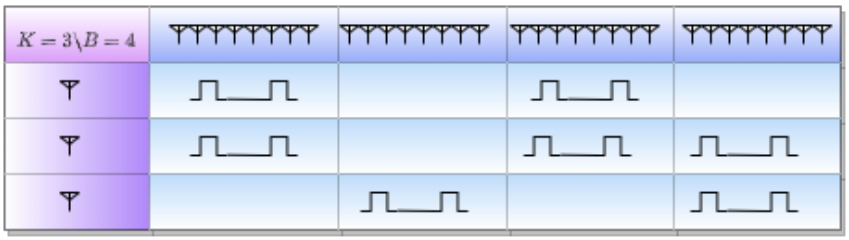

Figure B.2 – Arbitrary UL arrangement with $P_a = 1$, $K = 3$ UEs (single antennas), $M = 32$, $B = 4$ SAs ($M_b = 8$ antennas) and $\tau_p = 5$ available pilot sequences. In this example, all UEs selected the same RA pilot.

The conventional SUCRe protocol depends on massive MIMO properties:

$$\frac{\|\mathbf{h}_k^{(b)}\|^2}{M_b} \xrightarrow{M_b \to \infty} \beta_k^{(b)}, \quad \forall k, b \tag{B.3}$$

$$\frac{\mathbf{h}_k^{(b)H}\mathbf{h}_{k'}^{(b')}}{M_b} \xrightarrow{M_b \to \infty} 0, \quad \forall (k,b) \neq (k',b'). \tag{B.4}$$

From (B.3), in the XL-MIMO scenario we can assume

$$\sum_{j \in \mathcal{V}_k} \frac{\|\mathbf{h}_k^{(j)}\|^2}{M_b} \xrightarrow{M_b \to \infty} \sum_{j \in \mathcal{V}_k} \beta_k^{(j)}, \quad \forall k. \tag{B.5}$$

Notice that (B.5) is the total channel gain associated with UE k.

B.3 Proposed protocol

In this section, the proposed ACBPC-XL RA protocol is presented. The protocol steps are described in the sequel, and illustrated in Fig. B.3; also, the direction of uplink (UL) and downlink (DL) messages exchange are indicated.

***Step 1**: Random Pilot Sequence UL Transmission with Power Control.* Adapting from (Marinello et al., 2020), the transmit power of UE k is:

$$\rho_k^{pc} = \min\left\{\frac{\overline{\rho}}{\sum_{b \in \mathcal{V}_k} \beta_k^{(b)}}, \rho^{\max}\right\}, \tag{B.6}$$

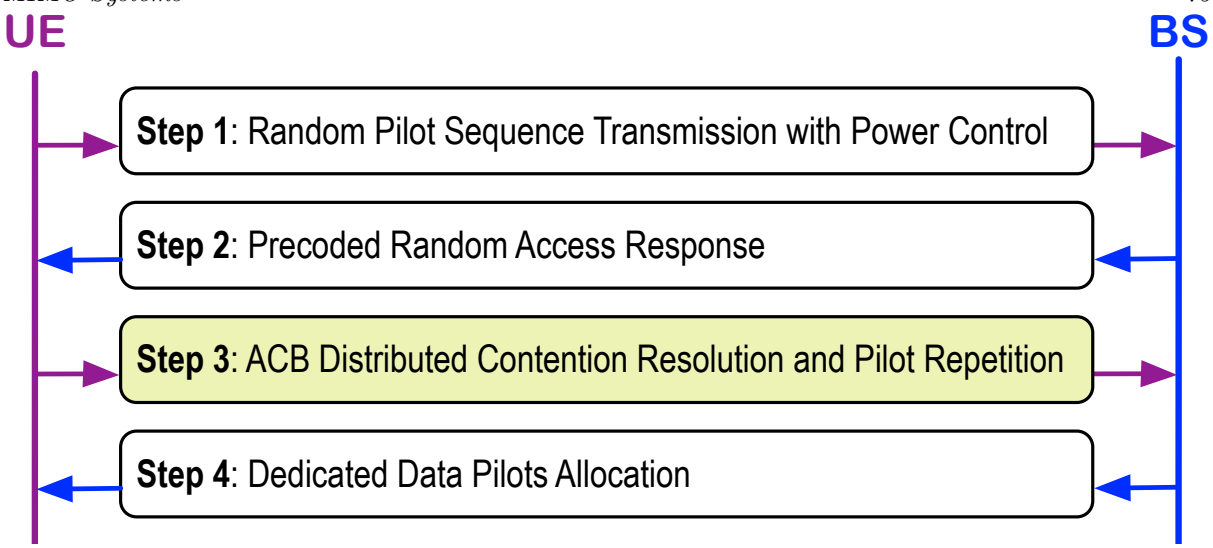

Figure B.3 – Diagram of the ACBPC-XL protocol; direction: UL (→) and DL (←)

where $\overline{\rho}$ is the average received power at the BS, and $\rho^{\max}$ is the the maximum transmit power available per user. With (B.6), inactive UEs that want to establish connection transmit RA UL pilot sequences, causing SA b to receive signal

$$\mathbf{Y}^{(b)} = \sum_{k\in\mathcal{K}} \sqrt{\rho_k^{pc}}\mathbf{h}_k^{(b)}\boldsymbol{s}_t^T + \mathbf{N}^{(b)}, \tag{B.7}$$

where $\mathbf{Y}^{(b)} \in \mathbb{C}^{M_b\times\tau_p}$, and $\mathbf{N}^{(b)} \in \mathbb{C}^{M_b\times\tau_p}$, with entries drawn from $\mathcal{CN}(0,\sigma^2)$, is the receiver noise. So each SA correlates (B.7) using an arbitrary normalized pilot $\boldsymbol{s}_t$, yielding

$$\mathbf{y}_t^{(b)} = \mathbf{Y}^{(b)}\frac{\boldsymbol{s}_t^*}{\|\boldsymbol{s}_t\|} = \sum_{i\in\mathcal{S}_t}\sqrt{\rho_i^{pc}\tau_p}\mathbf{h}_i^{(b)} + \mathbf{n}_t, \quad b = 1,\ldots,B \tag{B.8}$$

where $\mathbf{n}_t = \mathbf{N}\frac{\boldsymbol{s}_t^*}{\|\boldsymbol{s}_t\|}\mathbf{n}_t \sim \mathcal{CN}(0,\sigma^2\mathbf{I}_{M_b})$, is the effective receiver noise. From (B.3) and (B.4), the following holds (Nishimura et al., 2020):

$$\frac{\|\sum_{b\in\mathcal{M}}\mathbf{y}_t^{(b)}\|^2}{M_b} \xrightarrow{M_b\to\infty} \underbrace{\sum_{b\in\mathcal{M}}\sum_{i\in\mathcal{S}_t}\rho_i^{pc}\beta_i^{(b)}\tau_p}_{\alpha_t} + B\sigma^2. \tag{B.9}$$

Property (B.9) allows UEs $i \in \mathcal{S}_t$ to estimate α_t, which is the *sum of signal gains* associated with pilot t.

***Step 2**: Precoded Random Access DL Response.* SAs generate a precoded DL pilot,

$$\mathbf{V}_{\text{XL}} = \sqrt{\frac{q}{B}}\sum_{t=1}^{\tau_p}\frac{\sum_{b\in\mathcal{M}}\mathbf{y}_t^{(b)*}}{\|\sum_{b\in\mathcal{M}}\mathbf{y}_t^{(b)}\|}\boldsymbol{s}_t^H. \tag{B.10}$$

where $\mathbf{V}_{\text{XL}} \in \mathbb{C}^{M_b\times\tau_p}$ and q is the BS transmit power. In this case, UEs in $\mathcal{S}_t$ receive signal $\mathbf{z}_k^T \in \mathbb{C}^{1\times\tau_p}$ in the reciprocal channel with receiver noise $\boldsymbol{\eta}_k \sim \mathcal{CN}(0,\sigma^2\mathbf{I}_{\tau_p})$,

$$\mathbf{z}_k^T = \sum_{m\in\mathcal{V}_k}\mathbf{h}_k^{(m)T}\mathbf{V}_{\text{XL}} + \boldsymbol{\eta}_k^T. \tag{B.11}$$

From (B.11), each UE correlates the signal with its RA pilot $\boldsymbol{s}_t$,

$$z_k = \mathbf{z}_k^T \frac{\boldsymbol{s}_t}{\|\boldsymbol{s}_t\|} = \sqrt{\frac{q\tau_p}{B}} \sum_{m\in\mathcal{V}_k} \mathbf{h}_k^{(m)T} \frac{\sum_{b\in\mathcal{M}} \mathbf{y}_t^{(b)*}}{\|\sum_{b\in\mathcal{M}} \mathbf{y}_t^{(b)}\|} + \eta_k, \tag{B.12}$$

where $\eta_k = \boldsymbol{\eta}_k^T \frac{\boldsymbol{s}_t}{\|\boldsymbol{s}_t\|} \sim \mathcal{CN}(0, \sigma^2)$ is the effective receiver noise. To obtain (B.9) at the UE side, we divide (B.12) by $\sqrt{M_b}$ and consider properties (B.3) and (B.4):

$$\begin{aligned}\frac{z_k}{\sqrt{M_b}} &= \sqrt{\frac{q\tau_p}{B}} \frac{\left(\sum\limits_{m\in\mathcal{V}_k} \mathbf{h}_k^{(m)H} \sum\limits_{b\in\mathcal{M}} \mathbf{y}_t^{(b)}\right)^*}{M_b \sqrt{\frac{1}{M_b}\left\|\sum\limits_{b\in\mathcal{M}} \mathbf{y}_t^{(b)}\right\|^2}} + \frac{\eta_k}{\sqrt{M_b}} \\ &\xrightarrow{M_b\to\infty} \tau_p \sqrt{\frac{q\rho_k^{pc}}{B}} \frac{\sum\limits_{m\in\mathcal{V}_k} \beta_k^{(m)}}{\sqrt{\sum\limits_{b\in\mathcal{M}} \sum\limits_{i\in\mathcal{S}_t} \rho_i^{pc} \beta_i^{(b)} \tau_p + B\sigma^2}}.\end{aligned} \tag{B.13}$$

Taking $\Re(z_k)$ can mitigate noise and estimation errors:

$$\frac{\Re(z_k)}{\sqrt{M_b}} \approx \tau_p \sqrt{\frac{q\rho_k^{pc}}{B}} \frac{\sum\limits_{m\in\mathcal{V}_k} \beta_k^{(m)}}{\sqrt{\alpha_t + B\sigma^2}}. \tag{B.14}$$

Thus, UEs in $\mathcal{S}_t$ are now able to estimate α_t. Considering (Björnson et al., 2017) and similarly to (Nishimura et al., 2020), for ACBPC-XL the estimator is:

$$\begin{aligned}\widehat{\alpha}_{t,k} = \max \Bigg[&\rho_k^{pc} \sum_{m\in\mathcal{V}_k} \beta_k^{(m)} \tau_p \,, \\ &\left(\frac{\Gamma(M_b + 1/2)}{\Gamma(M_b)}\right)^2 \frac{\rho_k^{pc} q \tau_p^2 \left(\sum_{m\in\mathcal{V}_k} \beta_k^{(m)}\right)^2}{B[\Re(z_k)]^2} - B\sigma^2 \Bigg].\end{aligned} \tag{B.15}$$

Step 3*: ACB Distributed Contention Resolution and Pilot Repetition.* Due to (B.6), the *sum of the signal gains* is:

$$\alpha_t = \sum_{i\in\mathcal{S}_t} \left(\rho_i^{pc} \sum_{b\in\mathcal{V}_i} \beta_i^{(b)} \tau_p \right) = \overline{\rho} \tau_p |\mathcal{S}_t|. \tag{B.16}$$

Notice that the last equality in (B.16) is not true when $\rho_i^{pc} = \rho^{\max}$ for some UE. However, as stated in (Marinello et al., 2020), these cases are very rare and do not impact performance significantly. To exemplify, in Fig. B.4, is evaluated the a probability of $\rho^{pc} = \rho^{\max}$ for several numbers of inactive UEs (K) and SAs (B). This probability remains in $\approx 0\%$ in all cases, guaranteeing that the proposed protocol operates as expected when the power control policy introduced in eq. (B.6) is adopted.

Now, substituting ρ_k^{pc} in (B.15), each UE can take an estimate of the number of the contending UEs using pilot t:

$$|\widehat{\mathcal{S}_t}|_k = \frac{\widehat{\alpha}_{t,k}}{\overline{\rho}\tau_p}. \tag{B.17}$$

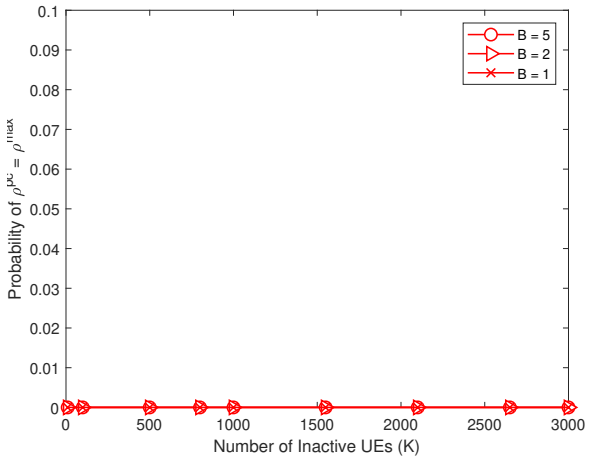

Figure B.4 – Probability of $\rho^{pc} = \rho^{\max}$ for different numbers of inactive UEs (K) and SAs (B).

Then, we define an ACB factor $\zeta_k = |\widehat{\mathcal{S}}_t|_k^{-1}$, where the kth UE makes a decision with probability ζ_k instead of using the decision rule defined in (Nishimura et al., 2020).

Step 4*: Allocation of Dedicated Data Pilots.* Finally, the BS defines four possible contention cases: ***i***) Non-overlapping UEs win (false positive), as for instance in Fig. B.2 users 1 and 3 win; ***ii***) Only one UE wins; ***iii***) None of the UEs win (false negative); ***iv***) Overlapping UEs win (false positive), as for example in Fig. B.2, users 1 and 2 or 2 and 3 win.

For cases ***i*** and ***ii*** above, and taking into account the obtained channel estimates, the BS tries to decode the message sent in Step 3, containing the user identifier. If the decoding is successful, it is an indication that the channel estimate is not contaminated, with no collision in step 3. A successful RA attempt is thus detected with the subsequent allocation of the dedicated payload pilots for the non-overlapping winners. Unsuccessful UEs need to try again after a random backoff.

B.3.1 Computational complexity and differences with SUCRe-XL

Regarding the SUCRe-XL (Nishimura et al., 2020), the computational complexity increasing from the proposed ACBPC-XL protocol is not significant. Table B.1 presents a brief description of the complexity and differences of both protocols, for the UE and the BS sides. UEs need to compute (B.6) to obtain the transmit power, generate a uniformly-distributed random number, and compare it with ζ_k to evaluate the ACBPC retransmission criterion. The main differences from (Marinello; Abrão, 2019) and (Marinello et al., 2020) are that, in the proposed scheme: ***i***) the kth UE transmit power is calculated by (B.6) to attain maximum fairness across all users in XL-MIMO scenarios; ***ii***) the decision rule for retransmission in Step 3 is substantially modified.

Notice that increasing the number of SAs (B), the number of antennas per SA (M_b) reduces, which degrades both protocols' connectivity performance. As analysed in section

Table B.1 – Differences and associated steps' complexities for the ACBPC-XL against SUCRe-XL protocols at the UE and BS side.

XL protocol	**At the UE**	**At the BS**
ACBPC-XL	Step 1: UE k selects an RA pilot and realizes the eq. (B.6), computing $\lvert\mathcal{V}_k\rvert$ summations, a multiplication and a comparison. Step 3: UE k calculates eq. (B.12), eq. (B.15), eq. (B.17), generates a random number and realizes a comparison.	Step 2: the BS calculates eq. (B.8) B times and eq. (B.10). Step 4: the BS verifies which that consider themselves winners, are not overlapping and allocates the payload data pilots.
SUCRe-XL (Nishimura et al., 2020)	Step 1: UE k selects an RA pilot. Step 3: UE k calculates eq. (B.12), eq. (B.15), realizes a comparison, 3 multiplications and $\lvert\mathcal{V}_k\rvert + 1$ summations, considering the bias term (Nishimura et al., 2020).	

B.4, the proposed ACBPC-XL presents satisfying collision resolution probability and the average number of access attempts for small numbers of SAs in (over)crowded scenarios.

B.4 Numerical results

We assume a circular cell with internal and external radius of 20 m and 200 m, respectively, where K iUEs in a crowded scenario ($K > M$) are distributed uniformly, as in Fig. B.1. Each UE becomes active with probability $P_a = 0.01$, randomly choosing one RA pilot out of $\tau_p = 10$ available. The BS is a ULA located in the center of the cell with $M = 400$ antennas uniformly spaced in a 40 m length, and divided into B SAs, each visible with probability $P_b = 0.5$. It is adopted $\bar{\rho} = \sigma^2$, which can be easily informed to all UEs, and $q = \rho^{\max} = \rho^{\text{SUCRe-XL}} = 1$ W to guarantee that the transmit power of UEs using ACBPC-XL do not surpass that used in SUCRe-XL.

A baseline performance is added for comparison in the following simulation. This baseline is an ALOHA-like protocol that resolves pilot collisions by instructing contending UEs to retransmit RA pilots after a random backoff time (Björnson et al., 2017). Nevertheless, to make a fair comparison, this baseline also takes advantage of the spatial non-stationarity feature provided by the XL-MIMO scenarios. Thus, cases where non-overlapping visibility regions from distinct inactive UEs that eventually selected the same RA pilot, and are realizing an access attempt, are considered successful (free of collision condition).

Simulations are generated in sequential RA blocks, which are represented by 10^4 Monte Carlo realizations. In each round, new iUEs carry out an access attempt following (B.2). UEs that failed at the first attempt retransmit their RA pilots with probability 0.5

in the next blocks. It is considered a failed access attempt if a UE do not succeed after 9 retransmissions.

The ***Probability to Resolve Collision*** (PRC) is calculated as the total number of resolved collisions per total number of occurred collisions. Fig. B.5 presents the PRC for the three protocols. SUCRe-XL and ACBPC-XL obtain beneficial effects of spatial non-stationarities when the number of SA's (B) increases, taking *Case* ***i*** from *Step 4* as an advantage. However, the occurrence of *Case* ***i*** where more than one UE is accepted per resolved collision becomes rare when B grows. That is because the probability of all contending UEs not presenting overlapping VRs (Nishimura et al., 2020), given by:

$$P_{no} = ((1 - P_b)^{|\mathcal{S}_t|} + |\mathcal{S}_t| P_b (1 - P_b)^{|\mathcal{S}_t|-1})^B, \tag{B.18}$$

decreases with B. This effect is explored in more details later in Fig. B.8, where only the ACBPC-XL protocol takes advantage of more than one accepted UE per resolved collision. Since the number of antennas per SA follows the ratio $M_b = M/B$, massive MIMO properties[1] also degrade with the increasing number of SAs. In such situation, the ACBPC-XL protocol is more affected negatively. However, ACBPC-XL outperforms SUCRE-XL in all scenarios considered in Fig. A.4, with a maximum percentual PRC advantage at $B = 2$ SAs of $\approx 12.3\%$ when $K = 1000$, and increases to $\approx 22.1\%$when overcrowded scenarios arise, *i.e.,* $K = 2000$ iUEs. In this first metric, $M = 800$ antennas have been adopted aiming to suitably demonstrate how the ACBPC-XL PRC surpasses the SUCRe-XL protocol at a favorable system scenario configuration. Besides, the baseline ALOHA-like performance remains around zero for the considered number of iUEs. Therefore, we ignore its low performance in the following numerical simulations.

The ***Average Number of Access Attempts*** (ANAA) performance metric is depicted in Fig. B.6(a), which confirms the ACBPC-XL advantage for reduced $B = 2$ and 5 SAs, in overcrowded scenarios *i.e.*, when $K \geq 1000$ iUEs. Besides, Fig. B.6(b) shows the same behavior for ***Fraction of Failed Access Attempts*** metric, meaning the probability that UEs fail to establish connection for different numbers of iUEs. Elaborating further, Fig. B.6(a) shows that with $K = 1500$ iUEs, the ANAA reduces from 8.6 attempts for SUCRe-XL to 7.4 attempts under ACBPC-XL for $B = 2$, representing a reduction of 14%. This gain leads to a significant access delay reduction, as well as transmit power savings in the initial RA steps. At the same circumstances for $B = 2$, Fig. B.6(b) presents a reduction of $\approx 18\%$ in terms of failed access.

Fig. B.7 also displays the ANAA, but with respect to the distance between the UEs and the BS, considering four crowded scenarios: (a) $K = 900$, (b) $K = 1000$, (c) $K = 2000$, and (d) $K = 2600$ iUEs. The figure highlights the unfair behavior of SUCRe-XL, since the ANAA performance of UEs not very close to the BS degrades rapidly. On the other hand, ACBPC-XL successfully attains connectivity fairness, maintaining almost equal

[1]Channel hardening and favorable propagation.

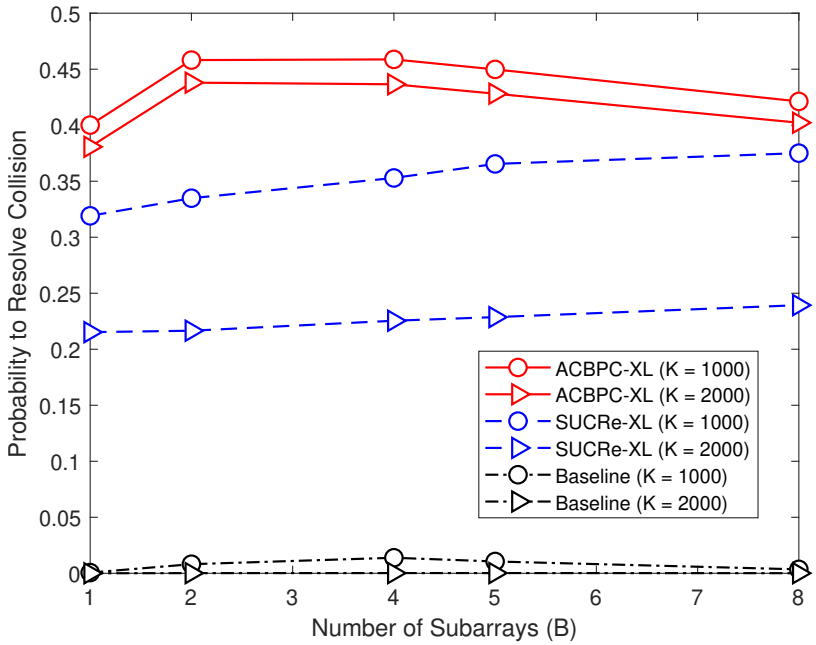

Figure B.5 – PRC for ACBPC-XL, SUCRe-XL and Baseline, $M = 800$ antennas.

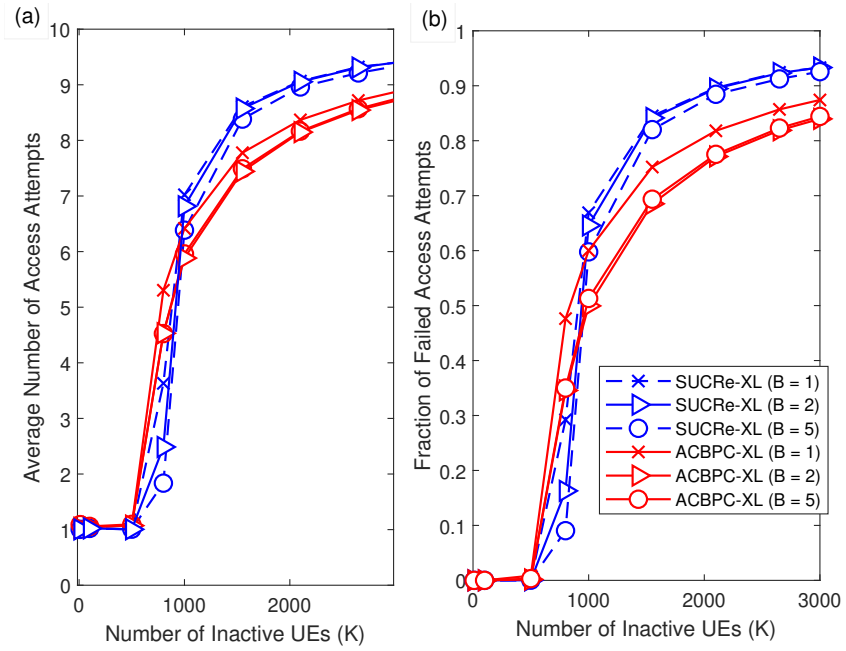

Figure B.6 – ACBPC-XL and SUCRe-XL performance. (a) Average Number of Access Attempts *vs.* number of iUEs (K). (b) Fraction of failed access attempts for different numbers of iUEs.

connection chances across the cell in all scenarios. Although ACBPC-XL curves shift up when K grows, due to the scarcity of RA pilots, the proposed ACBPC-XL protocol clearly results in advantage for most users. One may judge the high portion of negatively affected UEs closer to the BS when the number of iUEs is lower. This may be a disadvantage of the ACBPC-XL concerning the SUCRe-XL protocol if the main focus of the considered scenario is ultra-low latency. However, in the non-crowded scenario ($K = 900$), both protocols have satisfactory results, successfully managing $\approx 100\%$ of access attempts as shown in Fig. B.6.

Table B.2 presents the ANAA performance crossing points of ACBPC-XL over the SUCRe-XL protocol, obtained from Fig. B.7. When K grows to 2600 iUEs, ACBPC-XL can benefit $\approx 90\%$ of UEs comparing to the SUCRe-XL protocol, due to the crossing point of ≈ 65 m. In contrast, although increasing B may decrease delay access in overcrowded scenarios (Fig. B.6), it slightly decreases the portion of benefited UEs. As depicted in Fig. B.5 and Table B.2, the proposed protocol is advantageous only for small number of subarrays $B \in [1; 5]$, *i.e.*, configuration in which massive MIMO properties hold for M_b.

Table B.2 – Distance [meters] and % of Benefited Users when the ANAA metric for ACBPC-XL becomes smaller than SUCRe-XL, Fig.B.7.

B	**1**		**2**		**5**	
$K = 900$	119	65%	120	65%	140	52%
$K = 1000$	108	72%	115	68%	120	65%
$K = 2000$	70	89%	75	87%	80	85%
$K = 2600$	63	91%	65	90%	70	89%

Fig. B.8(a) presents the ***Success Probability*** versus P_b, for $K = 1000$ iUEs. Since P_b determines the probability of a SA being visible and considering the constraint $|\mathcal{V}_k| > 0$, the variation of P_b does not affect the success probability for stationary cases ($B = 1$). Furthermore, in non-stationary conditions ($B = 2,\ 5$), it is intuitive to expect reduced pilot collisions along the array as P_b decreases. This is confirmed in Fig. B.8(a) for ACBPC-XL, which has its success probability improved at lower values of P_b. In contrast, the cases with unique retransmitting UEs are more frequent for SUCRe-XL, due to its user retransmission criterion, which rarely results in false positives. ACBPC-XL leads to more cases of two or more UEs repeating their pilots, taking advantage of non-overlapping VRs. To support this claim, Fig. B.8(b) presents the ***Average Number of Accepted UEs per Resolved Collision*** (ξ) for different numbers of SAs (B). Notice that the SUCRe-XL protocol attains $\xi = 1$ in all cases, different from ACBPC-XL.

B.5 Final Remarks

Random access combined to massive number of antennas is a key technique to fulfill 5G massive MIMO systems requirements. New concepts and challenges appear with recent

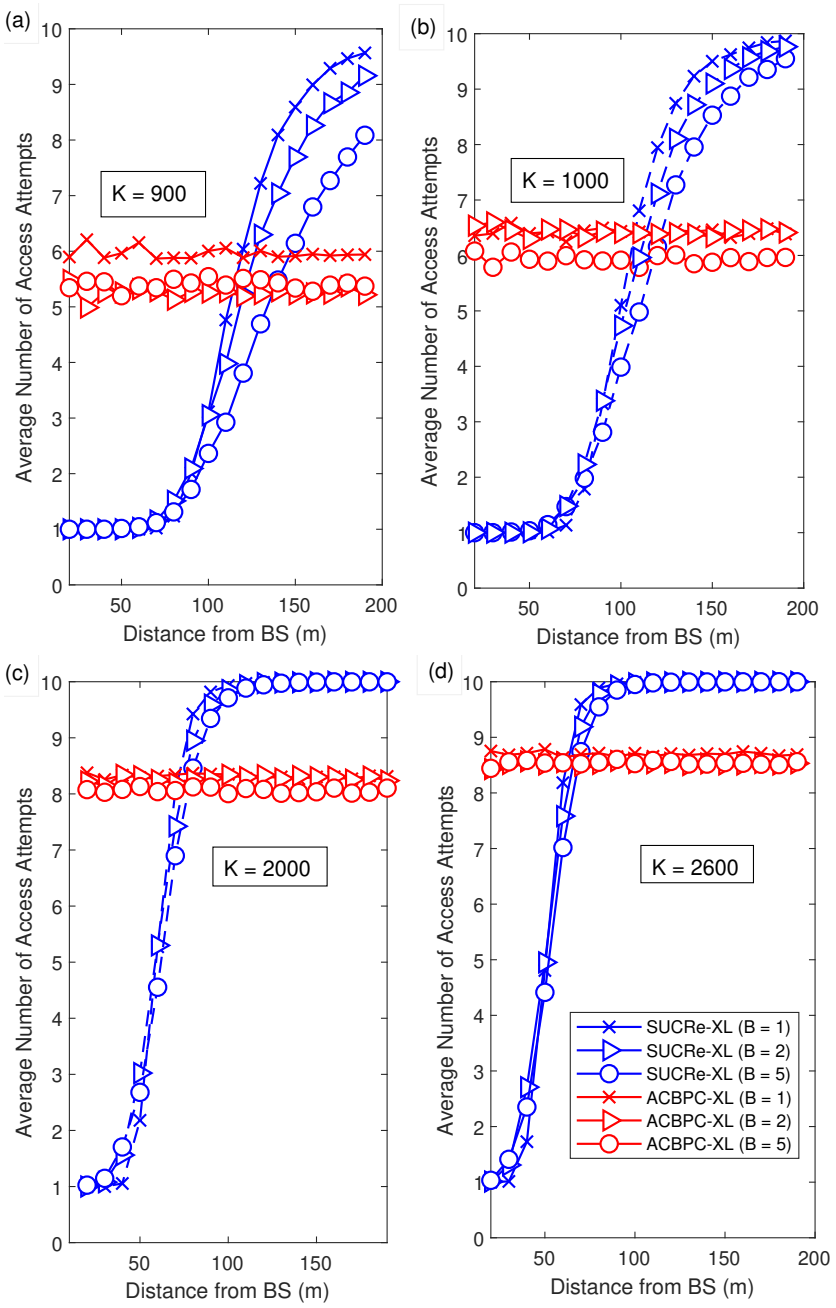

Figure B.7 – ACBPC-XL and SUCRe-XL performance. Average number of access attempts *vs.* distance from the BS for (a) $K = 900$; (b) $K = 1000$; (c) $K = 2000$; (d) $K = 2600$ iUEs.

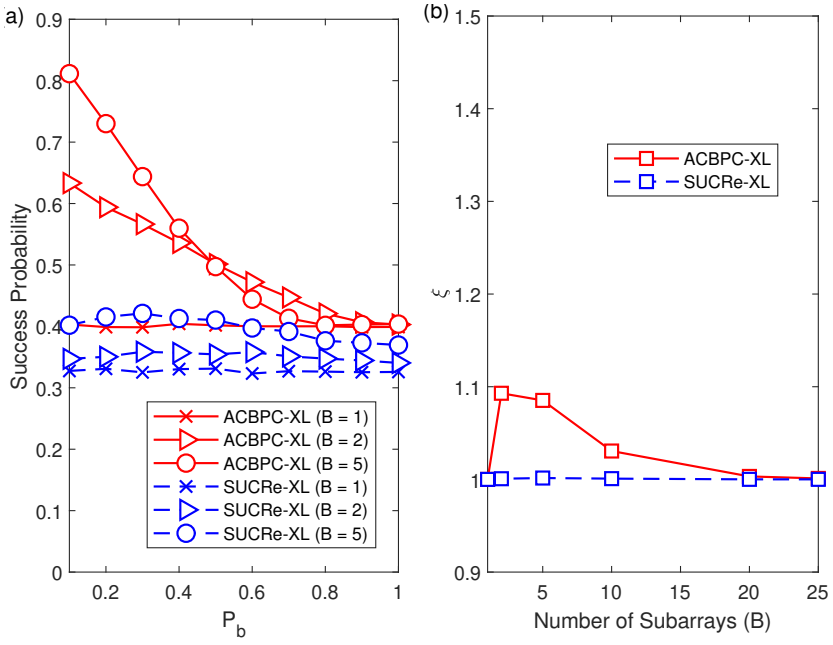

Figure B.8 – ACBPC-XL and SUCRe-XL, $K = 1000$ iUEs. (a) Success probability *vs.* P_b, for different numbers of SAs (B). (b) Average number of accepted UEs per resolved collision (ξ) *vs.* number of SAs (B), with $P_b = 0.5$.

structures under development, such as XL-MIMO. In this sense, the proposed grant-based ACBPC-XL RA protocol targets user access fairness while exploiting XL-MIMO features adapting the conventional ACBPC protocol to the new system setup. Numerical results indicate an improved performance of the proposed protocol in overcrowded scenarios and fairness along the entire cell, benefiting a significant amount of UEs.

Acknowledgment

This work was supported in part by the National Council for Scientific and Technological Development (CNPq) of Brazil under Grant 304066/2015-0, Fundação Araucária under Grant 302/2012, and in part by State University of Londrina – Paraná State Government (UEL) (scholarship)

APPENDIX C – A Graph-Based Random Access Protocol for Extra-Large Massive MIMO Systems

Otávio Seidi Nishimura, José Carlos Marinello Filho, Taufik Abrão

Abstract

Extra-large massive multiple-input multiple-output systems (XL-MIMO) is a new promising structure expected to provide sufficient access for massive number of user equipments (UEs). As this new paradigm emerge, conventional massive MIMO random access can be adapted to function appropriately, possibly bringing several improvements. This paper proposes a random access protocol relying on near field properties of the XL-MIMO, as an additional degree of freedom. Results show an improvement in access delay, with a slight increase in computational complexity and overhead at the base station (BS).

Keywords: Random access protocol, grant-based protocols, massive MIMO, XL-MIMO, non-stationarity, visibility region (VR), SIC.

C.1 Introduction

The rapid growth of UEs due to the development of technologies as Internet-of-Things and massive-Machine-Type-Communications is inevitable (Fallgren; AL, 2013). Furthermore, the current massive MIMO combined with random access is an acceptable strategy to manage this huge amount of data and intermittent access attempts required by the 5G wireless systems (Carvalho et al., 2017). These methods can already be considered as conventional and, although with acceptable performance, there are several approaches to explore and improvements to establish in overcrowded cases. One of the approaches is implementing novel structures as the XL-MIMO. This novel system can be installed in several large infrastructures as buildings, shopping malls, stadiums, or airports (Martínez et al., 2014).

In this paper, we propose a random access protocol in the new crowded XL-MIMO system. This protocol relies on the scenario near field propagation and visibility regions (VRs) to increase intermittent UE access in the entire cell. As the number of obstacles

increase, VRs become more scattered, which brings more collision free transmissions. With this feature, and adding one step in the time domain, the number of accepted UEs increase. *Notation*: Let $\mathbb{C}$ be the spaces of complex-valued numbers, $\mathcal{N}(.,.)$, $\mathcal{CN}(.,.)$ and $\mathcal{B}(.,.)$, a Gaussian, a circularly-symmetric complex Gaussian, and a binomial distribution, respectively. $|\cdot|$ denotes the cardinality of a set and $\|\cdot\|$, the Euclidean norm of a vector. We represent the conjugate, transpose and conjugate-transpose of matrix $\mathbf{A}$ as $\mathbf{A}^*$, $\mathbf{A}^T$ and $\mathbf{A}^H$, respectively. The $M \times M$ identity matrix is defined by $\mathbf{I}_M$.

C.2 System model

We adopt a time-division-duplexing (TDD), where UEs' channels are considered constant during a time slot. The base station (BS) is an 40 m extra-large uniform linear array (ULA) with M antennas, localized at the top center of a semicircle cell represented in Fig. C.1. To simplify, this ULA is equally divided into B subarrays (SAs), each composed by $M_b = M/B$ antennas (Amiri et al., 2018). Let $\mathcal{M}$ be the set with all SAs indexes $(b = 1, \ldots, B)$ and $\mathcal{V}_k \subset \mathcal{M}$ be the subset of SAs indexes of UE k visibility region (VR). We randomly generate a binary vector to represent $\mathcal{V}_k$, being 1 for visible and 0 for invisible SA. Each SA has the same probability P_b of being visible, following a Bernoulli distribution.

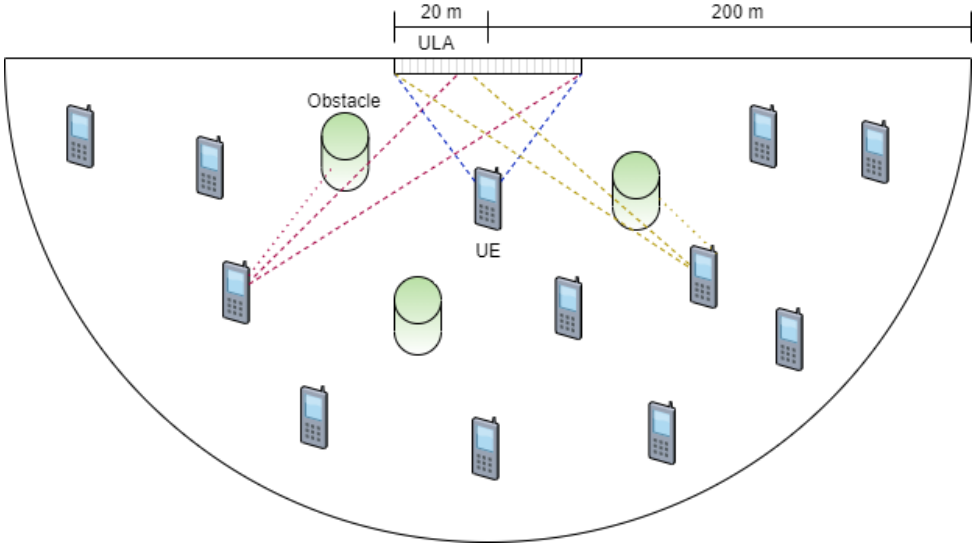

Figure C.1 – Representation of the considered crowded scenario composed by an XL ULA and uniformly distributed UEs with their respective VRs.

Let $\mathcal{K} = \mathcal{U} \backslash \mathcal{A}$ be the set of inactive user equipments (UEs) in the cell, where $\mathcal{U}$ is the set of UEs in the cell and $\mathcal{A} \subset \mathcal{U}$ is the set of active UEs, each one with its dedicated pilot. We consider τ_p mutually orthogonal pilot sequences available, $\boldsymbol{s}_1, ..., \boldsymbol{s}_{\tau_p} \in \mathbb{C}^{\tau_p \times 1}$. Inactive UEs must select a RA pilot from this pool to transmit payload data. Therefore, considering $\mathcal{S}_t \in \mathcal{K}$ as the set of UEs indices that selected pilot t,

$$|\mathcal{S}_t| \sim \mathcal{B}\left(K, \frac{P_a}{\tau_p}\right) \tag{C.1}$$

is the number of UEs that selected the same pilot, where $P_a \leq 1$ is the probability of transmission and $K = |\mathcal{K}|$ is the number of inactive UEs in the cell.

It is considered a Rayleigh fading channel vector $\mathbf{h}_k^{(b)} \in \mathbb{C}^{M_b \times 1}$ between UE k and SA b. The channel follows distribution $\mathbf{h}_k^{(b)} \sim \mathcal{CN}(0, \beta_k^{(b)} \mathbf{I}_{M_b})$, where $\beta_k^{(b)}$ is the large scale fading coefficient, which follows a urban micro scenario (3rd Generation Partnership Project, 2018). Due to near field propagation, we consider one coefficient per antenna, so $\beta_{k,m}^{(b)}$ is the large scale fading between UE k and antenna m of SA b, and

$$\beta_{k,m}^{(b)} = 10^{-\kappa \log(d_{k,m}^{(b)}) + \frac{g+\varphi}{10}}. \tag{C.2}$$

In this equation $d_{k,m}^{(b)}$ is the distance between UE k and antenna m ($m = 1, ..., M_b$) of SA b, $\kappa = 3.8$ is the pathloss exponent, $\varphi \sim \mathcal{N}(0, \sigma_{sf}^2)$ is the shadow fading, with standard deviation $\sigma_{sf} = 10$ dB, , and $g = -34.53$ dB is the pathloss at the reference distance. Similarly as in (Nishimura et al., 2020), we adopt the simplification $\beta_k^{(b)} = \frac{1}{M_b} \sum_{m=1}^{M_b} \beta_{k,m}^{(b)}$, and blocked SAs have $\beta_k^{(b)} = 0$.

C.3 Proposed Protocol

The proposed protocol (inspired by (Han et al., 2017b) and (Sorensen et al., 2018)) consists in applying SIC in a bipartite graph generated by pilot hopping. In the following we present the three steps of the graph-based pilot access for XL-MIMO (GBPA-XL) represented in Fig. C.2.

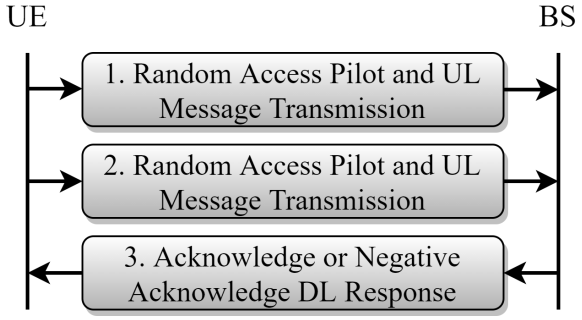

Figure C.2 – GBPA-XL protocol.

Step 1: All UEs that want to access the BS select two UL RA pilot sequences from the same pool $\mathcal{P}_0 = \{\boldsymbol{s}_0, \boldsymbol{s}_1, \boldsymbol{s}_2, \dots \boldsymbol{s}_{\tau_p}\}$, where the element $\boldsymbol{s}_0$ represents an inactivity state, not a pilot, when a UE chooses to not transmit any signals. Let $\{0', 1', \dots, \tau_p'\}$ denote the indexes of the second RA pilot selected. In this case, considering that double inactivity $\{\boldsymbol{s}_0, \boldsymbol{s}_{0'}\}$ is not an option, there are $P_t = \frac{(\tau_p+1)!}{(\tau_p-1)!} - 1$ possible choices. Then UE k transmits the first of the two selected RA pilots $\{\boldsymbol{s}_{r(k)}, \boldsymbol{s}_{r(k)'}\}$ to the BS, where $r(k) \in \{0, \dots \tau_p\}$ is the pilot index selected by UE k. The resulting received signal for each subarray is given by

$$\mathbf{Y}_{p,step1}^{(b)} = \sum_{k \in \mathcal{K}} \sqrt{\rho_k} \mathbf{h}_k^{(b)} \boldsymbol{s}_{r(k)}^H + \mathbf{N}^{(b)}. \tag{C.3}$$

Where ρ_k is the transmit power of UE k and $\mathbf{N}^{(b)}$ is the receiver noise at SA b. Additionally, each UE also needs to transmit a UL message with the encoded indexes of the selected pilots, to make the SIC algorithm possible. Defining N_p as the symbol length of the selected pilots indexes, SA b then receives

$$\mathbf{Y}^{(b)}_{d,step1} = \sum_{k\in\mathcal{K}} \frac{\mathbf{h}^{(b)}_k \boldsymbol{x}_k}{\sqrt{\beta^{(b)}_k}} + \mathbf{N}^{(b)}. \tag{C.4}$$

Where $\boldsymbol{x}_k = (x^1_k, x^2_k, \ldots, x^{N_p}_k)$ is the UL message of UE k. Now each SA can obtain the channels of UEs involved in pilot t by realizing a least squares estimation with the same sequence as

$$\mathbf{y}^{(b)}_{step1,t} = (\boldsymbol{s}^H_t \boldsymbol{s}_t)^{-1} \mathbf{Y}^{(b)}_{p,step1} \boldsymbol{s}_t = \sum_{i\in\mathcal{S}_t} \sqrt{\rho_i}\mathbf{h}^{(b)}_i + \mathbf{n}_t, \ \forall b. \tag{C.5}$$

Step 2: The same UEs in *Step 1* repeat the process now with the second UL pilot transmission. Similar to $\mathbf{Y}^{(b)}_{p,step1}$, each SA receives signal $\mathbf{Y}^{(b)}_{p,step2}$:

$$\mathbf{Y}^{(b)}_{p,step2} = \sum_{k\in\mathcal{K}} \sqrt{\rho_k}\mathbf{h}^{(b)}_k \boldsymbol{s}^T_{r(k)'} + \mathbf{N}^{(b)}. \tag{C.6}$$

The message remains the same, $\mathbf{Y}^{(b)}_{d,step2} = \mathbf{Y}^{(b)}_{d,step1}$. With the transmitted information, each SA is capable of realizing a SIC algorithm.

The SIC algorithm at the BS: Fig. C.3 presents an example of UL RA pilot transmissions with the VRs experienced by five UEs, each selecting one pilot per step. Fig. C.4 illustrates the resulting bipartite graph for SA1 and the SIC process to estimate the channels. As factor nodes we have the selected RA pilots of *Steps* 1 and 2, and as variable nodes, the four UEs having SA1 as a VR. To simplify, we consider ideal interference cancellation. Let $\mathbf{f}^{(b,t)}_j$ be the factor node, or channel response, in iteration j, SA b and pilot t. The algorithm first detect degree one factor nodes, *i.e.*, pilots that were selected by only one UE in a particular step and SA. In this case, the channel of a single UE can be readily estimated and his message decoded. In the example of Fig. C.4(a), $\mathbf{f}^{(1,1)}_1$ is a degree one factor node, $\mathbf{f}^{(1,1')}_1$, a degree two, and $\mathbf{f}^{(1,2)}_1$, a degree three. Message detection in pilot t and SA b, at any iteration j, is realized according to eq. C.7,

$$\hat{\mathbf{x}}^{(b,t)}_k = \frac{(\mathbf{f}^{(b,t)}_j)^H \mathbf{Y}^{(b)}_{d,step1}}{\|\mathbf{f}^{(b,t)}_j\|\sqrt{M_b}} = \sum_{k\in\mathcal{K}} \frac{(\mathbf{f}^{(b,t)}_j)^H \mathbf{h}^{(b)}_k}{\|\mathbf{f}^{(b,t)}_j\|\sqrt{\beta^{(b)}_k M_b}} \mathbf{x}^{b,t}_k + \boldsymbol{\eta}^{(b)}. \tag{C.7}$$

If the decoding is successful, BS now knows the pilots indexes selected by UE1, which were $\{\boldsymbol{s}_1, \boldsymbol{s}_{1'}\}$, and updates $\mathbf{f}^{(1,1)}_2 = \mathbf{f}^{(1,1)}_1$ and $\mathbf{f}^{(1,1')}_2 = \mathbf{f}^{(1,1')}_1 - \mathbf{h}^{(1)}_1$. It results in Fig. C.4(b), where the process is repeated identifying $\mathbf{f}^{(1,1')}_2$ and acquiring the channel and message of UE2. The SIC algorithm finishes at Fig. C.4(c), since there is no more degree one factor nodes.

Step 3: For the DL response, the BS utilizes only the SAs with successful estimated channels of the respective UEs. Therefore, the BS sends an acknowledge (ACK) and allocate

a payload data pilot for UEs with successful decoded message(s) using at least one SA. In contrast, if deconding fails in all visible SAs, unsuccessful UEs become aware of the negative acknowledge (NACK), due to absence of DL response. These UEs must realize another access attempt after a random time period.

Step 1	UE1	UE2	UE3	UE4	UE5
SA1	s_1	s_2	s_2	s_2	
SA2	s_1		s_2		s_3
SA3		s_2			

Step 2	UE1	UE2	UE3	UE4	UE5
SA1	s_1	s_1	s_3	s_3	
SA2	s_1		s_3		
SA3		s_1			

Figure C.3 – Arbitrary UL arrangement with five UEs trying to access the BS. VRs do not change during the process. UEs select a RA pilot, or remain inactive, in *Step 1* and can choose to repeat, reselect or remain idle in *Step 2*. As shown in this example, remaining idle may diminish pilot collisions in each SA, giving more chances of estimating the channels.

C.4 Preliminary Numerical results

Fig. C.5 presents P_{index}, the probability of the BS correctly decoding the index of UEs pilots. For this simulation, all SAs are visible for randomly distributed UEs along the cell. It is considered BPSK modulation, $N_p = 10$ and $\tau_p = 10$. To simplify, there is no pilot collision, so P_{index} represents the probability of decoding pilot indexes only at degree one factor nodes.

To compare the performance of the proposed protocol, we present the results of the strongest-user-collision-resolution protocol (SUCRe-XL) (Nishimura et al., 2020), and the named direct-channel-estimation for XL-MIMO (DCE-XL). The latter is similar to the GBPA-XL, not considering the SIC algorithm. In this case, the DCE-XL only accepts UEs with degree one factor nodes in the two UL transmission steps. To simplify, the following simulations consider perfect channel estimation and interference cancellation. The probability of transmission is $P_a = 1\%$ and $M = 400$ BS antennas.

Fig. C.6 presents the *Average Number of Access Attempts* (ANAA) for three XL-MIMO random access protocols, for different number of SAs at the BS. The GBPA-XL and DCE-XL protocols have satisfying performance under a specific number of UEs, access to inactive UEs with only one attempt. However, it degrades abruptly subsequently, not being capable to manage overcrowded scenarios. Also, with the increase of the number of

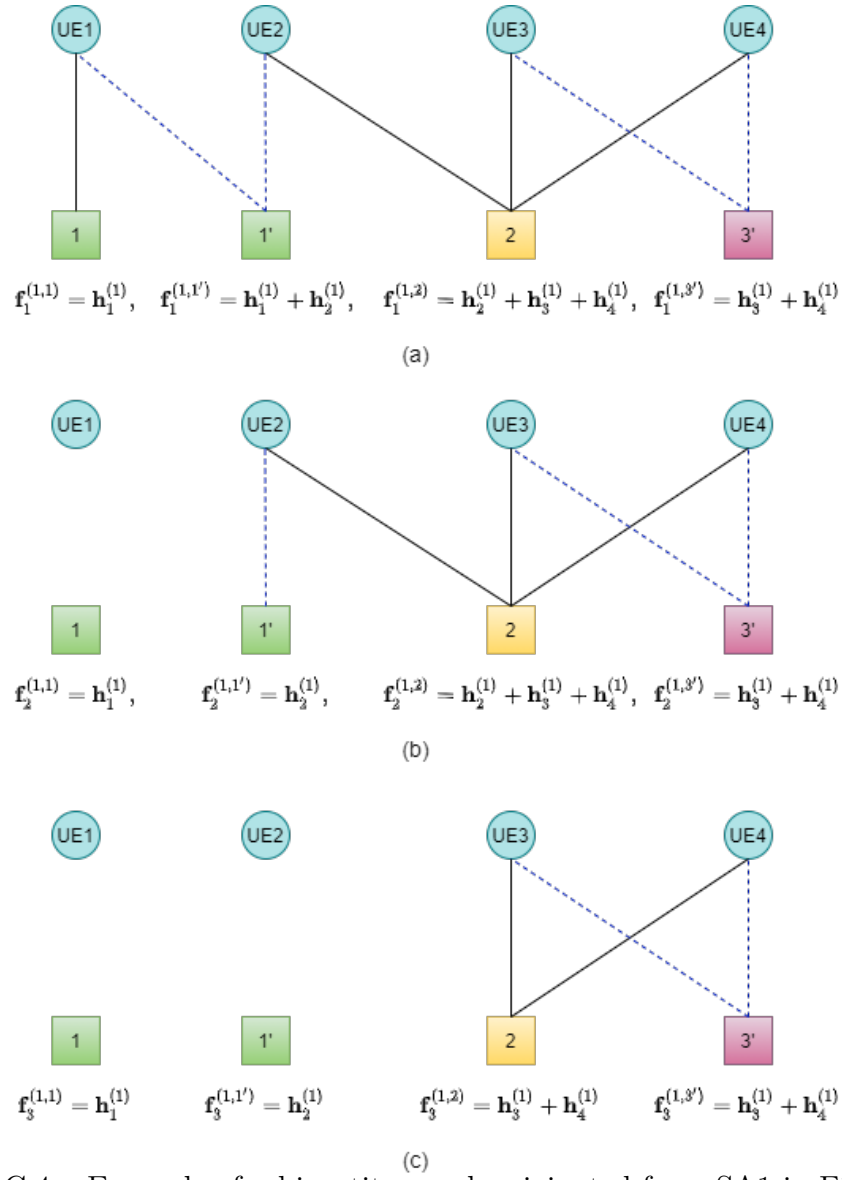

Figure C.4 – Example of a bipartite graph originated from SA1 in Fig. C.3.

SAs the ANAA curves shift right for both protocols. The SUCRe-XL protocol degrades more softly with the increase of inactive UEs, however its performance worsens with less number of UEs comparing with the proposed protocols. Fig. C.7 shows the *Fraction of Failed Access Attempts* and its curves are similar from Fig. C.6. From Fig. C.7 it is possible to visualize how performance worsens to unacceptable levels, 100% of access attempts fails after a specific number of inactive UEs. However, before that, 100% of the access attempts are successful.

Fig.C.8 presents the *Normalized Number of Accepted UEs*, which shows a similar behavior to previous results. Approximately all access attempts are successful until it degrades abruptly for overcrowded scenarios.

Currently, the proposition is to handle the massive attempts with a hybrid method, where it uses the GBPA-XL for lower number of inactive UEs and the SUCRe-XL or the ACBPC-XL protocols for overcrowded situations. The proposed GBPA-XL protocol

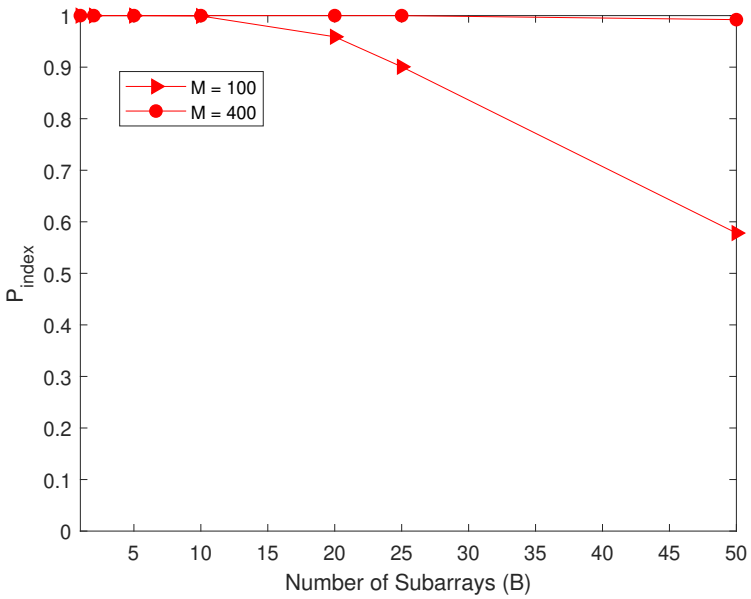

Figure C.5 – Probability of pilot indexes correct decodification *vs.* the number of subarrays (B) at the BS.

increases computational complexity considerably. However, for lower numbers of inactive UEs, the trade-off confirms to be advantageous. Furthermore, the choice between the GBPA-XL and the DCE-XL protocols will depend on the trade-off analysis of complexity and performance, which is only comparable for greater number of subarrays (B). In other words, the GBPA-XL has a better performance than the DCE-XL protocol only for greater number of subarrays, which in contrast increases complexity.

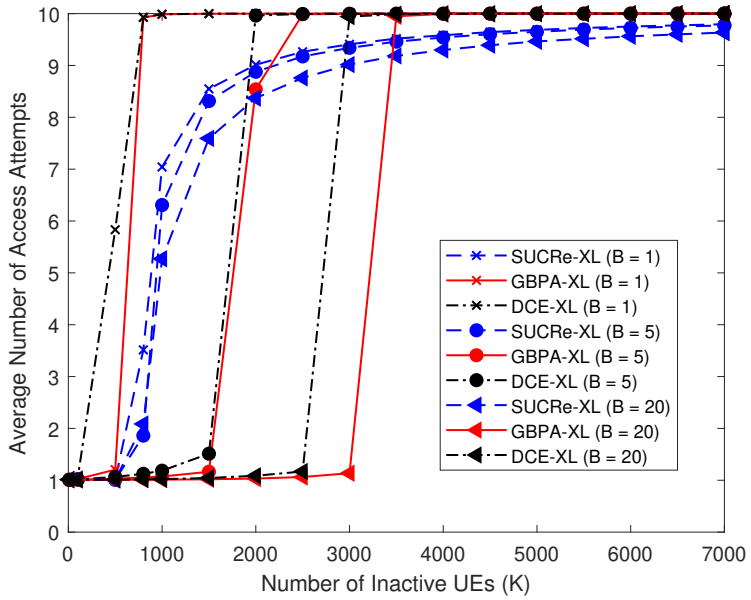

Figure C.6 – Average number of access attempts (ANAA) *vs.* number of inactive UEs (K) in the cell, for different numbers of subarrays (B).

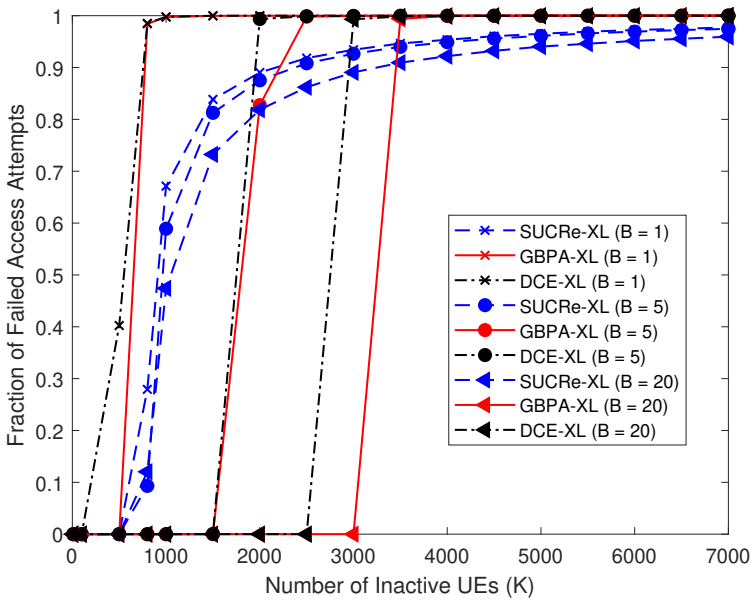

Figure C.7 – Probability of failed access attempt *vs.* number of inactive UEs (K) for different numbers of subarrays (B) at the BS.

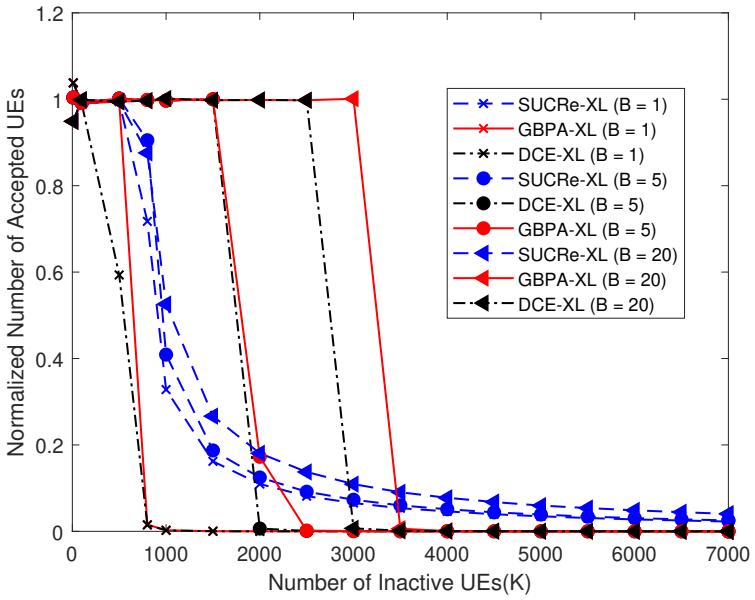

Figure C.8 – Normalized number of accepted UEs *vs.* number of inactive UEs (K) for different numbers of subarrays (B).

C.5 Remarks

Conventional massive MIMO protocols already present satisfactory results applied to 5G wireless systems, however new and higher requirements and challenges emerge with increase of UEs, data throughput and latency demands. Furthermore, the new XL-MIMO system is promising to accomplish higher standards for 5G and beyond. This work presented a new grant-based RA protocol to manage massive access attempts using its non-stationarities as a degree of freedom. Results show improvements for lower number of inactive UEs in the cell. In this case, a better approach would be a hybridd method to deal with different scenarios.